Stony Brook University

It's a NO for Bacterial Settlement: Nitric Oxide Regulated Biofilm Formation and Protein Expression

A Dissertation Presented

by

Yueming Xu

to

The Graduate School

in Partial Fulfillment of the

Requirements

for the Degree of

Doctor of Philosophy

in

Chemistry

Stony Brook University

August 2014

Stony Brook University

The Graduate School

Yueming Xu

We, the dissertation committee for the above candidate for the

Doctor of Philosophy degree, hereby recommend

acceptance of this dissertation.

Elizabeth M. Boon – Dissertation Advisor
Associate Professor, Department of Chemistry

Peter J. Tonge - Chairperson of Defense
Professor, Department of Chemistry

Orlando D. Schärer – Third Committee Member of Defense
Professor, Department of Chemistry

Stephen G. Walker – Outside Committee Member of Defense
Associate Professor, Department of Oral Biology and Pathology

This dissertation is accepted by the Graduate School

Charles Taber
Dean of the Graduate School

Abstract of the Dissertation

It's a NO for Bacterial Settlement: Nitric Oxide Regulated Biofilm Formation and Protein Expression

by

Yueming Xu

Doctor of Philosophy

in

Chemistry

Stony Brook University

2014

Nitric Oxide (NO) is a diatomic signaling molecule that regulates diverse bacterial behaviors. Its effect on cell motility has been established in many microbial systems, but the molecular mechanism remains understudied. Some bacteria have an H-NOX (Heme-Nitric oxide/OXygen-binding) domain that functions as an NO sensor. It is found in the same operon with two component signaling histidine kinases or diguanylate cyclases (DGC) that synthesize and degrade cyclic di-GMP (c-di-GMP). C-di-GMP is a secondary signaling molecule that regulates bacterial motile to sessile lifestyle transition. In this dissertation, we dedicated our effort toward understanding the effect on bacterial biofilm by NO/H-NOX regulated signaling pathway.

In *Vibrio harveyi*, NO mediates quorum sensing (QS) through the H-NOX/HqsK pathway. We show that NO regulates flagellar production and biofilm formation in a concentration dependent manner. At low nanomolar concentration of NO, repression of flagellin coincides with enhanced biofilm. As NO concentration increases (100~200nM), a global switch takes place in protein expression and results in decreased flagellar production and less promotion of biofilm.

In *Shewanella woodyi*, H-NOX binds a bifunctional DGC (*Sw*HaCE). Nanomolar levels of NO repress biofilm formation through c-di-GMP degradation, and enhance phosphodiesterase activity of *Sw*HaCE, leading to c-di-GMP hydrolysis. H-NOX regulation is not limited to

proteins in the same operon. *Sw*H-NOX can also interact with *Vh*HqsK homologue, *Sw*HK (Swoo_2833). Weaker biofilm phenotype in response to NO is attenuated when *Sw*HK gene is disrupted in *S. woodyi*.

In summary, NO mediates biofilm formation and protein expression via binding sensor protein H-NOX in multiple systems. Since biofilm is the predominant form of bacteria in natural aquatic environment, revealing the NO signaling mechanism would facilitate further understanding of bacterial group behavior.

Table of Contents

List of Figures

List of Tables

List of Abbreviations

AI	Autoinducer
AIP	Autoinducing Peptides
Amp	Ampicillin
c-di-GMP	Cyclic di-guanosine monophosphate
CLSM	Confocal Laser Scanning Microscope
CV	Crystal Violet
CV	Crystal Violet
DAP	2,3-diaminopropionic acid
DGC	Diguanylate Cyclase
EPS	Extracellular Polysaccharide Substance
GST	Glutathione S-transferase
HK	Histidine Kinase
H-NOX	Heme Nitric oxide/OXygen sensing domain
IPTG	Isopropyl-1-thio-β-D-glactopyranoside
Km	Kanamycin
LB	Luria Bertani
MM	Marine Media
NO	Nitric Oxide
PDE	Phosphodiesterase
QS	Quorum Sensing
RR	Response Regulator
sGC	Soluble Guanylate Cyclase
Sw	*Shewanella woodyi*
Vc	*Vibrio cholerae*
Vh	*Vibrio harveyi*
WT	Wild Type

Vita, Publications and/or Fields of Study

1. Liu, N., Xu, Y., Hossain, S., Huang, N., Coursolle, D., Gralnick, J. A., and Boon, E. M. (2012) Nitric Oxide Regulation of Cyclic di-GMP Synthesis and Hydrolysis in *Shewanella woodyi*. *Biochemistry* **51**, 2087-2099
2. Henares, B. M., Xu, Y., and Boon, E. M. (2013) A nitric oxide-responsive quorum sensing circuit in *Vibrio harveyi* regulates flagella production and biofilm formation. *Int. J. Mol. Sci.* **14**, 16473-16484, 16412 pp.

Chapter 1 Introduction

Abstract

Bacterial biofilms are cell aggregations covered in a self-secreted polysaccharide matrix at solid-liquid or liquid-air interfaces. A bacterium motile-to-sessile transition is correlated with the ubiquitous bacterial secondary signaling molecule Cyclic di-Guanosine Monophosphate. C-di-GMP is enzymatically synthesized and degraded by diguanylate cyclases with GG(D/E)EF domains and phosphodiesterases with ExL or HD-GYP domains respectively. In many single or multi-species microbial communities, the diatomic signaling molecule nitric oxide (NO) regulates biofilm level. The effects of NO on these species include biofilm formation and/or dispersion, virulence factor production and resistance to antibiotics. The hypothesized molecular mechanism is that upon NO exposure, bacterial NO sensor modifies protein expression or activity, bringing about a fluctuation in signaling pathways, ultimately resulting in regulation of biofilm formation. In several bacterial species that encodes for a *hnox* gene, the Heme Nitric oxide/Oxygen sensing protein is shown to serve as the NO sensor and mediates neighboring effectors.

1.1 Bacterial Biofilm

In 1933, Arthur T. Henrici immersed a microscope glass slide in an aquarium for a week and noticed “a thin and uniform coating of bacteria of various forms” firmly attached to the glass surface. The cell deposits were so strongly attached to slides that tap water could not remove them from the surface [1]. This was the first recorded observation of bacterial structured community that was later termed a biofilm [2]. Biofilm formation is a complicated process that requires cell-cell communication and multicellular behavior. Initialed by various environmental cues, platonic cells undergo structure changes and aggregate at phase interfaces. During the maturation stage, bacteria further adapt to a biofilm lifestyle. The surface cells secrete extracellular polysaccharide substance (EPS), and embedded cells reduce their metabolism rate and develop antimicrobial resistance. Upon sensing dispersal signals, cells in mature biofilms can detach and return to free swimming state [3] (Figure 1-1).

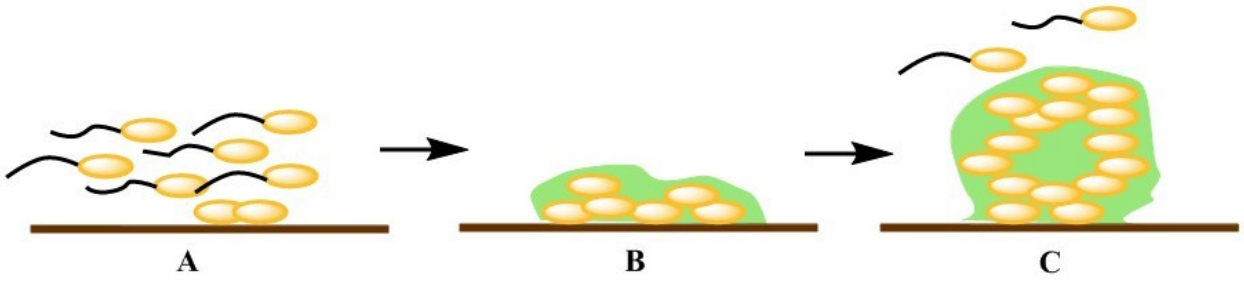

Figure 1-1. Three stages of bacterial biofilm formation. A) Platonic cells stop flagellar synthesis and initiate surface attachment. B) Bacteria further adapt to biofilm lifestyle and secrete EPS. C) Bacteria cells restart the flagellar formation and dissociate from mature biofilm.

Studying bacterial biofilms is a useful approach to understanding bacterial behavior because in natural aquatic systems, biofilms are the predominant form in which bacteria exist [1]. It has been shown that biofilm cells benefit from many advantages versus individual cells. Firstly, the

highly dispersed water channels throughout biofilm structure enhance nutrient and metabolite exchange within microbial structures [4]. In some multispecies biofilms systems, bacteria establish syntrophic relationships for metabolic energy production [5]. Secondly, biofilm formation is also an efficient bacterial self-defense mechanism. Many studies suggest that pathogenic bacteria adopt drug resistance by horizontal gene transfer, and since the majority of bacteria reside in biofilms, the exchange of genetic traits mostly likely takes place in biofilm via conjugation or phage infection [6]. Moreover, bacterial secreted EPS protects the community from antibiotic diffusion and hostile environment such as UV radiation, pH shift, heavy metals and desiccation [7].

Biofilm infections have increased public concern because cells in biofilms exhibit 10 to 1000 resistance to antibiotics in comparison to platonic cells [8]. Other than the drug resistance and difficulty in antimicrobial diffusion as mentioned above, traditional antibiotics that target growth-specific factors may fail to kill biofilm cells, as reports have shown that when bacteria settle and start to form micro-colonies, enclosed cells undergo dormancy and stop dividing [8, 9]. While highly active cells on the periphery might be killed quickly, deeper embedded cells can still survive [10]. Therefore, if medical treatment fails to eradicate biofilms from the host, persister cells can re-grow or disperse and resettle, causing reoccurring infection. In order to develop effective antibiofilm drugs, we need to further understand the unique lifestyle of biofilms and explore new targets that are specific for bacteria community.

1.2 Cyclic di-Guanosine Monophosphate (c-di-GMP) Metabolism and Signaling

C-di-GMP is a bacterial secondary messenger that is synthesized and degraded in bacteria as an output to extracellular signals. It was first identified as an allosteric cellulose synthase activator of *Gluconacetobacter xylinus* in 1987 [11]. Since then, the roles of c-di-GMP signaling have expanded to include a wide range of functions such as: sessility, virulence, environmental persistence, cell cycle, cell-cell communication regulation, and many others. [12].

In bacterial cells, diguanylate cyclases (DGC) and phosphodiesterases (PDE) are c-di-GMP metabolizing enzymes. DGCs that contain active GG(D/E)EF domains cyclize two molecules of guanosine triphosphate (GTP) into c-di-GMP [13, 14]. One such example is *Caulobacter crescentus* PleD, a response regulator required for pole development [15-17]. Upon phosphorylation, the N-terminal receiver domain mediates GGDEF domain dimerization and activates cyclase activity [13]. C-di-GMP specific PDEs that encode ExL or HD-GYP domains hydrolyze it into 5'-phosphoguanylyl-(3',5')-guanosine (pGpG) [11, 18] or two guanosine monophosphates (GMPs) [19](Figure 1-2). The PDE activity of EAL domain depends on the presence of Mn^{2+} or Mg^{2+}, and is strongly inhibited by Ca^{2+} or Zn^{2+} [18, 20].

In most cases c-di-GMP metabolizing enzymes respond to external signals via a sensory input domain, such as PAS, HAMP and REC domains [12, 17, 21-25]; or by protein-protein interaction with a stand-alone protein [26-29]. The sensors enable enzymes to sense external signals such as O_2, NO, CO, light, redox potential, and quorum sensing molecules [12, 21]. Some bacterial genomes encode for multiple DGCs and PDEs, each with their own sensor. For example, *Pseudomonas aeruginosa* has 41 putative c-di-GMP metabolizing proteins [30] and *Vibrio cholerae* (*V. cholerae*) encodes for 61 [31]. These enzymes with regulators comprise a

complex signaling network that can respond to various environmental cues, making c-di-GMP a universal signal molecule.

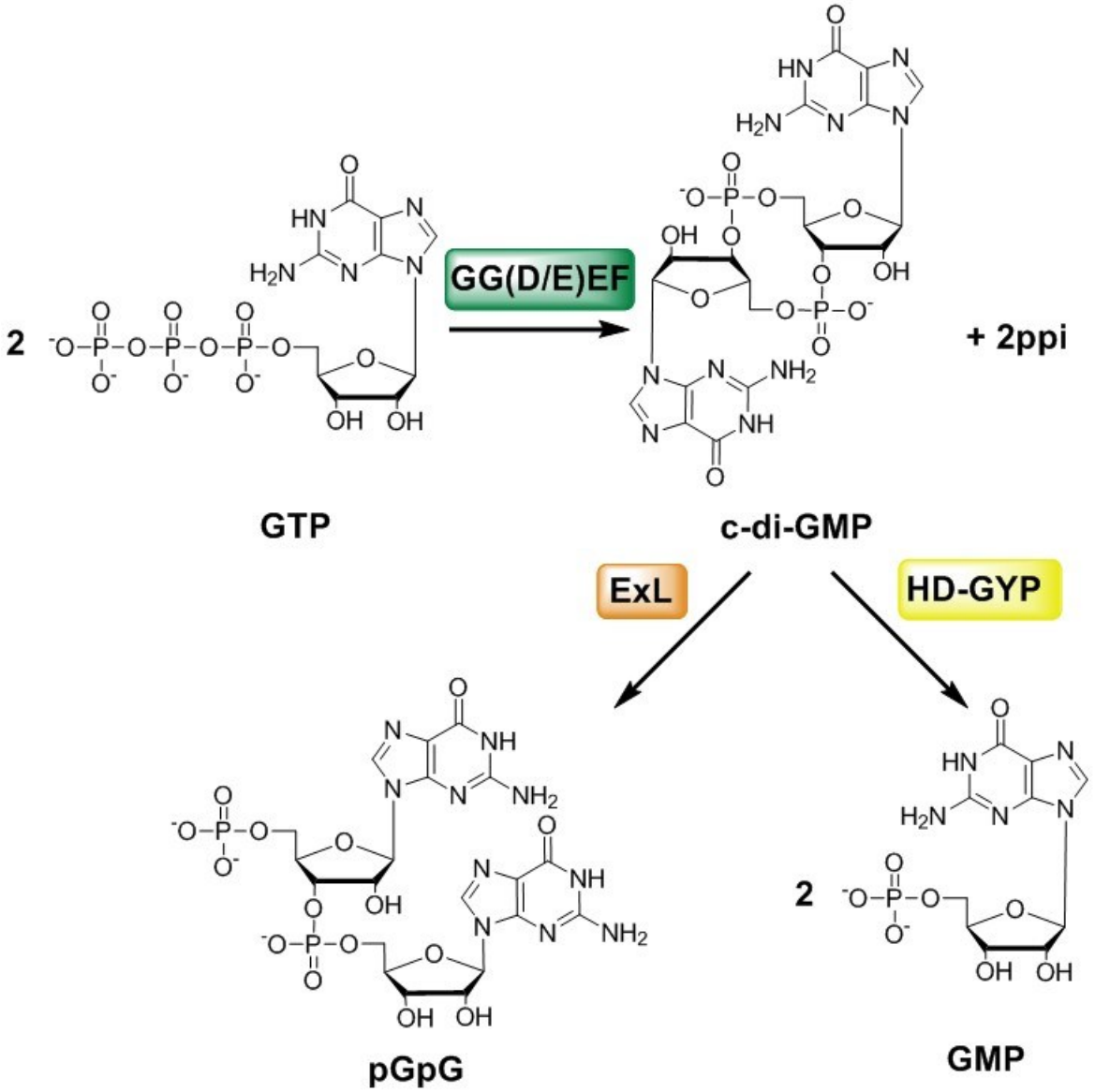

Figure 1-2. Enzymatic c-di-GMP metabolism. GG(D/E)EF domain cyclases two GTPs into c-di-GMP. Phosphodiesterases ExL and HD-GYP domains dehydrate c-di-GMP into pGpG and two GMPs respectively.

Receptors of c-di-GMP characterized include transcription factors, the PilZ domain, I sites, enzymatically inactive EAL and HD-GYP domains and riboswitches [32]. Transcriptional repression of genes related to virulence production by c-di-GMP has been observed in many systems such as *V. cholerae* and *Xanthomonas campestris* [33, 34]. The reversible sessile-motile lifestyle transition within biofilm communities is commonly controlled by c-di-GMP [11, 35-38]. One such effector is YcgR, the flagellar brake with a PilZ domain[21]. C-di-GMP-bound YcgR undergoes a structural change and interact with flagellar machinery, yielding a strong bias of flagellar counterclockwise rotation resulting in slower rotation speed [39, 40]. Decelerated cells that are unable to switch rotation direction are more likely to "smooth swim" towards a surface and transit to sessile mode [41]. Since surface attachment is the first step of biofilm formation, it is more than likely that c-di-GMP is a biofilm regulator. Indeed, many reports have shown that elevated c-di-GMP level promotes the expression of adhesive matrix components and biofilm formation [30, 35, 42-45]. The discovery of two classes of riboswitches in recent years extends c-di-GMP regulation to gene translation [46, 47]. The comprehensiveness of c-di-GMP signaling system and the abundance of receptors allow it to mediate cellular behavior on both a fast post-translational level and a long-term translational or transcriptional level [21].

1.3 Bacterial Quorum Sensing Circuits

The term quorum sensing (QS) describes the process of cell-density-dependent gene expression regulated by specific QS molecules [48-50]. The first discovered QS cases were the bioluminescence of two marine bacteria, *Vibrio harveyi* (*V. harveyi* or *Vh*) and *Vibrio fishceri* [51]. Since then QS has established a connection with many processes, including bioluminescence, biofilm formation, virulence, type III secretion, DNA uptake, plasmid conjugation, and microcin production [51-56]. QS molecules known as autoinducers (AIs) are

chemical signaling molecules secreted and monitored by bacteria as information of cell community density and species complexity. Expression of various genes is turned on in synchronicity when the AI concentration reaches a threshold as cell density increases [51]. QS species are able to switch lifestyle between a low cell density (LCD) mode that is favored by individual cells and a high cell density (HCD) mode that benefits groups [57]. For example, in the *V. fischeri* and bobtail squid symbiosis system, light production by *V. fischeri* at HCD counteracts shadows cast by the squid at night, protecting the squid from its predators. The squid in turn provides nutrients and a habitat for *V. fischeri* [58].

The molecular mechanisms of QS in different organisms vary from each other, but all characterized systems contain three essential steps involving AI production, release and detection [57, 59]. Gram-positive bacteria such as *Staphylococcus aureus* utilize autoinducing peptides (AIPs) as AIs (Figure 1-3). The extracellular level of AIP increases as it is produced and secreted. In some cases, AIP binds to a histidine kinase (HK) domain of a two-component receptor and activates kinase activity when it reaches a threshold. The HK domain further transfers phosphate groups to its cognate response regulator (RR) and initiates downstream translation of QS gene [60]. In other systems, AIP is transported back inside cells and directly interact with cytoplasm transcription factors [57]. The AIs for Gram-negative species are hormone-like small molecules such as acyl-homoserine lactones (AHLs) (Figure 1-4A) or compounds derived from *S*-adenosylmethionine (SAM) (Figure 1-4B) [61-63]. Amphipathic AHLs can diffuse freely through the membrane, and at HCD are sensed by transcription factors or two-component receptors. The following activation of gene expression is analogous to previously discussed Gram-positive systems [57].

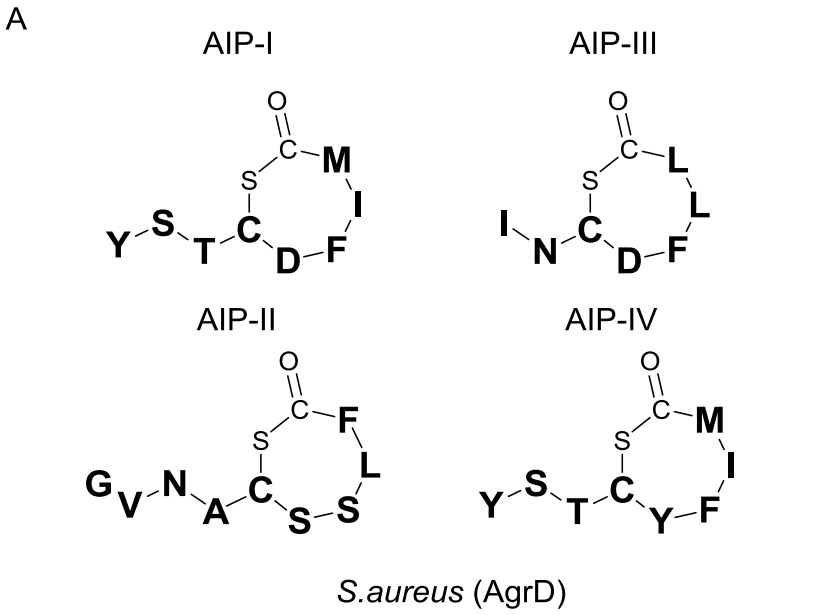

Figure 1-3. Structure of A) AIPs from *S. aureus* B) AIPs from other Gram-positive bacteria. Letters in bold correspond to the amino acids.

V. harveyi is a marine bacterium that is pathogenic to aquatic animals such as shrimp. The Bassler group identified three parallel signaling channels that mediate a shared QS regulatory pathway in this organism [64]. The receptors specifically detect three AIs that synergistically contribute to light production and are involved in inter- or intraspecies communication: HAI-1 (Figure 1-4A), AI-2 (Figure 1-4B), and CAI-1 (Figure 1-4C).

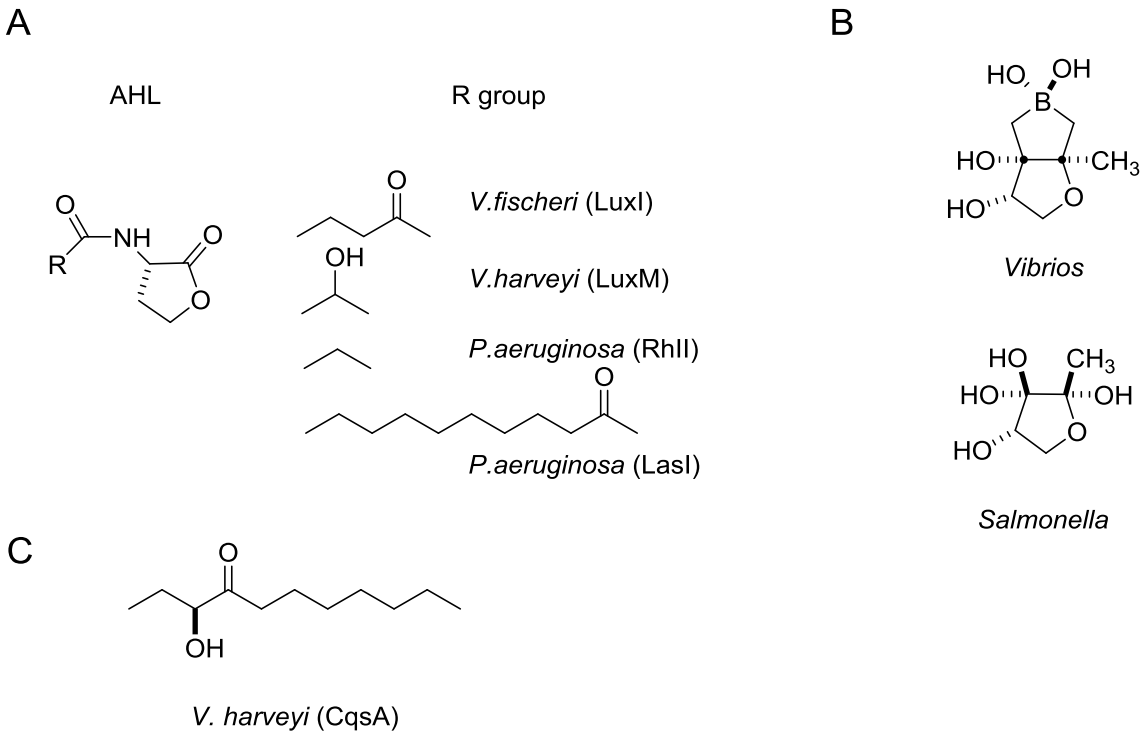

Figure 1-4. Structure of AIs for Gram-negatives. A) AHL analogues, B) SAM-based AIs , C) CAI-1 from *V. harveyi*. AI synthases are indicated in parentheses.

Figure 1-4 shows the detailed molecular mechanism of QS signal transduction. The first identified *V. harveyi* AI was HAI-1, an AHL-based 3OHC4-homoserine lactone synthesized by LuxM [65]. HAI-1 is detected by a membrane-bound cognate histidine kinase LuxN. HAI-1 is suggested as an intraspecies signal because LuxN is found in some closely related *Vibrio* species [64, 65]. The second *V. harveyi* QS circuit involves a furanosyl borate diester (AI-2) that is produced by LuxS [66-68]. The receptor for AI-2 is LuxP, a periplasmic protein that can bind to a histidine kinase LuxQ and serves as a sensor [69, 70]. AI-2 is considered a universal interspecies QS signal due to the frequent presence of LuxS in bacterial organisms [71]. The third signal CAI-1 is synthesized by CqsA and detected by CqsS [64]. CqsA/CqsS is conserved in many *Vibrio* species [64, 72, 73], hence CAI-1 may be a common signal among *Vibrios*.

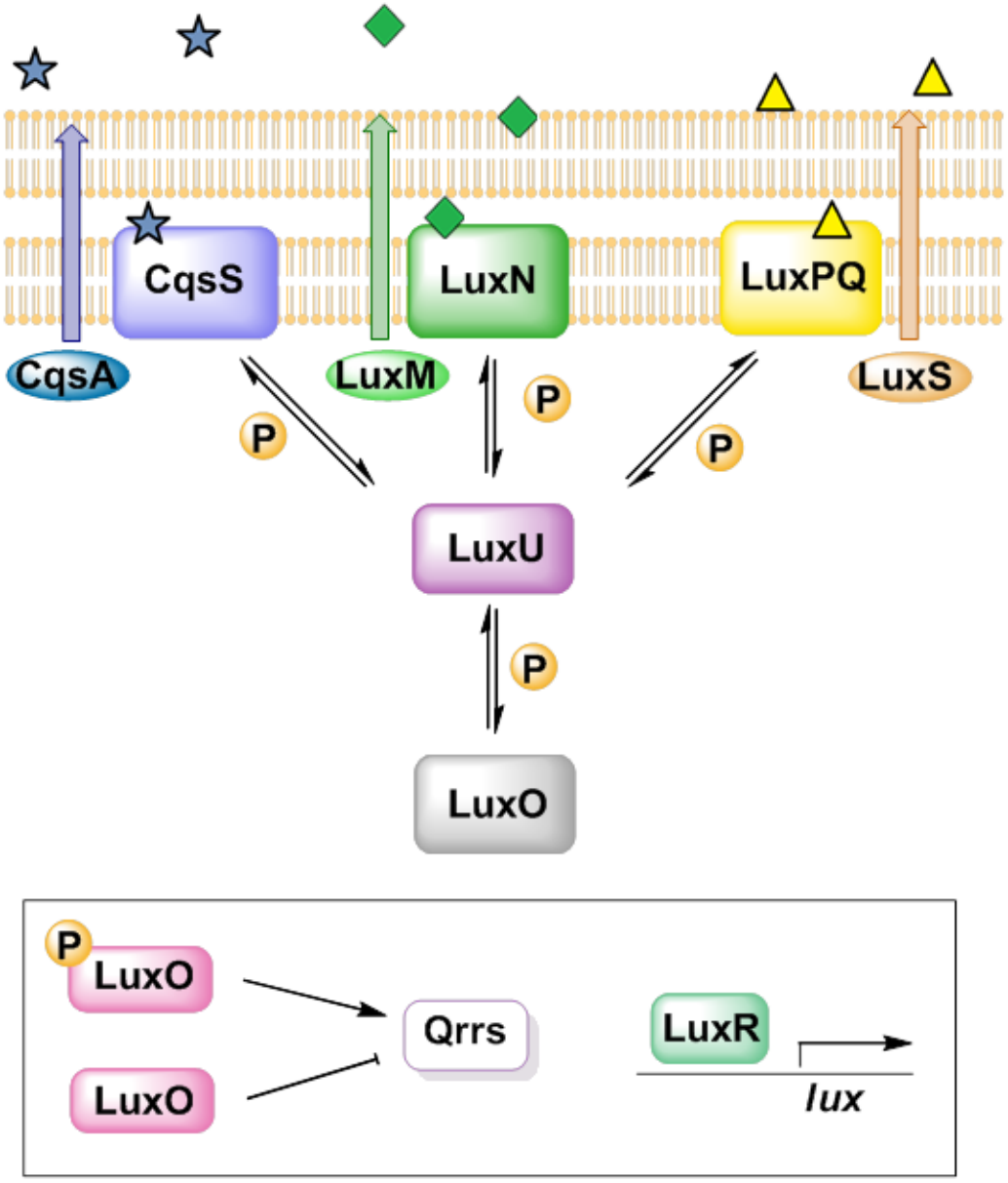

Figure 1-5. *Vibrio harveyi* parallel quorum sensing pathways. Blue stars, green diamonds and yellow triangles represent CAI-1, HAI-1 and AI-2 respectively.

The three parallel sensors, LuxN, LuxQ and CqsS, are all bi-functional enzymes with both kinase and phosphatase activity [64]. At LCD, AI-free sensors phosphorylates a two component phosphorylase, LuxU [74, 75], which in turn passes phosphate to response regulator LuxO [76]. Phosphrylated LuxO together with a transcription factor σ^{54} activates expression of five quorum regulatory RNAS (Qrr 1-5) [77]. The sRNAs bind to RNA chaperone Hfq and destabilizes the mRNA of LuxR [78], the activator of luciferase operon *luxCDABE* [79]. Hence light production is repressed under this condition. At HCD, AIs accumulate and bind to the sensors, inhibiting the kinase activity. The flow of signal transduction is, therefore, reversed, draining phosphates from LuxO. Unphosphorylated LuxO cannot initiate expressions of Qrrs. As a result, LuxR binds to promoters of *luxCDABE* and stimulate bioluminescence production [64].

1.4 Nitric Oxide (NO) and the NO Sensor

The diatomic molecule nitric oxide (NO) was first identified as a crucial signaling molecule in endothelial cells as a relaxing factor at low concentration [80]. It is an uncharged small radical that is stable enough to diffuse across cell membranes without being oxidized until binding its targets. Therefore, it is well suited for its role as a signaling molecule and was selected as molecule of the year by Science magazine in 1992 [81]. In eukaryotes, NO is synthesized by nitric oxide synthase (NOS) from L-arginine. The NO sensor soluble guanylate cyclase (sGC) [82] houses a heme molecule (Figure 1-5) that can bind gaseous molecules such as O_2, CO, and NO [83]. sGC is activated when a NO-heme complex is formed [84] and converts GTP into the secondary messenger cyclic GMP which in turn triggers downstream responses such as smooth muscle relaxation and platelet inhibition [85, 86]. Other than the NO/cGMP pathway, NO is also involved in various mammalian physiological processes such as mitochondrial cytochrome oxidase inhibition, neurotransmitter release, and immune response [87-91].

In recent years, researchers have also established the importance of NO in bacterial behavior regulation. Higher concentrations (~μM) of NO produced within macrophages cause oxidative and nitrosative stress as well as toxicity to pathogenic bacteria[92]. At non-toxic lower concentrations (~nM), NO functions as a signaling molecule and effectuates bacterial behavior such as biofilm formation [93-95] and quorum sensing (QS) [96, 97]. NO is also a broad-spectrum antimicrobial agent with minimal drug resistance because it targets multiple physiological pathways [98]. It has been applied as an anti-biofilm agent and displayed high potency owing to the biofilm dispersal effect in several pathogens and its phenomenal diffusion efficiency [99]. Aside from exogenous NO produced by mammalian NOS, bacteria can synthesize endogenous NO either by bacterial NOS (bNOS) (mostly Gram-positive strains) [100], or through anaerobic respiration by nitrite reductase as an intermediate of denitrification [101].

NO mediation of bacterial biofilm has been validated in many organisms [102-104]. For example, it has been shown that in *Nitromonas europaea*, NO induces biofilm dispersal at ~ 5 ppm (< 200 μM) while at higher levels (30 ppm = ~ 1 mM) promotes biofilm formation [102]. Barraud et al. established that *P. aeruginosa* biofilm dispersal is induced at 25-500 nM [103]. Although the phenotypes of NO regulation are verified, understanding of the molecular mechanisms is limited. Several possible mechanisms are suggested for *P. aeruginosa*, all by mediating PDE activity and depleting c-di-GMP [105, 106] . Li *et al*. identified an NO-induced biofilm dispersal locus A (NbdA) that specifically responds to NO [106]. NbdA is an active PDE that encodes a transmembrane MHYT domain (transmembrane domain with conserved Met, His, Tyr residues). Although NbdA is not a heme-protein, a bioinformatics study showed that the conserved Met and His residues could coordinate with copper ions and potentially sense NO

[107]. Upon NO exposure, NbdA expression is elevated. Accumulated NbdA degrades cellular c-di-GMP and induces biofilm dispersion [106]. A biofilm dispersal locus (BdlA) is also found to respond to many environmental cues such as succinate, salts of Ag^{+}, Hg^{2+}, As^{3+}, and NO, and prompts c-di-GMP degradation and biofilm dispersion [105, 108] because one PAS domain (PASa) of BdlA can bind heme and abrogate NO. However, it is yet unclear how BdlA regulates DGC or PDE activity.

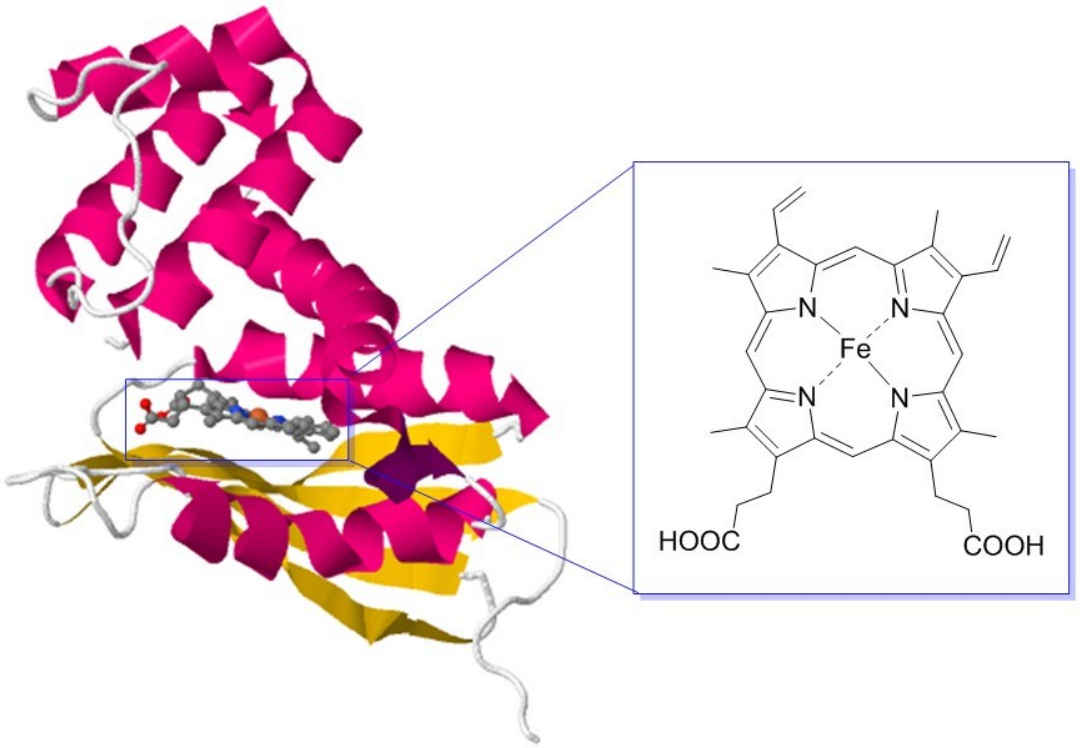

Figure 1-6. Crystal structure of a *Thermoanaerobacter tengcongensis* H-NOX (PDB ID:3SJ5; I5F Mutant with heme) [109]. The structure of heme polyporphyrin with a ferrous center is enlarged.

A homolog of the N-terminus NO sensory domain of eukaryotic sGC, heme-nitric oxide/oxygen (H-NOX) binding protein [110, 111], is encoded in many organisms [112]. The crystal structure

of an H-NOX protein with heme as a ligand is shown as Figure 1-5. Bioinformatics study suggests that in bacteria, this *hnoX* gene often encodes for a stand-alone protein, and is usually located within the same operon with diguanylate cyclases or histidine kinases (HK) [113]. Hence H-NOX is mostly likely serving as an NO sensor and regulating the activity of its neighboring effectors. In *S .oneidensis* and *V. harveyi*, NO bound H-NOX inhibits the autophosphorylation of downstream histidine kinase [97, 114]. In *Legionella pneumophila*, H-NOX directly interacts with a bi-functional DGC that can synthesize and degrade c-di-GMP [115]. With the emerging evidence of NO regulation of bacterial biofilms, we hypothesize that H-NOX will play a crucial role in the signaling process.

1.5 Overview of Research Projects

This dissertation is divided into 5 chapters. Chapter 2 explores H-NOX regulation of biofilm by mediating phosphorylation of H-NOX associated quorum sensing kinase (HqsK) in *Vibio harveyi*. Chapters 3 and 4 introduce NO regulation of c-di-GMP levels and biofilm formation through an H-NOX in *S. woodyi*, and extend the signaling pathway to a multi-effector network. The effects monitored in this study include biofilm and c-di-GMP levels, as well as global protein expression. Our findings suggested that bacteria respond to a low nanomolar level of NO by forming NO-H-NOX complex. Chapter 5 provides a summary of this thesis.

In Chapter 2, we seek to understand the connection between a characterized LuxO/LuxR QS pathway and biofilm formation. In *V. harveyi*, four parallel quorum-sensing systems have been identified to regulate light production. A previous study by Henares et *al*. established that through H-NOX/HqsK pathway, NO contributes to light production in *V. harveyi* through the LuxU/LuxO/LuxR quorum sensing network. Proteomics analysis indicates that NO also

regulates flagellar production and biofilm in a concentration dependent manner. Together with biofilm quantification by Bernadette Henares [116], our data suggest that *V. harveyi* switches between lifestyles in response to NO, possibly through QS pathway.

In Chapter 3, we explore the molecular mechanism of NO regulation of biofilm formation. In *S. woodyi*, the gene encoded for H-NOX is in the same operon with a bi-functional DGC-PDE enzyme (*Sw*DGC) that metabolizes c-di-GMP. *S. woodyi* biofilms as well as intracellular c-di-GMP levels of wild type and Δ*hnox* were quantified in the absence and presence of low concentrations of NO (~nM). The results are consistent with each other and have shown that upon binding NO, *Sw*H-NOX represses c-di-GMP accumulation and biofilm formation. Moreover, disruption of *hnox* gene abolishes NO regulation, implying *Sw*H-NOX is an NO sensor. *Sw*DGC itself, *in vivo*, acts as a cyclase as Δ*hnox* exhibits a biofilm deficient phenotype. Together with characterization of purified proteins by listed authors [93], we conclude that NO-bound *Sw*H-NOX promotes c-di-GMP degradation by directly binding to *Sw*DGC, leading to a decrease of biofilm level.

In Chapter 4, we further extend the H-NOX/HqsK from *V. harveyi* to other organisms. Although in *S. woodyi* the effector enzyme downstream of H-NOX is a DGC, SMART (Simple Module Architecture Research Tool) analysis suggests gene, swoo_2833, annotated as a histidine kinase (*Sw*HK) might interact with *Sw*H-NOX. Since BLAST search of *Sw*HK return as a homologue of *Vh* HqsK, the H-NOX/HqsK QS pathway may also exist in *S. woodyi*, although the two proteins are not in the same operon. Preliminary data indicate a protein-protein interaction between *Sw*HK and *Sw*H-NOX. Genetic knockout mutants of Δ*hk*, Δ*hnox*/Δ*hk*, and Δ*dgc*/Δ*hk* of *S. woodyi* were made to compare biofilm phenotype with wildtype. Results show that *Sw*HK

activity is indeed affected by *Sw*H-NOX. Disrupting *Sw*HK decreased biofilm formation as well as the response to NO. Further disruption of H-NOX in the Δ*hk* mutant abolished NO regulation. Therefore, the role of *Sw*H-NOX regulation as an NO sensor may not be limited to c-di-GMP pathway only, but also include two-component signaling pathways.

Chapter 2 A nitric oxide-responsive quorum sensing circuit in *Vibrio harveyi* regulates flagella production and biofilm formation

Key to the Chapter

This project explores NO regulation of *V.harveyi* biofilm through H-NOX/HqsK quorum sensing circuit. The project was finished in collaboration with Bernadette Henares. The crystal violet quantification of biofilm level was done by her, and iTRAQ proteomics analysis was done by me. We did confocal microscopic imaging of biofilms together.

Abstract

Cell signaling plays an important role in the survival of bacterial colonies. They use small molecules to coordinate gene expression in a cell density dependent manner. This process, known as quorum sensing, helps bacteria regulate diverse functions such as bioluminescence, biofilm formation and virulence. In *Vibrio harveyi*, a bioluminescent marine bacterium, four parallel quorum-sensing systems have been identified to regulate light production. We have previously reported that nitric oxide (NO), through the H-NOX/HqsK quorum sensing pathway contributes to light production in *V. harveyi* through the LuxU/LuxO/LuxR quorum sensing pathway. In this study, we show that nitric oxide (NO) also regulates flagellar production and enhances biofilm formation. Our data suggest that *V. harveyi* is capable of switching between lifestyles to be able to adapt to changes in the environment.

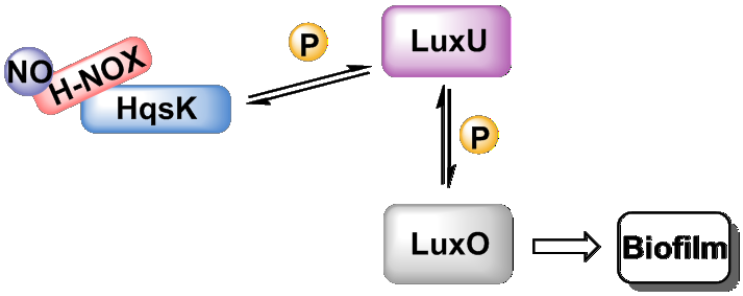

2.1 Introduction

Most bacteria are capable of switching between a free swimming, solitary, planktonic growth mode and sessile, biofilm living[117]. Biofilms are communities of surface-associated bacteria that form a complex, yet ordered, three-dimensional structure encapsulated in a self-secreted extracellular polysaccharide matrix (EPS). Members of a biofilm community have advantages such as access to nutrients, resistance to antimicrobial agents and protection against predators [118-120]. Biofilm formation is associated with quorum sensing (QS). Quorum sensing refers to the process by which bacteria coordinate social behaviors by secreting, detecting and responding to small molecules called autoinducers (AI) [50]. The sequential steps involved in biofilm formation require regulation of many genes across the bacterial community [117], thus, efficient communication is required. To achieve this remarkable feat, bacteria send out signals as soon as they enter the confines of the biofilm, since proximity to each other makes it more feasible for bacteria to communicate with one another and engage in the maintenance of the well-being of the community [50].

Vibrio harveyi is widely studied as a model bacterium for understanding quorum sensing. *V. harveyi* are well understood to regulate the gene expression of community behaviors such as bioluminescence and virulence gene production using QS circuits [52, 121, 122]. Furthermore, *V. harveyi,* are known to exist as free-swimming single cells, attached to abiotic surfaces as a biofilm, and in association with a host as a pathogen of marine animals [123]. Although it has been shown that *V. harveyi* can switch between these lifestyles, limited information is available about biofilm formation in *V. harveyi*, and there are even fewer studies that correlate QS and biofilm formation.

V. harveyi have (at least) four parallel quorum sensing sensor-kinases, each of which responds to detection of its cognate AI by a change in kinase activity [97]. Each of these kinases contributes to regulating the phosphorylation state of a common phosphorelay protein called LuxU [74, 97]. LuxU transfers phosphate to and from LuxO [76], a transcriptional regulator that controls the expression of LuxR, and ultimately, the quorum sensing response. We previously reported that one of the four known QS pathways responds to nitric oxide (NO) through the H-NOX/HqsK (heme-nitric oxide/oxygen binding domain; H-NOX-associated quorum sensing kinase) sensor/kinase pair [97]. We have shown that NO acts analogously with the other AIs and positively regulates light production.

Several studies have shown that LuxR and its homologues indirectly regulate biofilm formation through QS. Genetic studies done on *V. parahaemolyticus*, *V. vulnificus* and *V. fischeri* reveal that QS positively regulates biofilm formation [124, 125] through OpaR, SmcR, and LitR [126] (homologs of *V. harveyi* LuxR), respectively. An opposite regulation is observed in *V. cholerae* where vibrio polysaccharide (VPS, equivalent of EPS) gene expression is more abundant in the absence of HapR (LuxR homolog in *V. cholerae*), indicating a negative regulation of biofilm formation [127-129]. The ecological importance of this regulation in *V. cholerae* is still being investigated, but it has been suggested that being able to detach from the community is important in the transmission, colonization, and persistence of the next generation. Moreover, in a genetic study, LuxR, expressed as a function of AI concentration, is shown to negatively regulate the expression of *flagellar* operons in *V. harveyi* [3, 130]. A single polar flagellum provides bacteria an effective means of motility. In the initial stages of biofilm formation in *Vibrio*, attachment to a surface has been shown to involve the loss of flagellar genes [131]. Thus a loss of the flagellum is predicted to upregulate biofilm formation.

Interestingly, NO is well known to be involved in biofilm formation. Indeed, in many bacterial species such as *Shewanella woodyi* [132], *Shewanella oneidensis* [133], and *Legionella pneumophila* [115], NO is detected by H-NOX, which goes onto regulate biofilm formation through a pathway involving cyclic-di-GMP metabolism. Cyclic-di-GMP is a second messenger widely used by bacteria to regulate biofilm formation and EPS production [134, 135]. In these systems, NO is sensed by H-NOX and ultimately regulates the activities of a diguanylate cyclase and/or phosphodiesterase, either directly [115, 132], or indirectly through a histidine kinase [133], to control the intracellular concentration of cyclic-di-GMP.

In *Pseudomonas aeruginosa,* NO causes QS-mediated biofilm dispersal [103]. Thus we hypothesized that NO/H-NOX might contribute to regulation of biofilm formation through QS in *V. harveyi.* Here, using genetic, biofilm, and proteomic data, we demonstrate that NO/H-NOX regulates biofilm formation and flagellar formation in *V. harveyi.*

2.2 Materials and Methods

Bacterial strains and growth conditions. Strains used in this study are listed in Table 2-1. *V. harveyi* strains wild-type (WT), Δ*luxO*, and Δ*luxNS* were purchased from the American Type Culture Collection (ATCC). *V. harveyi* mutants Δ*hnoX* and *phnoX*/Δ*hnoX* are lab strains constructed as previously described [97]. Cell cultures were maintained in marine media (MM; 28 g/L; BD Difco) and grown at 30 °C with agitation at 250 rpm.

Table 2-1. Bacterial strains used in this work.

Bacterial strains	Relevant characteristics	Ref.
V. harveyi		
WT	BB120, *V. harveyi* WT, ATCC BAA-1116	ATCC
Δ*luxO*	BB721, *luxO*:Tn5 ATCC 700106	ATCC [136]
Δ*luxNS*	MM30, luxN::Cm, luxS::Tn5Kan, ATCC BAA-1120	ATCC [137]
Δ*hnoX*	BB120 ΔVIBHAR_01911	[97]
p*hnoX*/Δ*hnoX*	Δ*hnoX,* p*hnoX*, Km^r	[97]

Biofilm imaging by confocal microscopy. Microscopy images were recorded on a Zeiss LSM 510 Metanlo Two-Photon Laser Scanning Confocal Microscope System. An overnight culture of *V. harveyi* in marine media was diluted (1:1000) into fresh medium in a sterile 50 mL conical centrifuge tube containing a glass microscope slide. The medium also contained various concentrations of DPTA NONOate that had been predecayed for 3 hours at 30 °C, resulting in 0, 50, 100, and 200 nM NO in solution, as measured by a Sievers nitric oxide analyzer (NOA 280i, GE analytical instruments). Biofilms were grown under static conditions at 30 °C with slow agitation at 50 rpm for 12 h. Following the growth period, the slide was thoroughly rinsed with distilled water and the adhered biofilm cells were stained for imaging. Samples were stained with the 1% calcoflour white for 15 min to stain and image EPS. Cells for confocal microscopy were stained with LIVE/DEAD BacLight kit (Invitrogen) according to the manufacturer's protocol, for 15 min. The biofilm formed at the air−liquid interface was then imaged and analyzed. The air−liquid interface was ∼3 mm wide (in the X dimension, along the longest side of the microscope slide), as determined from crystal violet staining of identically obtained biofilms on

microscope slides. The biofilm thickness (X−Z dimension, i.e., the height of the biofilm measured from the surface of the microscope slide to the top of the biofilm) was measured at three different locations in each experiment and averaged to determine the mean biofilm thickness. The locations were chosen randomly, but generally one spot near the middle of the slide and one from each edge of the slide (in the Y dimension) were chosen. Multiple locations were measured because bacterial biofilms are often not of uniform thickness. These measurements may not account for all the variation in biofilm thickness, but they provide an estimate of biofilm thickness for comparison between different NO concentrations. Confocal images for each of three completely independently grown biofilms exposed to each NO concentration were separately grown and analyzed. The mean thickness from each trial was determined from measurements at multiple locations. The mean thickness from three independent trials ± one standard deviation is reported.

Crystal violet staining for biofilm quantification. Steady-state biofilm formation, at the air−liquid interface, in a shaking culture was examined in 96-well polyvinyl chloride (PVC) plates as previously described [132], with a few modifications. A 100 μL subculture (1:100 dilution of an overnight culture of *V. harveyi*) in marine media was incubated at 30 °C for 12 h with slow agitation (50 rpm). Some cultures included the addition of 50 nM NO (from NONOate) or cell-free medium from an overnight culture (contains a high concentration of AIs). The planktonic cells and media were then removed, and the remaining biofilm was rigorously washed with water followed by staining with 150 μL of 0.1% crystal violet (CV) in water for 15 min. Next the CV solution was removed, and the wells were rinsed three times with distilled water and allowed to thoroughly dry. Then 100 μL of DMSO was added to each well to solubilize the CV adsorbed by the biofilm cells. The DMSO/CV solution was removed from the

PVC plate and added to a polystyrene 96-well plate, and the optical density at 570 nm was measured with a Perkin-Elmer Victor X5 multilabel reader. The data are reported as the CV absorbance at 570 nm divided by the optical density of the planktonic and biofilm cells at 600 nm. Each biofilm condition was run a minimum of 10 times in one experiment, and the entire experiment was independently performed a minimum of three times. The mean measurement ± one standard deviation from 3 independent experiments is reported.

iTRAQ^{TM} analysis of *V. harveyi.* An overnight *V. harveyi* culture was inoculated (1:100 dilution) into autoinducer bioassay media [AB; 0.2% vitamin-free casamino acids, 0.3 M NaCl, 0.05 M $MgSO_4$, 10 mM potassium phosphate pH 7.0, 1 mM L-arginine, 1% (v/v) glycerol] [53] supplemented with DPTA NONOate that had been predecayed for 3 hours at 30 °C, resulting in 0, 50, 100, and 200 nM NO in solution, as measured by a Sievers nitric oxide analyzer (NOA 280i, GE analytical instruments). After 10 hours, the culture was harvested by centrifugation at 5000 rpm at 4 °C (Beckman Coulter, USA) and re-suspended in 300 µL Milli-Q water followed by repeated freeze- thaw cycles in liquid nitrogen. Cell lysates were treated by acetone precipitation and protein samples were re-suspended in dissolution buffer using the iTRAQ^{TM} kit (Applied Biosystems, USA). Protein mixtures were reduced and alkylated according to manufacturer's protocol. The total protein concentrations were then quantified using bicinchoninic acid (BCA) assay kit (Pierce). For each sample, 100 µg of total protein was digested with trypsin (Roche) at 37 °C overnight and labeled with iTRAQ^{TM} reagents. Then samples with different labels (corresponding to samples grown in different NO concentrations) were mixed together. Protein samples were analyzed on a Thermo Fisher Scientific LTQ Orbitrap XL ETD by the proteomics core facility center at Stony Brook University.

2.3 Results and Discussion

We have shown in our previous work that NO enhances light production at the initial stage of bioluminescence through LuxR and the QS pathway [97]. However, the *lux* operon is not the only set of genes regulated by QS [49]. Thus we hypothesize that other than light production, NO may also regulate biofilm formation by entering the QS pathway through the H-NOX/HqsK circuit. Our hypothesis is based on several literature observations. First, NO is well understood to be involved in biofilm formation in a wide range of bacteria [115, 132, 133], and in *P. aeruginosa*, NO has been reported to affect biofilm formation through QS processes [102, 103]. Furthermore, several lines of evidence in several strains of *Vibrio* have demonstrated that LuxR and QS indirectly regulate biofilm formation and expression of the flagella operon [131]. Thus, we expect QS to upregulate biofilm formation in the presence of NO.

To test this hypothesis, we investigated the effect of NO on biofilm formation by *V. harveyi* wild-type strain BB120. Using concentrations of NO that have no effect on a planktonic growth curve (Figure 2-1), biofilm architecture, biofilm thickness, and cell viability were determined using confocal laser scanning microscope (CLSM). The cells were allowed to grow on microscope slides for 12 hours at 30 °C. Biofilms that formed at the air-liquid interface were visualized by staining with SYTO 9 (green; stains live cells) and propidium iodide (red; stains dead cells only) for observation under confocal microscope while EPS production was viewed using calcoflour white under the phase-contrast method. Under the conditions in which the biofilms were obtained, most cells were viable and *V. harveyi* were able to form EPS and thick, biofilms under aerobic conditions (Figure 2-2A). Individual cells are difficult to see due to other substances present in the EPS matrix (DNA, protein). Cells exposed to 50 nM NO showed a remarkably thick biofilm in comparison to the culture grown without added NO (Figure 2-2B

and C). On the other hand, biofilm formation goes back to the without NO thickness at NO concentrations exceeding 100 nM. This observation was corroborated when we quantified biofilm formation of *V. harveyi* grown in 96-well plates using the crystal violet staining method [3]. As illustrated in Figure 2-3, a similar trend was observed; at 50 nM NO we observed more biofilm formation than in the absence of NO, while at higher NO concentrations, biofilm levels decreased.

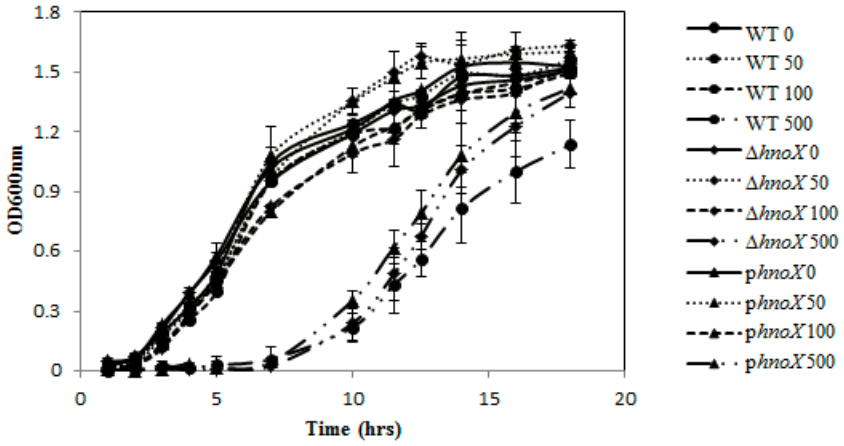

Figure 2-1. *V. harveyi* growth curves of wild-type, Δ*hnoX*, and Δ*hnoX*/p*hnoX* in the presence of NO (50 nM NO, 100 nM NO, 500 nM NO) at 30 ° C in AB medium. These data indicate that there is no significant delay in growth with less than 500 nM NO.

A.

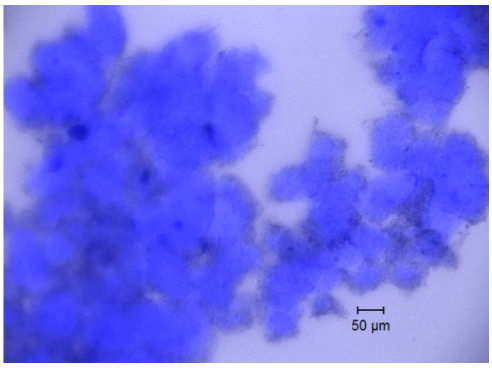

C.

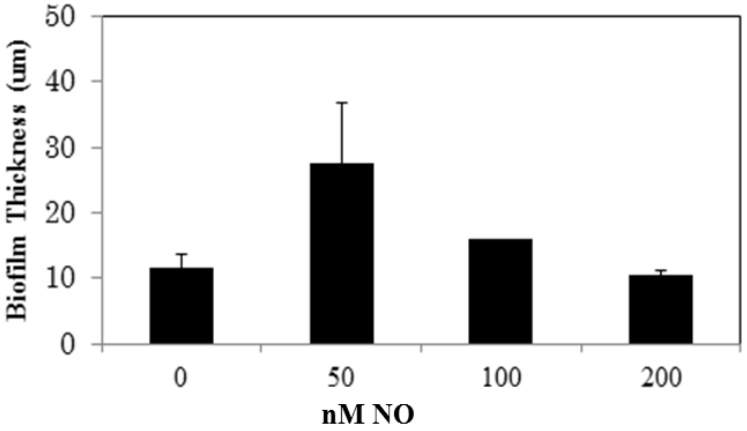

B.

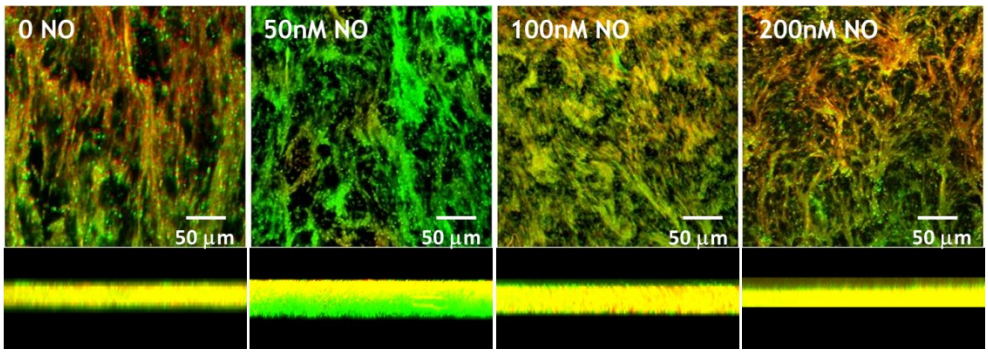

Figure 2-2. Effect of NO on biofilm thickness and cell viability quantified by CLSM. (A) Phase-contrast image of a biofilm at 10x magnification stained with calcofluor to show EPS production. This biofilm was grown without the addition of NO. (B) Confocal images of biofilm at 40x magnification, grown in the presence of the indicated amount of NO. Cells were stained with SYTO 9 (green; stains all cells) and propidium iodide (red; stains dead cells only). Top pictures are the x-y view, bottom pictures show the y-dimension as viewed on the side. (C) Summary of biofilm thickness as a function of NO concentration.

It is not clear why there is a concentration-dependent switch in biofilm regulation in response to NO, although this NO phenotype has been previously observed in *Nitrosomonas europea*, where biofilm formation is induced at 30 ppm while a NO concentration below 5 ppm promotes dispersal [138]. It is possible that at higher NO concentrations, NO is detected by a less sensitive NO sensor that regulates an alternate biofilm response. It is also possible that NO, through H-NOX, induces dispersal of biofilm through a different (not QS) pathway. For example, like many histidine kinases, HqsK could transfer phosphate to more than one response regulator, thus feeding into several pathways.

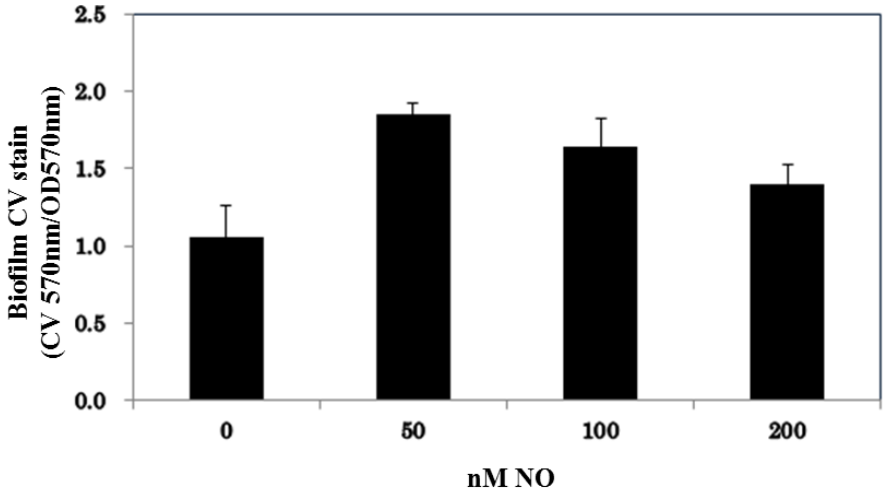

Figure 2-3. Effect of NO on biofilm formation in *V. harveyi* WT strain quantified using the crystal violet staining method. Normalized CV is reported as the CV absorbance at 570 nm divided by OD of all cells, planktonic and biofilm, at 570nm. Error bars represent one standard deviation from the mean of triplicate experiments.

These data demonstrate that NO enhances biofilm formation in *V. harveyi* at low concentration, consistent with our hypothesis that biofilm is positively regulated by NO/H-NOX, possibly through QS. Next we investigated the effect of NO on biofilm formation of WT and several QS

mutants. As shown in Figure 2-4, biofilm formation is enhanced in WT cultures grown in the presence of 50 nM NO, which is consistent with our CLSM and CV assays discussed above. As expected, deletion of the *hnoX* gene results in decreased biofilm and does not elicit the same biofilm enhancement in the presence of NO, indicating that H-NOX positively regulates biofilm formation. Furthermore, complementation of the Δ*hnoX* mutant strain with H-NOX expressed on a plasmid (the Δ*hnoX*/*phnoX* strain) rescues the NO-induced increase in biofilm phenotype. These data confirm that H-NOX is the NO sensor responsible for the increase in biofilm in the presence of NO. Interestingly, the addition of cell-free medium from an overnight culture, which contains a high concentration of all the autoinducers that trigger QS pathways in *V. harveyi* (+ AI), does not result in as large an increase in biofilm as NO, suggesting that NO/H-NOX is the primary QS circuit affecting biofilm formation.

The mutant strain Δ*luxO*, which is used as positive control for QS, showed a much higher biofilm than WT, verifying that QS and LuxR positively regulate biofilm formation. This strain contains a Δ*luxO* mutation which renders the production of LuxR independent of AI concentration, thus this strain is constitutively bright and locked at the high cell density state. The addition of NO and excess AI do appear to further increase biofilm formation, these increases in CV staining could be due to other response regulators that are regulated by HqSK but not through LuxU/LuxO/LuxR quorum sensing circuit. It is also possible that there is an alternative NO-mediated pathway that affects biofilm formation, as discussed above. However, because there is no effect on NO in the Δ*hnoX* mutant, we do not believe this is the most likely explanation. Taken together, these results are supportive of NO-mediated regulation of biofilm formation through QS via the H-NOX/HqsK system. In our previous studies we demonstrated

that H-NOX responds to NO by regulating the flow of phosphate into the QS circuitry through the H-NOX-associated quorum sensing kinase (HqsK).

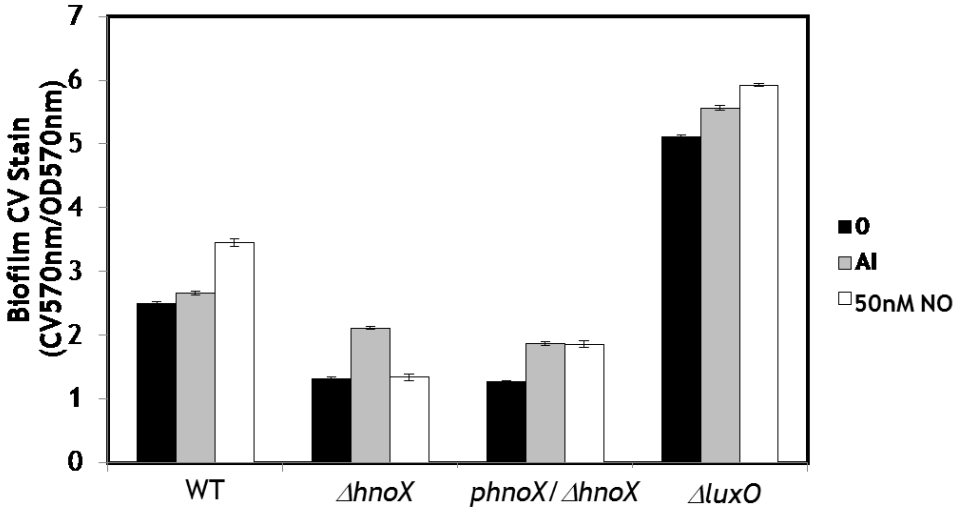

Figure 2-4. Effect of NO on biofilm formation in *V. harveyi* WT, Δ*hnoX*, p*hnoX*/Δ*hnoX*, and Δ*luxO* strains. Normalized CV is reported as the CV absorbance at 570 nm divided by OD of all cells, planktonic and biofilm, at 570nm. The black bars indicate no additives, the grey bars indicate the addition of cell-free medium from an overnight culture, which is rich in AIs, and the white bars indicate the addition of 50 nM NO. Error bars represent one standard deviation from the mean of triplicate experiments.

To support our biofilm analysis, we performed an iTRAQ proteomics analysis on *V. harveyi* exposed to varying concentrations of NO. In our analysis, we identified a total of 529 proteins from ~4800 predicted proteins in the *V. harveyi* genome. Of the 529 proteins, 493 were identified by two or more significant peptides. Protein mixtures obtained under 0, 50, 100, 200nM NO growth condition were labeled with isobaric tags that produce signature ions at m/z 114, 115, 116 and 117 respectively. The effect of NO on the proteome was determined based on the ratio of an isobaric tag ion peak at a given NO concentration over that same tag peak area in the

absence of NO (Appendix 2). We selected proteins whose expression ratios fell outside of 1.000 ± 0.2 as being significantly affected by NO.

A number of proteins displayed a NO concentration-dependent trend. In Figure 2-5, these peptides are indicated in the overlapping areas of the Venn diagram. Among the downregulated proteins (Figure 2-5A), 65.9% of 116/114 (100 nM/ 0 nM NO) also showed up in 117/114 (200 nM/ 0 nM NO), while 52.7% overlapped with 115/114 (50 nM/ 0 nM NO). 57.8% and 54.3% of upreglated proteins (Figure 2-5B) overlapped with 115/114 and 117/114, respectively. Some protein levels were strongly decreased at 50 nM NO, but were restored as NO concentration was increased. Therefore, the pattern of proteome at 50 nM is slightly different from 100 nM and 200 nM. A higher similarity between 100 nM/0 nM NO and 200 nM/0 nM NO might be an indication of a NO concentration dependent switch of bacterial protein expression. Interestingly this is the same NO-dependent pattern we observed for biofilm formation, indicating there is possibly a global switch that takes place in protein expression as NO is increased from 50 to 100 nM.

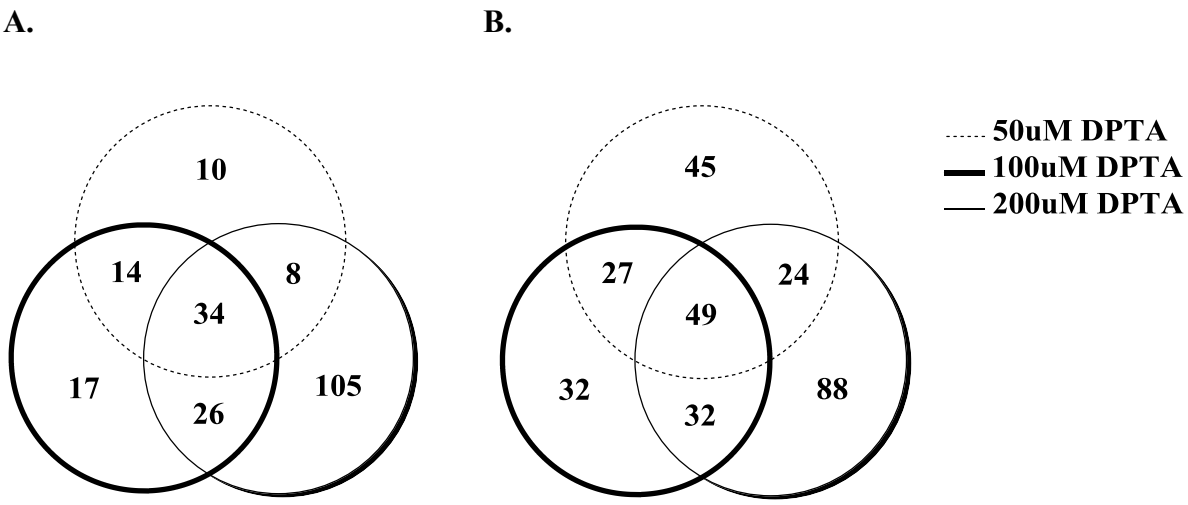

Figure 2-5. Summary of *V. harveyi* iTRAQ analysis. Proteins that were down-regulated (A) or upregulated (B) by at least 20% were selected and compared under different NO concentrations. Numbers in the common areas indicate proteins that show the same trend as a function of NO concentration. Remaining numbers represent proteins that are up- or down-regulated only under one condition.

Here we highlight and further analyze several proteins that are known to be involved in biofilm formation (Table 2-2). All five *V. harveyi* flagellin proteins display the same NO-concentration dependent trend. They show a significant decrease at 50 nM NO and are restored to the same levels as without NO as the NO concentration is increased. A functional flagella has been proven to be critical in initial attachment [139-141] of Gram-negative bacteria and early exopolysaccharide synthesis. Furthermore, CheY protein expression is unchanged at 50 nM NO, but is repressed upon exposure to higher NO concentration. CheY can bind to FilM at the base of flagellar motor and modify flagellar behavior [142]. It is reported in *E.coli* that an overexpression of CheY can enable clockwise rotation [143-145] and reduce bacteria motility.

Although the experiments were carried out with agitation and no biofilm was observed, when taken together, these results imply an upregulation in biofilm due to a decrease in motility and enhanced surface attachment at low NO concentration, followed by a return to normal motility as NO continues to increase. Interestingly, this is exactly the same trend that we observed in our biofilm analysis: an increase in biofilm at low NO concentration followed by a decrease as NO concentration is increased. In the presence of NO, flagellin and CheY might synergistically contribute to bacterial initial attachment. A microarray study in *Vibrio fischeri* has shown that several flagellins and flagellar basal-body proteins are negatively regulated by quorum sensing system [146]. Based on our results, we suggest that in *V. harveyi*, NO regulates flagella production through QS.

Table 2-2. Selected biofilm-associated proteins as a function of NO.

Gene ID	Protein ID	50 nM NO fold change[a]	100 nM NO fold change[a]	200 nM NO fold change[a]	Annotation
Vibhar_01300	A7MT73	0.364	0.625	0.813	Flagellin
Vibhar_01301	A7MT74	0.421	0.637	1.012	Flagellin
Vibhar_03171	A7MS06	0.443	0.673	0.955	Flagellin
Vibhar_03173	A7MS08	0.425	0.705	1.000	Flagellin
Vibhar_03174	A7MS09	0.553	0.856	0.925	Flagellin
Vibhar_03143	A7MS30	1.052	0.953	0.455	CheY

[a]Determined by the peptide abundance after growth in the presence of NO divided by the abundance of the same peptide after growth in the presence of 0 nM NO.

2.4 Conclusion

In the natural environment, bacteria are often part of a multicultural community. They spend most of their time in social communes where they are covered with an EPS matrix that confers protection against environmental stress. Biofilm regulation is not well understood, although

cyclic-di-GMP signaling and QS are known to play a role [42, 147] . A global regulatory mechanism is needed to achieve biofilm formation because it involves the concomitant expression and repression of tens or even hundreds of unlinked genes in a cell-density dependent manner [148]. It appears that QS reciprocally influences cyclic-di-GMP signaling pathways, together providing an integrated network for assimilating numerous external stimuli into a community-wide response [149, 150].

Our data suggest that, at low concentration, NO acts as a stimulus to promote *V. harveyi* biofilm formation. In several bacteria, NO/H-NOX regulates cyclic-di-GMP synthesis and/or hydrolysis to contribute to EPS production and biofilm regulation [115, 132, 133]. Here, we report QS-mediated biofilm formation through regulation of flagellar proteins via the H-NOX/HqsK pathway. It is interesting that all NO/H-NOX pathways characterized to date are involved in biofilm regulation, although the details of the signaling pathway appear to vary from organism to organism. These results serve as a starting point to study in detail the mechanism involved in formation of biofilms through QS. Biofilms involve community-wide changes in gene expression, and thus QS plays a critical role that is still being uncovered.

Chapter 3 NO Regulation of C-di-GMP Metabolism and Biofilm Formation

Key to the Chapter

This project explores NO regulation of *S. woodyi* biofilm through H-NOX/DGC c-di-GMP signaling pathway. It was in collaboration with listed authors in publication 1 [93]. My contribution to the work was generation of knockout and complementary mutant strains (received knockout donor plasmid from Gralnick Group) and all the phenotype analysis (growth rate of bacterial strains with NO donor, CLSM image of *S. woodyi* biofilm, crystal violet quantification and intracellular c-di-GMP concentration measurement of mutant strains).

Abstract

Although several reports have documented nitric oxide (NO) regulation of biofilm formation, the molecular basis of this phenomenon is unknown. In many bacteria, a H-NOX (heme-nitric oxide/oxygen binding) gene is found near a di-guanylate cyclase (DGC) gene. H-NOX domains are conserved hemoproteins that are known NO sensors. It is widely recognized that cyclic-di-GMP is a ubiquitous bacterial signaling molecule that regulates the transition between motility and biofilm. Therefore, NO may influence biofilm formation through H-NOX regulation of DGC, thus providing a molecular-level explanation for NO regulation of biofilm formation. This work demonstrates that, indeed, NO/H-NOX negatively affects biofilm formation by directly regulating c-di-GMP turnover in *Shewanella woodyi* strain MS32. Exposure of wild-type *S. woodyi* to nanomolar NO resulted in the formation of thinner biofilms, and less intracellular c-di-GMP, than in the absence of NO. Also, a mutant strain in the gene coding for *Sw*H-NOX showed decreased biofilm formation (and decreased intracellular c-di-GMP) with no change observed upon NO addition. Furthermore, using purified proteins, it was demonstrated that *Sw*H-NOX and *Sw*DGC are binding partners. *Sw*DGC is a dual-functioning DGC; it has di-guanylate cyclase and

phosphodiesterase activities. These data indicate that NO-bound *Sw*H-NOX enhances c-di-GMP degradation, but not synthesis, by *Sw*DGC. These results support the biofilm growth data and indicate that *S. woodyi* senses nanomolar NO with a H-NOX domain and that *Sw*H-NOX regulates *Sw*DGC activity, resulting in a reduction in c-di-GMP concentration and decreased biofilm growth in the presence of NO. These data provide a detailed molecular mechanism for NO regulation of c-di-GMP signaling and biofilm formation.

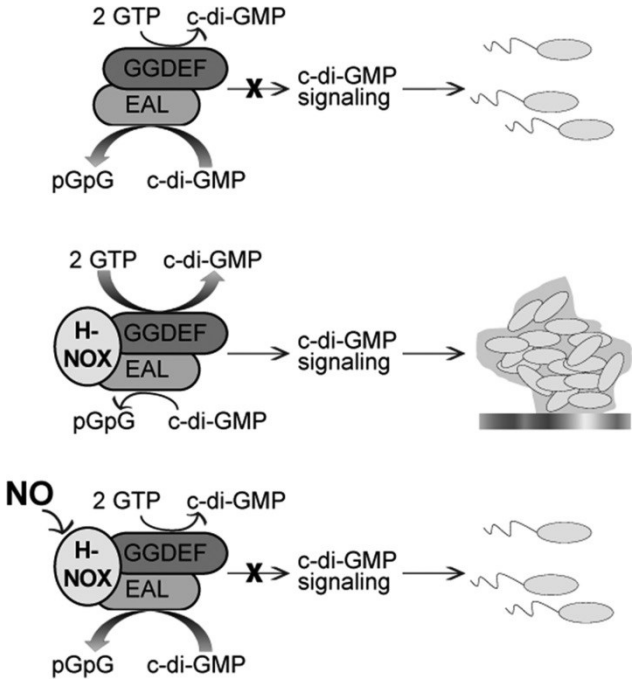

3.1 Introduction

Most bacteria can switch between sessile and planktonic growth to adapt to varying environmental conditions. Biofilms, sessile, surface-attached bacterial communities, are widespread, persistent, and highly resistant to antibiotics [151]. Effective new strategies for controlling biofilms are needed, but the biochemical pathways underlying their regulation must first be elucidated.

Nitric oxide, a well-known signaling molecule in mammals [89], has been shown to regulate bacterial biofilms at physiological concentrations. For example, in *Nitrosomonas europaea*, NO levels above 30 ppb result in biofilm formation and below 5 ppb in biofilm dispersal [102]. NO also plays an important signaling role in biofilm dispersal in the cystic fibrosis-associated pathogen *Pseudomonas aeruginosa* [103]. The dispersal of *P. aeruginosa* biofilms was observed upon treatment with the NO donor sodium nitroprusside at 25 nM, a sub-lethal concentration. Taking advantage of the observation that NO can disperse biofilms, several methods have been developed to treat biofilms using NO-releasing materials [152-154]. Despite these observations, the NO signaling pathway that regulates biofilm formation is not known.

Biofilm formation is a complex processes with fundamental regulatory mechanisms still widely debated [155]. Nonetheless, it is clear that bis-(3'-5')-cyclic dimeric guanosine monophosphate (cyclic-di-GMP; c-di-GMP) is a secondary messenger widely used by bacteria to regulate biofilm formation [135, 156, 157]. As the intracellular concentration of c-di-GMP goes up, bacteria enter biofilm or persistence growth modes [158]. The intracellular concentration of c-di-GMP is controlled through two enzymatic activities. Di-guanylate cyclases synthesize c-di-GMP from two molecules of GTP and phosphodiesterases hydrolyze c-di-GMP to pGpG. Di-guanylate

cyclase activity is predicted by a conserved GG(D/E)EF amino acid motif [159]; similarly, EAL [158] or HD-GYP [19] amino acid motifs are conserved in phosphodiesterases for the degradation of c-di-GMP. Thus, in bacteria, GG(D/E)EF and EAL or HD-GYP domains inversely regulate c-di-GMP levels [160].

Invariably, there are input sensory domains associated with GG(D/E)F and EAL/HD-GYP domains, suggesting that c-di-GMP concentrations are controlled by signal transduction from a variety of environmental stimuli [161]. Stimuli known to regulate c-di-GMP formation and hydrolysis include blue light [162], intercellular molecules [163], and oxygen [22]. Interestingly, the Kjelleberg group has shown that NO mediates phosphodiesterase activity to enhance biofilm dispersal in *P. aeruginosa* [105]; the NO sensor and NO-sensitive phosphodiesterase have not been identified, however.

H-NOX (heme-nitric oxide/oxygen-binding) domains are a family of hemoprotein sensors that include the heme domain of soluble guanylate cyclase (sGC), the well-studied mammalian NO sensor [164]. Like sGC, bacterial H-NOX proteins bind NO sensitively and selectively [111, 113, 165, 166]. Bioinformatics studies have revealed that several common effectors may be associated with H-NOX, including methyl-accepting chemotaxis proteins, histidine kinases, and di-guanylate cyclases [112]. Biochemical studies have indicated that NO/H-NOX is capable of regulating the enzymatic activity of associated effectors in several species [114, 115, 167]. For example, an H-NOX in *Legionella pneumophila* has been found to inhibit biofilm formation, likely through regulation of an associated di-guanylate cyclase [115]. Direct evidence for H-NOX and di-guanylate cyclase interaction and the mechanism of NO regulation of cyclase activity has not been demonstrated, however.

We have previously shown that *Swoo_2750* (*Sw*DGC) from *Shewanella woodyi* strain MS32 (*Sw*MS32; crosslisted as strain ATCC 51908), has both c-di-GMP synthesis and hydrolysis activities, as predicted from the presence of a GGDEF and an EAL domain in its primary structure [168]. Here we demonstrate that NO regulates biofilm formation in *S. woodyi* through changes in c-di-GMP concentration and that *Sw*H-NOX (*Swoo_2751*) and *Sw*DGC are responsible for this NO biofilm phenotype. Furthermore, these results indicate that *Sw*H-NOX and *Sw*DGC directly interact and that NO-bound H-NOX regulates the enzymatic activity of *Sw*DGC. The data presented here, reveal for the first time, a molecular mechanism detailing NO regulation of c-di-GMP metabolism and biofilm formation.

3.2 Materials and Methods

Bacterial strains and growth conditions. Strains used in this study are listed in Table 3-1. *E. coli* strains DH5α, BL21(DE3)pLysS, Tuner(DE3)pLysS, and Rossetta2(DE3) were used throughout this study for plasmid amplification and protein purification. *E. coli* were typically grown in Luria Broth (LB; 20 g/L; EMD chemicals) at 37 °C with agitation at 250 rpm. *E. coli* strain WM3064 was used as a donor for conjugation and was grown in LB complemented with 2,3-Diaminopropionic acid (DAP; 0.36 mM; Sigma Aldrich) at 37 °C with agitation at 250 rpm (VWR™ International). *Sw*MS32 was grown in Marine Media Broth (MM; 28 g/L; BD Difco) at 25 °C with agitation at 250 rpm. *Sw* transconjugants were grown on LB (10 g/L) / MM (14 g/L) / Bacto Agar (BA; 10 g/L; BD Difco) plates at 25 °C.

Table 3-1. Strains, plasmids and primers used in this chapter.

Strains and plasmids	Relevant characteristics	Ref.
Bacterial strains		
S. woodyi		
*Sw*MS32 (WT)	*Shewanella woodyi* MS32, ATCC 51908	(36)
Δ*hnox*	*Sw*MS32 Δ*Swoo_2751*	This work
Δ*hnox/*p*hnox*	*Sw*MS32 Δ*hnox* p*hnox*, Km^r	This work
E. coli		
WM3064	Mating strain	(25)
BL21(DE3) pLysS	Expression strain	
Plasmids		
pSMV3	Deletion vector, Km^r, *sacB*	(25)
pBBR1MCS-2	Broad range cloning vector, Km^r	(27)
pΔ*hnox*	pSMV3 with1kbp upstream and downstream of *hnox*	This work
p*hnox*	pBBR1MCS-2 with *hnox* and 32bp upstream of *hnox*	This work
Primers		
Gene deletion primers		
*Sw*2751-up-fw	*NNNGGATCCCACATAGTTTGGACACCTAAG	
*Sw*2751-up-rev	*NNNGAATTCAACATTAGCCCCTGTTTTAA	
*Sw*2751-down-fw	*NNNGAATTCTTATGAGTGCACTTGAGGACA	
*Sw*2751-down-rev	*NNNNNNNNNGCGGCCGCCACAATAGAGAACTCATCTC	
Confirmation primers		
hnox-up-fw	GGATCTGCTCCGCTTGC	
hnox-down-rev	GGTTACTTTGTTGACACAGTGG	
Complementation primers		
hnox-comp 1	CAACGAATTCGAGTACTTATTAAAAC	
hnox-comp 2	CAAACTCGAGACGTCGTGTAATATTA	
RT-PCR primers		
hnox-f	TTACCTGTGATCGTTTAGGCG	
hnox-r	AATAACGTCGGTCTCGGAATC	
dgc-f	TGAAGCCTTGATCCGTTGG	
dgc-r	GTGATAGGAAGTGCGATGGAG	

* Ns represent random nucleobases that are designed to protect restriction sites.

Construction of in-frame gene disruption mutant strains. PCR was used to amplify regions of genomic DNA flanking the H-NOX gene (Swoo_2751) from *Shewanella woodyi* strain MS32 genomic DNA (ATCC strain 51908) using Phusion® polymerase (New England Biolabs). The upstream genomic DNA was amplified with forward and reverse primers (Sw2751-up-fw,

Sw2751-up-rev) containing NotI and EcoRI restriction sites, respectively. The downstream genomic DNA was amplified with forward and reverse primers (Sw2751-down-fw, Sw2751-down-rev, Table 3-1) containing EcoRI and BamHI restriction sites, respectively. The up- and downstream fragments were fused by ligation at the common EcoRI restriction site. This fused product was cloned into pSMV3 [169] using the NotI and BamHI restriction sites and sequenced (Stony Brook DNA sequencing facility). The resulting vector (pΔhnox, Table 3-1) was transformed into the plasmid donor strain *E. coli* WM3064 and grown on LB/DAP/BA plates with kanamycin added to a concentration of 10 μg/ml. WM3064 transformed with the deletion vector was mated with *Sw*MS32 in a 1:3 ratio on LB/MM/DAP agar for 2 days at 25 °C. The *S. woodyi* transconjugants containing the deletion vector were selected on LB/MM/BA plates supplemented with 60 μg/mL kanamycin and verified by colony PCR (hnox-up-fw, and hnox-down-rev, Table 3-1). The selected colonies were then plated on LB/MM/BA plates containing 5% sucrose at 25 °C in order to select for double recombination events. Plates were then replica printed onto LB/MM/BA plates with and without added kanamycin (60 μg/mL) at 25 °C; kanamycin sensitive colonies were screened by colony PCR for gene deletion using primers hnox-up-fw, and hnox-down-rev (Table 3-1).

Construction of gene disruption mutant complementation plasmids. PCR was used to amplify Swoo_2751 from *Shewanella woodyi* genomic DNA (ATCC) using *Pfu* Turbo polymerase (Agilent). Upstream and downstream primers contained BamHI and EcoRI restriction sites, respectively, as well as 26 base pairs of upstream target gene sequence so that all ribosome binding sites would be identical (hnox-comp 1, and hnox-comp 2, Table 3-1). The amplified PCR products were cloned into the broad host range plasmid pBBR1MCS-2 [170] and

sequenced (Stony Brook DNA sequencing facility). The resulting p*hnox* plasmid (Table 3-1) was introduced into the gene disrupted strains via conjugation as previously described [169].

Biofilm imaging by confocal microscopy. Microscopy images were obtained on a Zeiss LSM 510 Metanlo Two-Photon Laser Scanning Confocal Microscope System. 15 mL of a 1:1000 dilution of an overnight culture of *S. woodyi* in MM was added to a sterile 50 mL conical centrifuge tube containing a glass microscope slide. Biofilms were grown under steady-state conditions at 25 °C with slow agitation at 50 rpm for 24 hours. Following the growth period, the slide was thoroughly rinsed with distilled water and the adhered biofilm cells were stained with the LIVE/DEAD BacLightTM kit (InvitrogenTM), according to the manufacturer's protocol, for 15 minutes. The biofilm formed at the air-liquid interface was then imaged and analyzed. The air-liquid interface was ~3 mm wide (in the X dimension, along the longest side of the microscope slide), as determined from crystal violet staining of identically obtained biofilms on microscope slides. The biofilm thickness (XZ dimension, i.e., the height of the biofilm measured from the surface of the microscope slide to the top of the biofilm) was measured at 3 different locations in each experiment and averaged to determine the mean biofilm thickness. The locations were chosen randomly, but generally one spot near the middle of the slide and one from each edge of the slide (in the Y dimension) were chosen. Multiple locations were measured because bacterial biofilms are often not of uniform thickness. These measurements may not account for all the variation in biofilm thickness, but they provide an estimate of biofilm thickness for comparison between wild-type and Δhnox mutant *S. woodyi* strains. Biofilm mass was quantified using crystal violet staining (see below). Confocal images for each of three independently grown biofilms of each strain (wild-type and Δhnox mutant *S. woodyi*) were separately obtained and analyzed. The mean thickness from each trial was determined from

measurements at multiple locations. The mean thickness from three independent trials ± 1 standard deviation is reported.

Crystal violet (CV) staining for biofilm quantification. Steady-state biofilm formation, at the air-liquid interface, in shaking culture was examined in 96-well polyvinyl chloride (PVC) plates as has been previously described [140], with a few modifications. A 100 µL subculture (1:100 dilution of an overnight culture of *S. woodyi*) in MM was incubated at 25 °C for 24 hours with slow agitation (50 rpm). The planktonic cells and media were then removed and the remaining biofilm was rigorously washed with water followed by staining with 200 µL of 0.1% CV in water for 15 minutes. Next the CV solution was removed and the wells were rinsed 3 times with distilled water and allowed to thoroughly dry. Then 100 µL of DMSO was added to each well to solubilize the CV adsorbed by the biofilm cells. The DMSO/CV solution was removed from the PVC plate and added to a polystyrene 96-well plate and the OD_{570} was measured by a Perkin Elmer Victor^{TM} X5 multilabel reader. The data are reported as the CV absorbance at 570 nm divided by the optical density of the planktonic and biofilm cells at 600 nm. For biofilms grown in the presence of NO, the 100-fold diluted overnight culture was diluted into MM supplemented with 200 µM diethylenetriamine NONOate (DETA/NO; Cayman Chemicals; DETA/NO $t_{1/2}$ = 20 hours and 56 hours at 37 °C and 22-25 °C, respectively) that had been decaying for 20 hours at 37 °C (~1 half-life; it was cooled to 25 ºC before inoculation). NONOates are NO donating compounds that are stable as solids, but spontaneously release NO in a pH-dependent manner in solution. Using a Nitric Oxide Analyzer 280i (Sievers) it was determined that this resulted in a solution NO concentration of less than 100 nM (slowly decreased from ~80 nM to ~60 nM) during the length of NO exposure. From there the protocol was identical. Each biofilm condition

was run a minimum of ten times in one experiment and the entire experiment was performed a minimum of three times. The mean ± 1 standard deviation is reported.

Quantification of c-di-GMP. Intracellular c-di-GMP concentrations were quantified as has been described [171], with slight modifications. Briefly, a single *S. woodyi* wild-type or mutant colony from a MM/BA plate was grown to an optical density of 1.5 at 600 nm at 25 °C with agitation at 250 rpm in MM. Cultures were then diluted 1:1000 and grown at 25 °C with agitation at 250 rpm for 24 hours. Formaldehyde (final concentration 0.18%) was then added to prevent c-di-GMP degradation. 1 mL of this culture was pelleted by centrifuging at 6000 rpm for 5 minutes. The pellet was then resuspended in 400 µL ice cold extraction buffer (40% methanol, 40% acetonitrile, 0.1% formic acid, 19.9% Milli-Q water) and vortexed for 30 seconds followed by incubation on ice for 15 minutes. The resultant lysates were centrifuged at 14,000 rpm for 5 minutes and the pellets were discarded. The supernatant was then dried by rotary evaporation and the remaining pellet was resuspended in 50 µL Milli-Q water. C-di-GMP was separated and quantified for each sample by HPLC (Shimadzu LC-2010A HT) using a Shimadzu Shimpack XR-ODS c-8 column. Separations were conducted in 0.1 M TEAA (triethylammonium acetate) solution (pH 6.0) at 0.1 mL/min rate with 10% methanol. C-di-GMP concentration was determined by comparison to a standard curve generated from known concentrations of c-di-GMP (Biolog Life Science Institute) run on the HPLC under identical conditions. The HPLC peak assigned to c-di-GMP was confirmed by MALDI mass spectrometry (a peak in the mass spectrum at m/z = 691 g/mol was observed; the expected mass for c-di-GMP is 690 g/mol). To introduce NO, 50 µM diethylamine NONOate (DEA/NO; Cayman Chemicals; DEA/NO $t_{1/2}$ = 2 mins and 16 mins at 37 °C and 22-25 °C, respectively) was added 20 minutes before harvesting the cells. The DEA/NO had been pre-decayed for at 25 ºC before addition to the *S. woodyi*

cultures. A Nitric Oxide Analyzer 280i (Sievers) was used to determine that the solution NO concentration was less than 100 nM (decayed from ~80 nM to ~50 nM) during the length of NO exposure in these experiments. The result was normalized by cell mass. Each data set was independently obtained a minimum of three times. The mean c-di-GMP concentration, relative to the wild-type strain, ± 1 standard deviation is reported.

Pull-down assay. Glutathione S-transferase (GST) fusions of *Sw*DGC, *Sw*GGAAF, and *Sw*AAL were created by subcloning *Sw*DGC and mutants from pET28b(+) into a pGEX4t-2 (GE Life Science) vector by PCR amplification using Pfu Turbo polymerase. Upstream and downstream primers contained *Bam*HI and *Xho*I restriction sites, respectively. GST constructs were purified from Rosetta2(DE3) cells (induced with 250 μM IPTG overnight at 16 ºC). Glutathione sepharose beads with protein bound were washed in 50 mM Tris, 300 mM NaCl, 1 mM PMSF, 2 mM DTT and 0.5% Triton X-100. Following washing, 10 μM His_6 tagged *Sw*H-NOX was added to the beads in a final volume of 1 mL in the same buffer and incubated overnight at 4 ºC with gentle rocking. Beads were then washed 3 times with the same buffer and then boiled in 50 μL of SDS sample buffer. 10 μL of this reaction was loaded onto a 12.5% Tris glycine gel for Western Blot analysis. Polyclonal anti-His antibody (Abcam) was used in 5% milk to detect the presence of His_6 tagged *Sw*H-NOX.

Steady-state kinetics analysis. Steady-state kinetic parameters for di-guanylate cyclase activity were determined using *Sw*AAL. *Sw*AAL (50 nM) was incubated with various concentrations of GTP (0.5 – 50 μM) at 25 ºC in buffer containing 75 mM Tris·HCl, pH 7.5, 250 mM NaCl, 25 mM KCl, and 10 mM $MgCl_2$. Initial velocities were determined by following the production of pyrophosphate (PPi) using the PhosphoWorks™ kit (AAT bioquest) on a Perkin Elmer Victor™ X5 multilabel reader. In this assay, PPi (a c-di-GMP co-product of di-guanylate cyclase activity)

is detected by a turn-on flurorescent PPi sensor. To obtain the actual product concentration (used for calculation of the initial velocity and other kinetic parameters), the raw values of the fluorescence versus time data were normalized to a standard curve generated by plotting the fluorescence of known concentrations of commercial pyrophosphate detected using the PhosphoWorks assay.

Steady-state kinetic parameters for phosphodiesterase activity were determined using *Sw*GGAAF. *Sw*GGAAF (50 nM) was incubated with various concentrations of c-di-GMP (0.5 – 25 μM) at 25 ºC in buffer containing 50 mM Tris, 1 mM $MgCl_2$, pH 7.5. Initial velocities were determined by following the production of phosphate using a modified Invitrogen EnzChek™ kit on a Cary 100 spectrophotometer equipped with a constant temperature bath set to 25 ^{o}C. 1U of calf intestinal phosphatase (CIP from New England Biolabs; 10 unit/mL) was added to the kit contents to convert the product pGpG to phosphate (for detection by EnzChek) and GpG. To obtain the actual product concentration (used for calculation of the initial velocity and other kinetic parameters), the raw values of the absorbance versus time data were normalized to a standard curve generated by plotting the absorbance of known concentrations of commercial pGpG (Biolog) detected using the modified EnzChek assay.

In both assays, the initial velocity (V_i) was determined by plotting the corresponding product concentration versus time and fitting the date with the linear regression formula ([product] = V_i*t + C), where C is basal absorbance and t is time. V_{max} and K_M were determined by plotting V_i versus substrate concentration and fitting with the Michaelis-Menten equation [(V_i = (V_{max}*[substrate])/([substrate] + K_M)]. k_{cat} was calculated from V_{max} (k_{cat} = V_{max}/[enzyme]). Origin 7.0 was used for all fittings. In reactions containing *Sw*H-NOX, pre-incubation of *Sw*H-NOX (varying concentration, 1 – 20 μM) with *Sw*AAL or *Sw*GGAAF was carried out for 20

minutes at 25 ºC before the addition of substrate to initiate the reaction. All of the coupling enzymes used in the EnzChek kit™ assay as well as including CIP were determined not to be rate limiting (doubling the concentration of each coupling enzyme did not affect the initial velocity measured; see Table 3-2).

Table 3-2. Phosphodiesterase steady-state kinetics assay coupling enzyme control reactions. Initial velocity of phosphodiesterase cyclase activity (standard conditions: [*Sw*GGAAF] = 50nM; [c-di-GMP] = 10μM; [a][PNP] = 1U; [b][CIP] = 1U; changes where noted) at 25ºC. Error analysis was determined from at least three independent trials.

Enzyme	**Notes**	[c]V_i **(min^{-1})**
*Sw*GGAAF	standard conditions	0.026 ± 0.007
[d]2x*Sw*GGAAF	100 nM *Sw*GGAAF	0.055 ± 0.005
2xCIP	2U CIP	0.022 ± 0.004
2xPNP	2U PNP	0.024 ± 0.006

[a]We used the EnzChek phosphate detection kit from Invitrogen; 1U of PNP (purine nucleoside phosphorylase, standard kit component) was used as per Invitrogen's protocol in our standard assay conditions. [b]CIP (calf intestinal phosphatase; New England Biolabs) was added to each phosphodiesterase assay at a concentration of 1U in our standard assay conditions. [c]The V_i values reported in this table are for the raw absorbance data plotted versus time. They are not normalized to a standard curve for pGpG concentration. [d]These data indicate that *Sw*GGAAF phosphodiesterase activity, and not CIP or PNP activity, is the rate limiting step in our assays, thus we are indeed reporting the V_i of *Sw*GGAAF activity.

Congo red (CR) visualization of extracellular polysaccharide matrix production. A vector expressing both *Sw*H-NOX and *Sw*DGC was created by subcloning each gene into pETDuet-1 (Novagen) by PCR amplification using Pfu Turbo polymerase. Upstream and downstream primers contained *Nde*I and *Xho*I restriction sites, respectively for *Sw*H-NOX and *Not*I and *Nco*I, respectively for *Sw*DGC. Vectors expressing only *Sw*H-NOX or only *Sw*DGC were also created. Transformed *E. coli* constructs were grown in LB containing 25 μg/mL CR, ± 0.1 mM IPTG, and ± ~60 nM NO (200 μM dipropylenetriamine NONOate [Cayman Chemicals; $t_{1/2}$ = 3 hours at

37 °C]). EPS production was measured by removal of CR from the media upon binding to EPS, as we have previously described [168].

Growth Curve. Sub-cultures (1:1000 ratio dilution of an overnight culture) of *S. woodyi* and mutants were grown at 25°C with agitation at 250 rpm in MM; *E. coli* were grown at 37°C with agitation at 250 rpm in LB. The optical density at 570 nm was recorded at various time points and plotted as shown here. For *S. woodyi* cultures grown in the presence of NO, the 1000-fold diluted overnight culture was diluted into media supplemented with varying amounts of DETA/NO that had been decaying for 20 hours at 37 °C. For *E. coli* cultures grown in the presence of NO, the 1000-fold diluted overnight culture was diluted into media supplemented with varying amounts of DPTA/NO that had been decaying for 2 hours at 37 °C. From there the protocols were identical.

Reverse transcription. Total RNA was extracted from *S. woodyi* cells using PureLink^{TM} RNA mini kit (Invitrogen). The RNA mixture was then subjected to a reverse transcription (RT) reaction using the Dynamo^{TM} cDNA synthesis kit (Thermo Scientific). The cDNA products of RT were used as the template in the following PCR reactions. The PCR products were separated on a 1.2% agarose gel.

3.3 Results

Despite intense research efforts, regulation of biofilm development is not well understood [6]. However, it has become apparent that the signaling molecule NO plays a role in biofilm development [102, 103, 105]. In order to provide molecular details concerning how NO affects biofilm growth, in this report we investigate our hypothesize that NO influences biofilm formation through H-NOX regulation of c-di-GMP metabolism.

3.3.1 Correlation of biofilm thickness on *Sw*H-NOX

In order to determine if H-NOX plays a role in biofilm growth in *S. woodyi*, biofilms of wild-type and Δ*hnox* mutant *S. woodyi* strains were grown on microscope slides. Deletion of the *Sw*H-NOX gene does not lead to any delay in cell growth (Fig. 3-1). Biofilms formed at the air-liquid interface were stained with SYTO®9 (green; stains live cells) and propidium iodide (red; stains dead cells only) and imaged by confocal microscopy [172]. In this experiment the thickness and density of biofilm formation, as well as cell viability, can be visualized. As illustrated in Fig. 3-1 and 3-2, wild-type *S. woodyi* forms robust biofilms under aerobic conditions. We call *S. woodyi* biofilms robust because we consistently get thick, well-adhered films; the cells are not easily scraped off the surface and one can visually see a band of cells at the liquid-air interface. As shown in Fig. 3-2, in comparison to wild-type, deletion of *Sw*H-NOX results in a visible decrease in the density and thickness of the biofilm formed (average biofilm coverage: *Sw*MS32 = ~100%; Δ*hnox* = ~50%, average biofilm thicknesses: *Sw*MS32 = 6.9 ± 0.4 μm; Δ*hnox* = 5.0 ± 0.9 μm). In all cases, the biofilm cells were healthy; live/dead staining indicated few dead cells. Therefore we conclude that *Sw*H-NOX affects biofilm appearance in *S. woodyi*. These findings led us to further investigate, and quantify, the role of *Sw*H-NOX and NO in biofilm formation.

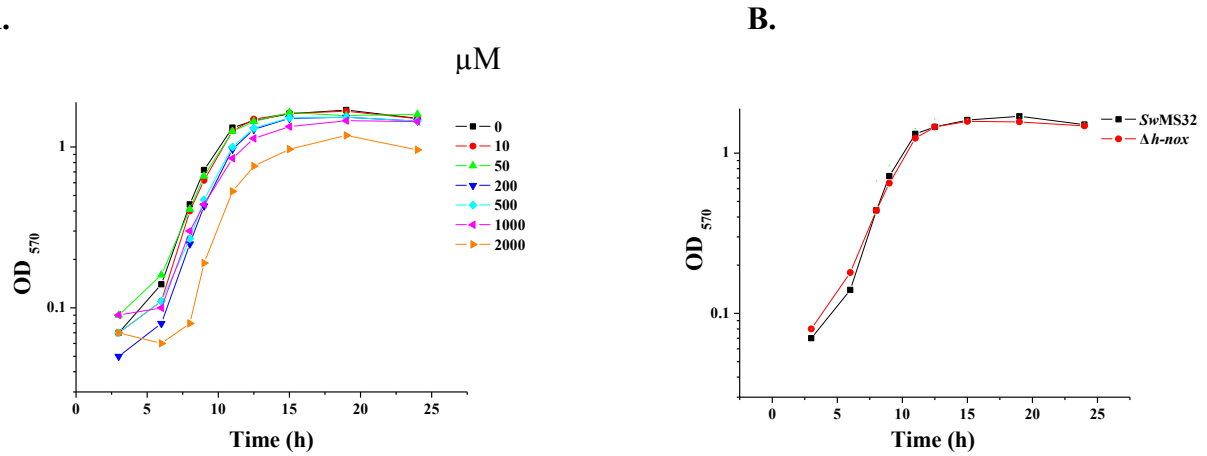

Figure 3-1. Growth curves of wild-type and Δ*hnox* mutant *S. woodyi.* **A)** DETA/NO (DETA/NO $t_{1/2}$ = 20 hours and 56 hours at 37 °C and 22-25 °C, respectively), which is used as an external NO source in this study, is non-toxic to *S. woodyi* up to ~1 mM under the experimental conditions tested. **B)** In-frame disruption of the *hnox* gene does not affect the growth rate of *S. woodyi*.

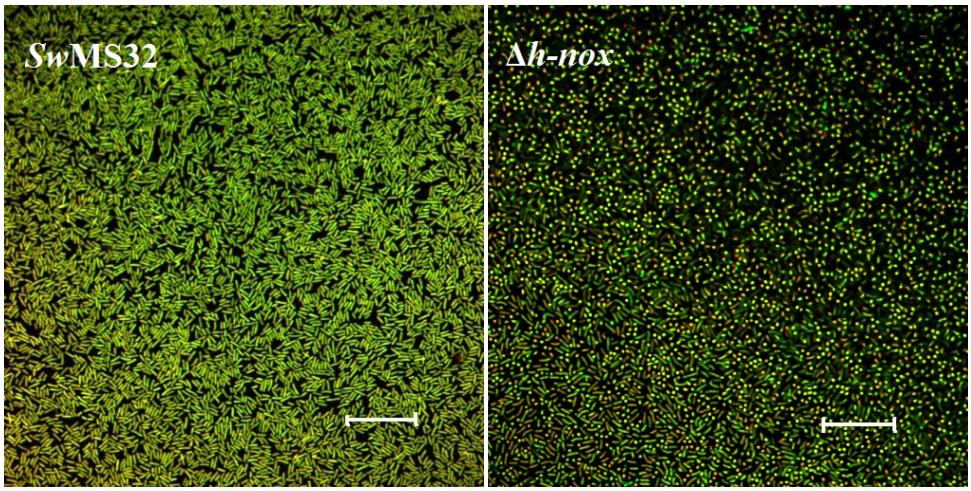

Figure 3-2. *Sw*H-NOX regulates biofilm formation. Biofilms of wild-type and Δ*hnox* mutant *S. woodyi* stained with SYTO®9 (green; stains all cells) and propidium iodide (red; stains dead cells) and imaged by confocal laser scanning microscopy. Top: XY view of a *Sw*MS32 biofilm; bottom: XY view of a Δ*hnox* biofilm. Bar = 20 μm.

3.3.2 Effect of NO/H-NOX on c-di-GMP concentration and biofilm thickness in *S. woodyi*

Having established that *Sw*H-NOX affects biofilm growth in *S. woodyi*, we sought to quantify the effect of NO and *Sw*H-NOX on biofilm formation. Biofilms of wild-type and mutant *S. woodyi* were grown in the presence and absence of NO. Biofilm growth at the air-liquid interface was analyzed by crystal violet staining of biofilms grown in a 96 well plate (27).

All of the biofilm experiments reported here were open to air and diethylenetriamine NONOate (DETA/NO) was used as an NO donor [173]. NONOates are stable as solids but spontaneously release NO in a pH-dependent manner in solution [174]. The non-lethal concentration range of NONOate was determined using planktonic growth curves measured with exposure to varying concentrations of NONOate (Fig. 3-1). We established that NONOates are non-toxic (no decrease OD relative to no NONOate) up to ~1 mM with our strains under the conditions tested. Further, the concentration of NO in solution throughout the entire length of the biofilm experiment was measured using a Nitric Oxide Analyzer 280i (Sievers). By allowing the NONOate (DETA/NO $t_{1/2}$ = 20 hours and 56 hours at 37 °C and 22-25 °C, respectively) to decay for ~1 half-life before inoculation, the NO concentration throughout the experiment stayed relatively constant for over 24 hours. Under the experimental conditions used here, 200 μM DETA/NO resulted in a relatively steady concentration of less than 100 nM NO (slowly decayed from ~80 nM to ~60 nM) during the full course of biofilm growth. This is consistent with solution (cell medium) NO concentrations previously reported using DETA/NO [175, 176].

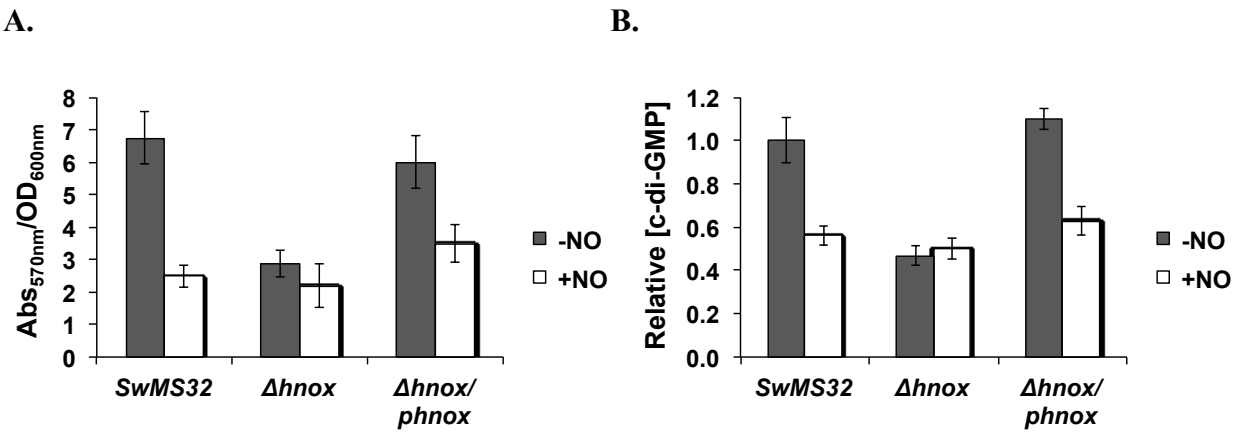

Figure 3-3. *Sw*H-NOX mediates an NO-dependent reduction in intracellular c-di-GMP concentration and biofilm formation. **A)** Biofilms of wild-type, Δ*hnox* and Δ*hnox/phnox* mutant *S. woodyi* formed at the liquid-air interface of PVC plates after 24 hours of growth, in the presence and absence of NO (gradual decrease from ~80 to ~60 nM during the 24 growth period), quantified by CV staining. Each biofilm condition was run a minimum of twelve times in one experiment and the entire experiment was performed a minimum of three times. The mean ± 1 standard deviation is reported. **B)** Intracellular c-di-GMP concentration of wild-type, Δ*hnox* and Δ*hnox/phnox* mutant *S. woodyi* in the presence and absence of NO (decrease from ~80 to ~50 nM during exposure). The c-di-GMP concentration relative to the concentration of c-di-GMP in *Sw*MS32 in the absence of NO (~1400 pmol/mg cell) is reported. Each data set was independently obtained a minimum of three times. The mean c-di-GMP concentration, relative to wild-type, ± 1 standard deviation is reported. Taken together, these data indicate that *Sw*H-NOX and *Sw*DGC regulate biofilm formation in response to NO through c-di-GMP concentration changes.

Figure 3-3A illustrates the results of biofilm growth after 24 hours analyzed by crystal violet staining. The amount of biofilm observed in the absence (closed bars) and presence (open bars) of NO is compared for wild-type and Δ*hnox* strains. The key observations are as follows. First,

the wild-type strain exhibits a marked decrease in biofilm growth in the presence of nanomolar NO. Second, the *Sw*H-NOX gene is required for this NO biofilm phenotype, as evidenced by decreased biofilm in the Δ*hnox* strain both with and without NO. Finally, the decreased biofilm phenotype in the Δ*hnox* construct is correlated with the absence of *Sw*H-NOX, as complementation of the deletion strain with the *hnox* gene on a plasmid restores wild-type activity.

In order to determine if the decrease in biofilm growth observed in Fig. 3-2 and 3-3A was, as we hypothesized, correlated with a decrease in cellular c-di-GMP levels, we quantified the amount of c-di-GMP present in *S. woodyi* cell lysates in the presence and absence of NO. In these experiments, *S. woodyi* strains were exposed to <100 nM NO from DEA/NO for 20 minutes before c-di-GMP extraction. This short NO exposure was designed to maximize the changes in c-di-GMP concentration resulting from changes in enzyme activity and minimize the possibility of changes in c-di-GMP concentration caused by changes in gene expression.

As illustrated in Fig. 3-3B, the c-di-GMP quantification results are consistent with the biofilm growth experiments. A decrease in the concentration of c-di-GMP in the wild-type strain (wild-type [c-di-GMP] is ~1400 pmol c-di-GMP/mg cells) upon exposure to NO, and a similar decrease in the Δ*hnox* strain in both the presence and absence of NO, was observed. For the Δ*hnox* mutant, plasmid complementation with the deleted gene restores wild-type activity. These data imply that the changes in biofilm growth observed in the presence of NO and/or the absence of *Sw*H-NOX (Fig. 3-3A) are the direct result of changes in the concentration of cellular c-di-GMP.

A reasonable NO sensing and signaling mechanism that would result in these data is that NO is sensed by *Sw*H-NOX, and that NO-bound *Sw*H-NOX decreases the c-di-GMP output of *Sw*DGC. This reduction in c-di-GMP production ultimately results in a decrease in biofilm formation.

3.3.3 Steady-state kinetics of the di-guanylate cyclase and phosphodiesterase activities of *Sw*DGC

In order to begin to explore the hypothesis that NO/H-NOX affects c-di-GMP concentrations and biofilm formation in *S. woodyi* through direct regulation of *Sw*DGC, we first determined the steady-state kinetics of each enzymatic activity of *Sw*DGC. In our previous study, we found *Sw*DGC to have both di-guanylate cyclase and phosphodiesterase activities [168]. We have confirmed that the activity of one domain (e.g., phosphodiesterase activity in the EAL domain) is not affected by a point mutation in the other domain (e.g., the GGDEF to GGAAF mutation in the cyclase domain does not affect phosphodiesterase activity; see Table 3-3 and 3-4). Thus, in order to simplify product detection and quantification, here, we measured the kinetics of each activity separately using point mutants that inactivate one or the other active site. As we have shown previously [168], *Sw*AAL has only di-guanylate cyclase activity (condensation and cyclization of two molecules of GTP to c-di-GMP) due to mutation of a key residue in the active site of the phosphodiesterase domain. *Sw*GGAAF, on the other hand, has only phosphodiesterase activity (hydrolysis of c-di-GMP to pGpG).

Table 3-3. Di-guanylate activity control reactions. Initial velocity of di-guanylate cyclase activity ([enzyme] = 50nM; [GTP] = 50μM; [*Sw*H-NOX] = 10μM, where noted) at 25ºC. Error analysis was determined from at least three independent trials.

Enzyme	Notes	[a]V_i (μM*s^{-1})
*Sw*DGC	wild-type enzyme	12.3 ± 1.7
*Sw*DGC	[b]no $MgCl_2$ in reaction	1.5 ± 1.1
*Sw*DGC/Fe^{2+}	+*Sw*H-NOX Fe^{2+}	49.7 ± 8.9
*Sw*DGC/Fe^{2+}-NO	+*Sw*H-NOX Fe^{2+}-NO	14.4 ± 3.4
[c]*Sw*AAL	inactive PDE domain	12.1 ± 1.8
*Sw*AAL/Fe^{2+}	+*Sw*H-NOX Fe^{2+}	59.7 ± 2.9
*Sw*AAL/Fe^{2+}-NO	+*Sw*H-NOX Fe^{2+}-NO	11.2 ± 1.4
*Sw*GGAAF	inactive DGC domain	-0.7 ± 1.9

[a]The V_i values reported in this table are for the raw fluorescence data plotted versus time. They are not normalized to a standard curve for pyrophosphate concentration. [b]The 10mM $MgCl_2$ included in all other cyclase reactions was omitted in this reaction. [c]Mutation in the EAL domain does not affect activity in the GGDEF domain, as demonstrated by the fact that there is no significant difference between the initial velocity of di-guanylate cyclase activity for *Sw*DGC and *Sw*AAL (active cyclase but inactive phosphodiesterase domain) measured under the same experimental conditions.

TABLE 3-4. Phosphodiesterase activity control reactions. Initial velocity of phosphodiesterase cyclase activity ([enzyme] = 50nM; [c-di-GMP] = 10μM; [*Sw*H-NOX] = 10μM, where noted) at 25ºC. Error analysis was determined from at least three independent trials.

Enzyme	Notes	[a]V_i (μM*min^{-1})
*Sw*DGC	wild-type enzyme	0.027 ± 0.004
*Sw*DGC/Fe^{2+}	+*Sw*H-NOX Fe^{2+}	0.024 ± 0.005
*Sw*DGC/Fe^{2+}-NO	+*Sw*H-NOX Fe^{2+}-NO	0.047 ± 0.006
[b]*Sw*GGAAF	inactive DGC domain	0.026 ± 0.007
*Sw*GGAAF/Fe^{2+}	+*Sw*H-NOX Fe^{2+}	0.023 ± 0.005
*Sw*GGAAF/Fe^{2+}-NO	+*Sw*H-NOX Fe^{2+}-NO	0.040 ± 0.006
*Sw*AAL	inactive PDE domain	0.001 ± 0.001

[a]The V_i values reported in this table are for the raw absorbance data plotted versus time. They are not normalized to a standard curve for pGpG concentration. [b]Mutation in the GGDEF domain does not affect activity in the EAL domain, as demonstrated by the fact that there is no significant difference between the initial velocity of phosphodiesterase activity for *Sw*DGC and

*Sw*GGAAF (inactive cyclase and active phosphodiesterase domain) measured under the same experimental conditions.

To measure di-guanylate cyclase activity, the production of pyrophosphate (PPi), which along with c-di-GMP is a product of di-guanylate cyclase activity, by *Sw*AAL was monitored. A range of GTP concentrations were tested in order to obtain k_{cat} and K_M values for *Sw*AAL. As illustrated in Fig. 3-4A and Table 3-5, in the absence of *Sw*H-NOX, *Sw*AAL has a k_{cat} of 0.105 ± 0.005 s^{-1}, a K_M of 7.74 ± 0.90 μM, and a k_{cat}/K_M = 0.014 $s^{-1}\mu M^{-1}$. In comparison to other di-guanylate cyclases, these kinetics indicate that *Sw*AAL has moderate di-guanylate cyclase activity. The cyclase activity of *Sw*AAL is similar to PleD (k_{cat} = 0.102 ± 0.023 min^{-1}; K_M = 5.8 ± 1.2 μM; k_{cat}/K_M = 0.018 $s^{-1}\mu M^{-1}$) and lower than WspR (k_{cat} = 4.50 ± 0.12 s^{-1}; K_M = 5.97 ± 0.80 μM; k_{cat}/K_M = 0.75 $s^{-1}\mu M^{-1}$) [177, 178].

To determine the phosphodiesterase activity of *Sw*GGAAF, we developed the first continuous assay for monitoring the enzyme activity of EAL domains. We modified a phosphate detection kit from Invitrogen by coupling it to calf intestinal phosphatase (CIP) activity. In doing this, we were able to detect the production of pGpG, which produces stoichiometric inorganic phosphate upon CIP hydrolysis, whereas c-di-GMP, the substrate of the phosphodiesterase reaction, cannot be hydrolyzed by CIP due to its cyclic structure. Table 3-2 summarizes data that indicate *Sw*GGAAF activity is the rate-limiting step in this novel phosphodiesterase assay. Therefore, the measured kinetics in these experiments are those of *Sw*GGAAF phosphodiesterase activity. The results of the phosphodiesterase activity assays are shown in Fig. 3-4B, Table 3-4, and Table 3-5.

Table 3-5. Regulation of *Sw*DGC activity by *Sw*H-NOX; NO-bound *Sw*H-NOX results in a decrease in c-di-GMP concentration. Kinetic parameters for di-guanylate cyclase (*Sw*AAL) and phosphodiesterase (*Sw*GGAAF) activities as a function of *Sw*H-NOX in the ferrous unligated and ferrous NO-bound forms.

Enzyme	Regulator	k_{cat} (s^{-1})	k_{cat}/K_M ($s^{-1}*\mu M^{-1}$)
*Sw*AAL	without *Sw*H-NOX	0.105 ± 0.005	0.014 ± 0.002
(di-guanylate cyclase)	*Sw*H-NOX Fe^{2+}	0.209 ± 0.009	0.125 ± 0.023
	*Sw*H-NOX Fe^{2+}-NO	0.102 ± 0.011	0.011 ± 0.003
*Sw*GGAAF	without *Sw*H-NOX	1.52 ± 0.05	1.16 ± 0.20
(phosphodiesterase)	*Sw*H-NOX Fe^{2+}	1.04 ± 0.08	1.65 ± 0.59
	*Sw*H-NOX Fe^{2+}-NO	4.65 ± 0.14	15.5 ± 2.6

A. **B.**

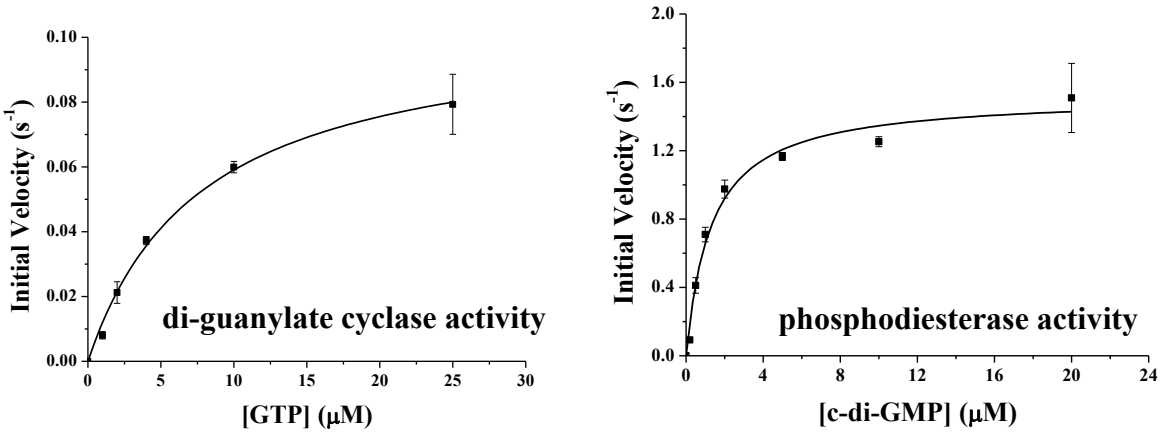

Figure 3-4. *Sw*DGC in the absence of *Sw*H-NOX is primarily a phosphodiesterase. **A.** Steady-state kinetic analysis of the di-guanylate cyclase activity of *Sw*DGC. Initial velocity of *Sw*AAL (50 nM) at 25 °C as a function of GTP concentration. **B.** Steady-state kinetic analysis of the phosphodiesterase activity of *Sw*DGC. Initial velocity of *Sw*GGAAF (50 nM) at 25 °C as a function of c-di-GMP concentration. The data were fitted with the Michaelis-Menten equation. Error analysis was determined from at least three independent trials.

Using this assays, a k_{cat} of 1.52 ± 0.05 s^{-1} and a K_M of 1.31 ± 0.22 μM for *Sw*GGAAF in the absence of *Sw*H-NOX was measured (Fig. 3-3B). In general, c-di-GMP phosphodiesterases have not been kinetically characterized, perhaps due to the lack of a good continuous assay for measuring steady-state kinetics. For comparison, CC3396 from *Caulobacter crescentus* [20], is a c-di-GMP specific phosphodiesterase that is activated by GTP. The c-di-GMP turnover rate for CC3396 in the absence of GTP has been reported as 0.040 ± 0.005 s^{-1}. In the presence of 100 μM GTP, its specific activity is 1.78 ± 0.03 (μM c-di-GMP)/(μM protein*s) and its K_M is 0.42 μM. The basal activity of *Sw*DGC (in the absence of activator) is several orders of magnitude higher than that measured for CC3396.

In comparison to the di-guanylate cyclase activity of *Sw*AAL, the k_{cat} of *Sw*GGAAF phosphodiesterase activity is 15 times higher and the K_M for c-di-GMP is 6 times lower. Therefore, as assessed by catalytic efficiency (k_{cat}/K_M), *Sw*DGC, in the absence of *Sw*H-NOX, is about 90 times more active as a c-di-GMP phosphodiesterase than a di-guanylate cyclase. Therefore, we conclude that *Sw*DGC, by itself, is predominately a phosphodiesterase.

3.3.4 Interaction of *Sw*H-NOX and *Sw*DGC

Keeping in mind our hypothesis that NO/*Sw*H-NOX regulates the activity of *Sw*DGC, and having characterized *Sw*DGC and *Sw*H-NOX separately, we next investigated whether or not *Sw*DGC and *Sw*H-NOX interact with each other. In bacteria, co-cistronic proteins are often functional partners. A single PCR fragment from reverse transcription of *S. woodyi* mRNA confirms that *Sw*DGC and *Sw*H-NOX are in the same operon (Fig. 3-5A).

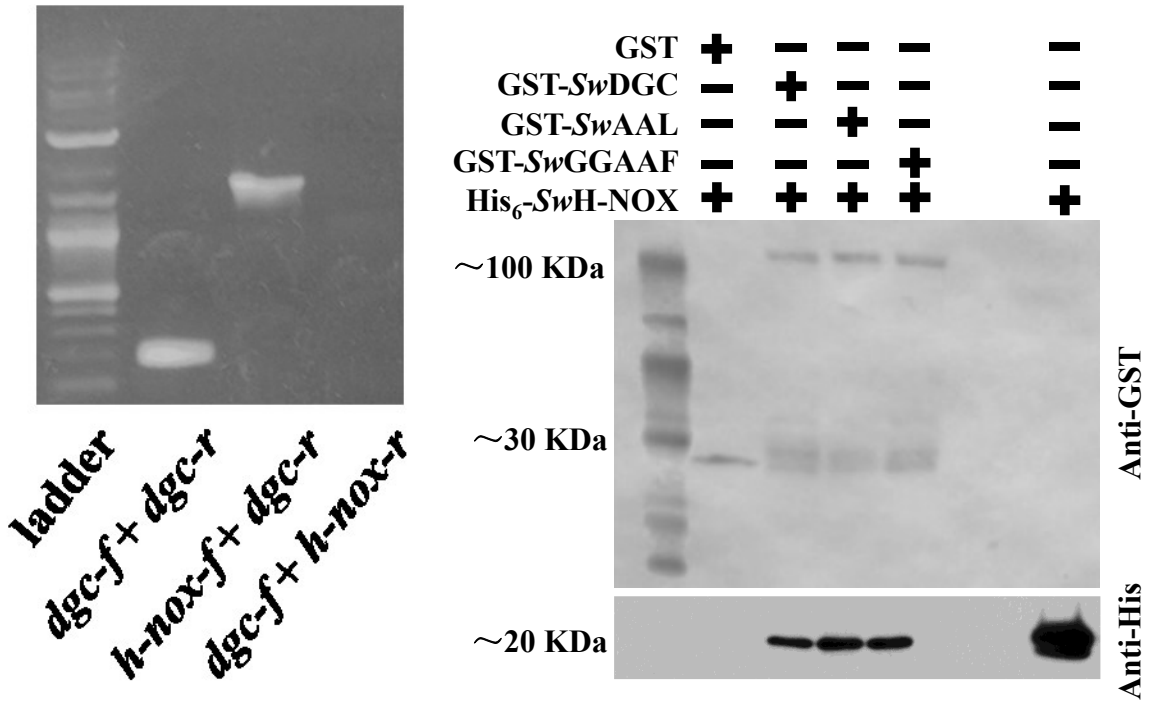

Figure 3-5. A) *Sw*H-NOX and *Sw*DGC are in the same operon. Lane 1, a 2-log DNA ladder was used as a molecular weight indicator. Lane 2, primers *dgc-f* and *dgc-r* were used as a positive control to amplify a ~200bp fragment internal to the *dgc* gene. Lane 3, primers *hnox-f* and *dgc-r* were used to demonstrate that *hnox* and *dgc* genes are indeed on the same mRNA transcript, and thus in the same operon. The ~1.6kb band present in lane 3 could only have been amplified if *hnox* and *dgc* were on the same mRNA, and thus the same piece of cDNA in the template DNA mixture. Lane 4, primers *dgc-f* and *hnox-r* served as a negative control. This reaction would only have generated a product if genomic DNA were contaminating the cDNA mixture. **B)** Precipitation of *Sw*H-NOX by *Sw*DGC. GST-tagged *Sw*DGC, *Sw*GGAAF, and *Sw*AAL were used to pull-down His_6-tagged *Sw*H-NOX from *E. coli* cell lysates. Top: Detection of GST via Anti-GST Western blot. The far left lane is a molecular weight marker; in the next lane to the

right, the bottom band is GST alone (~23 KDa; negative control); in the subsequent three lanes, the top bands are GST-*Sw*DGC, GST-*Sw*AAL, and GST-*Sw*GGAAF, respectively, and the bottom bands are GST domains proteolyzed from the larger GST-tagged constructs. Bottom: Detection of *Sw*H-NOX pulled-down by *Sw*DGC, *Sw*AAL, and *Sw*GGAAF via Anti-His Western blot. In the far left lane, GST alone does not pull down *Sw*H-NOX (negative control); in the subsequent three lanes, *Sw*DGC, *Sw*AAL, and *Sw*GGAAF, respectively, all efficiently precipitate *Sw*H-NOX; and in the far right lane His_6-*Sw*H-NOX (~21 KDa) was run as a positive control.

To investigate the interaction of *Sw*H-NOX and *Sw*DGC more directly, co-immunoprecipitation assays were performed. Using GST-tagged *Sw*DGC, *Sw*AAL, *Sw*GGAAF, and GST alone as bait, His_6-tagged *Sw*H-NOX was precipitated by GST-tagged *Sw*DGC, *Sw*AAL, and *Sw*GGAAF, but not GST alone, in a pull-down assay (Fig. 3-5B). This experiment demonstrates that *Sw*H-NOX and *Sw*DGC are binding partners. Furthermore, these data indicate that point mutations in the di-guanylate cyclase and phosphodiesterase active sites do not abolish *Sw*H-NOX binding by *Sw*DGC.

3.3.5 NO/*Sw*H-NOX regulation of *Sw*DGC activity

In order to quantify the effect of *Sw*H-NOX on *Sw*DGC activity, we determined the steady-state kinetics of both the di-guanylate cyclase and phosphodiesterase activities of *Sw*DGC in the presence and absence of NO and *Sw*H-NOX. First the effect of *Sw*H-NOX on *Sw*GGAAF phosphodiesterase activity was investigated. No change in the initial velocity of c-di-GMP (50 μM) turnover by *Sw*GGAAF (50 nM) was observed when varying concentrations of *Sw*H-NOX (1-20 μM) in the Fe^{2+} unligated complex were present in the reaction mixture. However, a

concentration-dependent enhancement in the initial velocity of phosphodiesterase activity was observed upon addition of NO-bound *Sw*H-NOX. In the presence of 20 μM *Sw*H-NOX in the Fe^{2+}-NO form, the initial rate of c-di-GMP hydrolysis is 1.5 times faster than in the presence of *Sw*H-NOX in the Fe^{2+} unligated form, or in the absence of *Sw*H-NOX (Fig. 3-6).

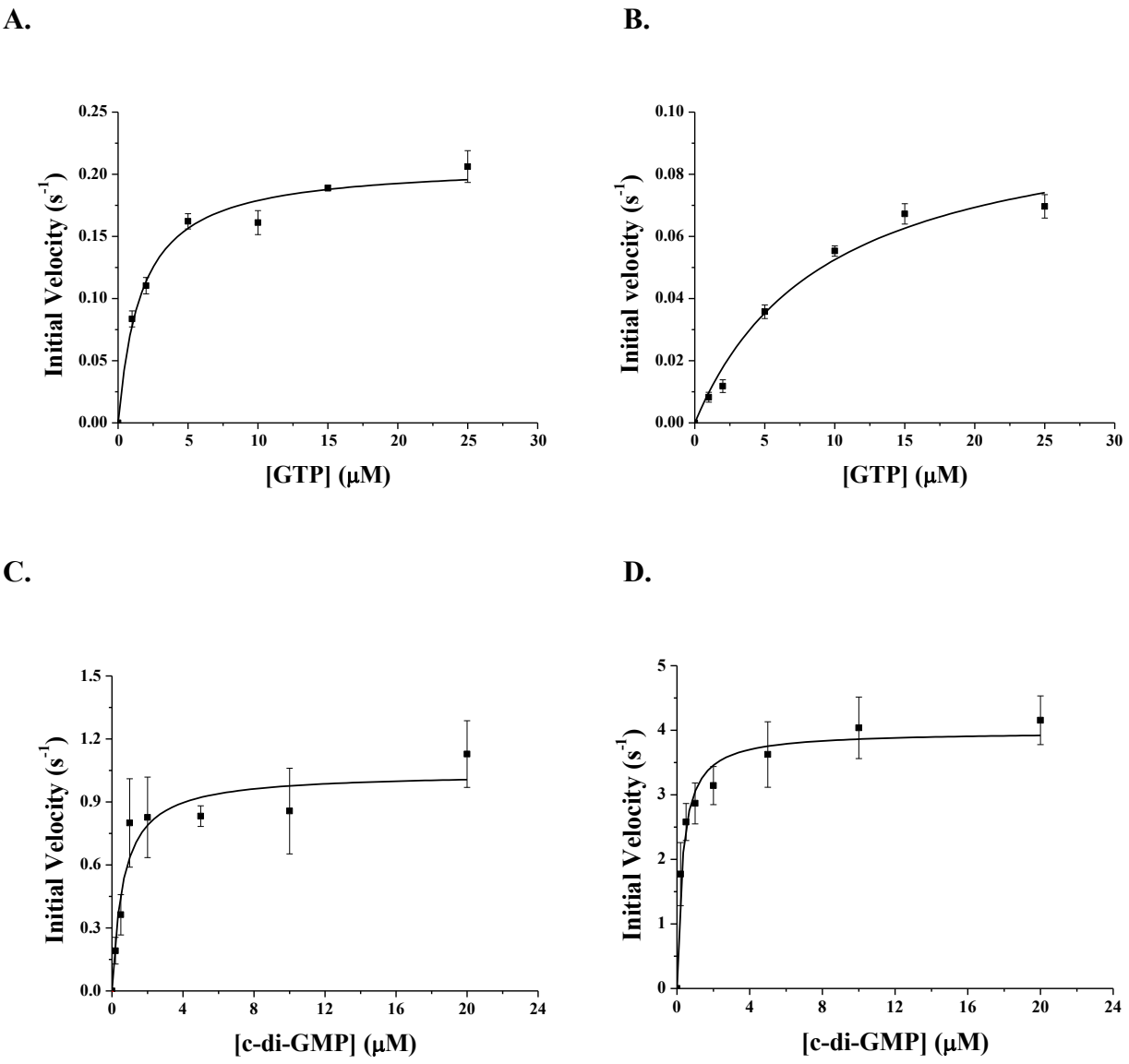

Figure 3-6. NO sensing synergistically reduces c-di-GMP concentrations. **A)** Steady-state kinetic analysis of the di-guanylate cyclase activity of *Sw*DGC in the presence of Fe^{2+}-unligated *Sw*H-NOX (10 μM). Initial velocity of *Sw*AAL (50 nM) at 25 °C as a function of GTP

concentration is plotted. **B)** Steady-state kinetic analysis of the di-guanylate cyclase activity of *Sw*DGC in the presence of NO-bound Fe^{2+} *Sw*H-NOX (10 μM). Initial velocity of *Sw*AAL (50 nM) at 25 °C as a function of GTP concentration is plotted. **C)** Steady-state kinetic analysis of the phosphodiesterase activity of *Sw*DGC in the presence of Fe^{2+}-unligated *Sw*H-NOX (10 μM). Initial velocity of *Sw*GGAAF (50 nM) at 25 °C as a function of c-di-GMP concentration is plotted. **D)** Steady-state kinetic analysis of the phosphodiesterase activity of *Sw*DGC in the presence of NO-bound Fe^{2+} *Sw*H-NOX (10 μM). Initial velocity of *Sw*GGAAF (50 nM) at 25 °C as a function of c-di-GMP concentration is plotted. The data were fitted with the Michaelis-Menten equation. Error analysis was determined from at least three independent trials.

Thus we performed a full kinetic characterization of *Sw*GGAAF phosphodiesterase activity in the presence of 10 μM *Sw*H-NOX in the Fe^{2+}-NO bound form (Fig. 3-6 and 3-7, and Table 3-5). In the presence of NO-bound *Sw*H-NOX, *Sw*GGAAF has a k_{cat} of 4.65 ± 0.14 s^{-1} and a K_M of less than 0.5μM (Table 3-5). Therefore, the catalytic efficiency parameter, k_{cat}/K_M, indicates a 13-fold or greater increase in phosphodiesterase activity when NO-bound *Sw*H-NOX is present (Fig. 3-7B).

The effect of *Sw*H-NOX on di-guanylate cyclase activity using the *Sw*AAL mutant (50 nM) was also investigated. Interestingly, a strong dose-dependent response in the initial velocity of di-guanylate cyclase activity (50 μM GTP) as a function of Fe^{2+} unligated *Sw*H-NOX concentration (1-10 μM) was observed, but there was no difference in the initial velocity of c-di-GMP synthesis as a function of Fe^{2+}-NO *Sw*H-NOX (Fig. 3-6). In the presence of 10 μM *Sw*H-NOX in the Fe^{2+} unligated form, the initial rate of c-di-GMP synthesis is 5.5 times faster than in the presence of *Sw*H-NOX in the NO-bound form, or in the absence of *Sw*H-NOX. Thus NO-bound

*Sw*H-NOX has exactly the opposite effect on c-di-GMP synthesis as it has on c-di-GMP hydrolysis.

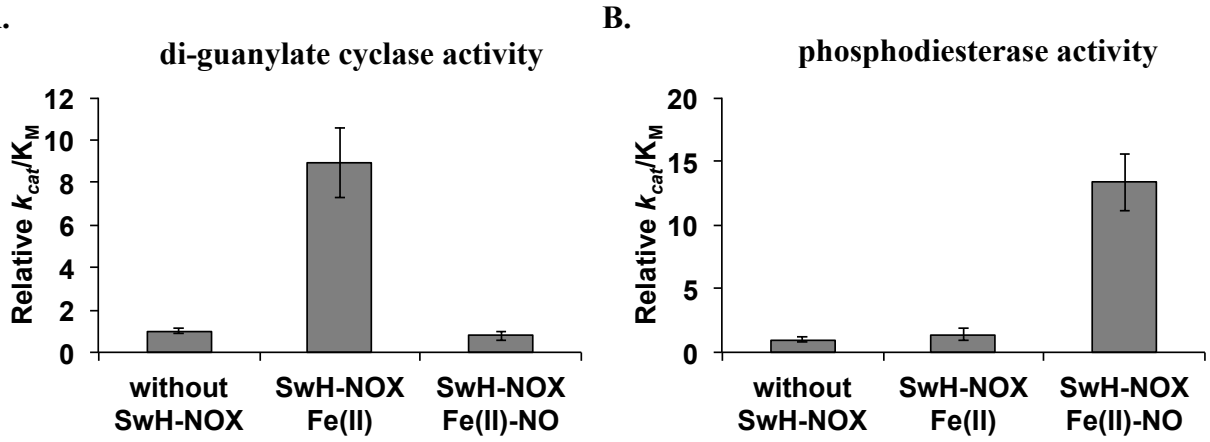

Figure 3-7. Upon NO binding, *Sw*H-NOX results in a decrease in c-di-GMP output by *Sw*DGC. **A)** Catalytic efficiency (k_{cat}/K_M) of *Sw*DGC di-guanylate cyclase activity (*Sw*AAL at 50 nM) in the presence of *Sw*H-NOX (10 μM) as the Fe^{2+}-unligated or Fe^{2+}-NO complex, relative to the catalytic efficiency of *Sw*AAL in the absence of *Sw*H-NOX. **B)** Catalytic efficiency (k_{cat}/K_M) of *Sw*DGC phosphodiesterase activity (*Sw*GGAAF at 50 nM) in the presence of *Sw*H-NOX (10 μM) as the Fe^{2+}-unligated or Fe^{2+}-NO complex, relative to the catalytic efficiency of *Sw*GGAAF in the absence of *Sw*H-NOX. Error analysis was determined from three independent experiments.

The full steady-state kinetic analysis of *Sw*AAL di-guanylate activity in the presence of 10 μM *Sw*H-NOX in the Fe^{2+} unligated form (Fig. 3-6 and 3-7, and Table 3-5) indicates that Fe^{2+} unligated *Sw*H-NOX enhances the cyclase activity of *Sw*AAL (k_{cat} = 0.209 ± 0.009 s^{-1}; K_M = 1.67 ± 0.30 μM) by about 10-fold in k_{cat}/K_M, as compared with *Sw*AAL di-guanylate cyclase activity in the presence of NO-bound H-NOX or in the absence of H-NOX (Fig. 3-7A and Table 3-5).

Therefore, unlike *Sw*DGC in the absence of *Sw*H-NOX, *Sw*H-NOX-bound *Sw*DGC acts as a di-guanylate cyclase in the absence of NO. Upon exposure to NO, however, *Sw*H-NOX regulated

changes in the activities of both the GGDEF and EAL domains take place. This should result in a rapid reduction in c-di-GMP concentration. This response to NO results because NO-bound *Sw*H-NOX relieves the augmentation of di-guanylate cyclase activity caused by Fe^{2+} unligated *Sw*H-NOX, and greatly activates phosphodiesterase activity.

3.4 Discussion

In addition to being important in many aquatic, industrial, and environmental processes, the National Institutes of Health has estimated biofilms to be responsible for up to 80% of all non-viral human microbial infections [179, 180]. Despite the well-documented role of NO in the regulation of biofilm production by some bacteria, the mechanism for NO regulation of biofilm formation is unknown [102, 103, 105].

We have hypothesized that the NO/H-NOX signaling pathway may be important for the development of bacterial biofilms. H-NOX domain-containing proteins are evolutionarily conserved heme proteins that include the well-characterized eukaryotic NO sensor, soluble guanylate cyclase [181]. In support of this hypothesis, H-NOX has been linked to biofilm formation [115] and in the genomes of many bacteria, an H-NOX gene is found near a predicted DGC gene [182]. The activity of some DGC proteins is strongly correlated with biofilm growth [183]. Here evidence from genetics, biofilm growth, and enzymology experiments is presented to substantiate the link between NO/H-NOX signaling and biofilm formation.

The results of the enzyme kinetics experiments (Fig. 3-4 and 2-7; Table 3-5) are in excellent agreement with the biofilm growth and c-di-GMP concentration determination studies (Fig. 3-2 and 3-3). Based on all of these data, we propose a model for NO regulation of biofilm formation in *S. woodyi* (Fig. 3-8).

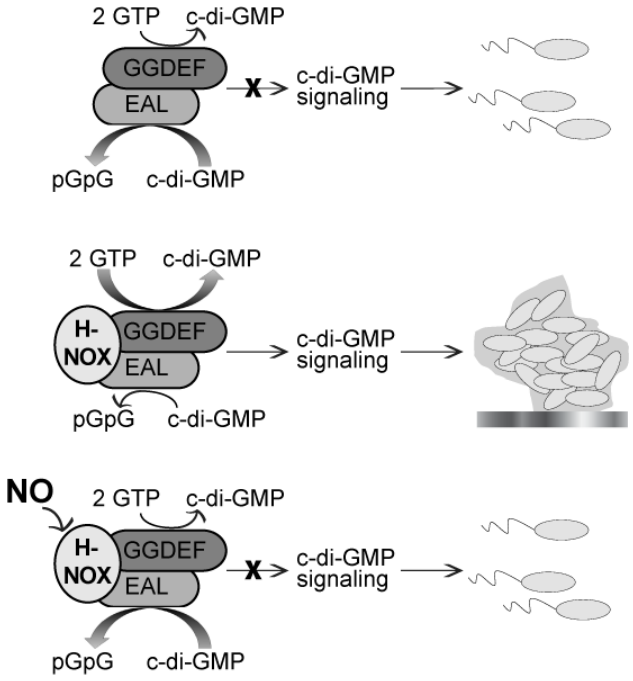

Figure 3-8. Our model for NO regulation of c-di-GMP synthesis in *S. woodyi*. In the absence of *Sw*H-NOX (such as in the Δ*hnox* mutant strain), *Sw*DGC is primarily a phosphodiesterase. However, it is likely that *in vivo*, *Sw*H-NOX and *Sw*DGC form a complex. In the absence of NO, *Sw*H-NOX is associated with *Sw*DGC and maintaining basal phosphodiesterase activity while enhancing di-guanylate cyclase activity. Upon detection of NO, *Sw*H-NOX down-regulates di-guanylate cyclase activity and activates phosphodiesterase activity. Therefore, NO reduces the c-di-GMP concentration in *S. woodyi*, leading to a reduction in biofilm formation.

3.4.1 NO causes a reduction in c-di-GMP concentration through *Sw*H-NOX regulation of both the di-guanylate cyclase and phosphodiesterase activities of *Sw*DGC

As illustrated in Fig. 3-2 and 3-3, deletion of *Sw*H-NOX from *S. woodyi* (i.e., the Δ*hnox* strain) results in decreased biofilm and decreased intracellular c-di-GMP concentration. This is consistent with the kinetic data presented in Table 3-5 and Fig. 3-4, indicating that in the absence of *Sw*H-NOX, *Sw*DGC is primarily a phosphodiesterase. In this study, the mutant strain in the

gene coding for *Sw*DGC was not constructed, thus we cannot explicitly conclude that *Sw*H-NOX and *Sw*DGC form a functional complex *in vivo*. However, as suggested by the fact that *Sw*H-NOX and *Sw*DGC are co-cistronic (Fig. 3-5A) and as demonstrated by our pull-down studies (Fig. 3-5B), we propose that it is likely that *Sw*H-NOX and *Sw*DGC form a stable complex *in vivo*. Thus, we suggest that the *Sw*DGC kinetic data most relevant to understanding the behavior of *S. woodyi*, are those in complex with *Sw*H-NOX (Fig. 3-7 and Table 3-5), as discussed below.

Based on the kinetics results presented in Table 3-5 and Fig. 3-7, we conclude that *Sw*DGC is primarily a di-guanylate cyclase in the presence of *Sw*H-NOX in the Fe^{2+} unligated form (absence of NO). In the absence of NO, induction of recombinant *Sw*DGC/*Sw*H-NOX expression in *E. coli* results in an increase in extracellular polysaccharide matrix production (Fig. 3-9). This is consistent with the activity of an enzyme that is primarily producing c-di-GMP, thus acting like a di-guanylate cyclase when *Sw*H-NOX, but not NO, is present. These *in vitro* results are supported by the biofilm growth and c-di-GMP quantification results illustrated in Fig. 3- 2 and 3-3, which demonstrate that wild-type *S. woodyi* (containing both *Sw*H-NOX and *Sw*DGC) have relatively high c-di-GMP concentrations and produce robust biofilms in the absence of NO.

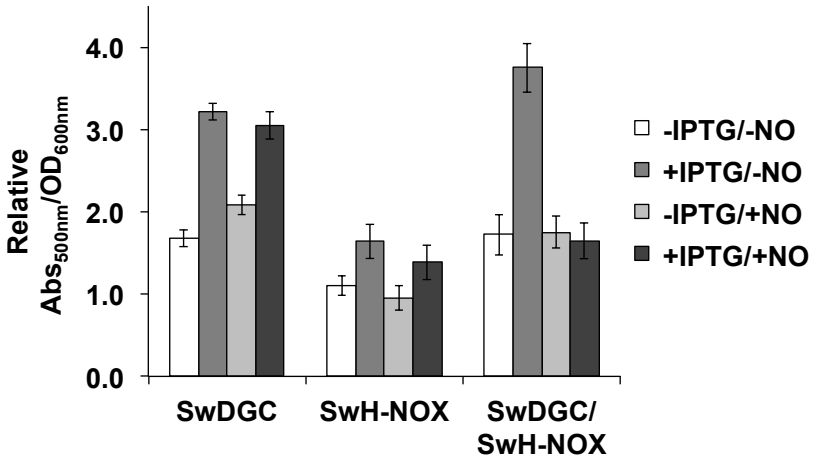

Figure 3-9. Expression of recombinant *Sw*H-NOX and *Sw*DGC reduces *E. coli* EPS production upon exposure to NO. CR absorbance at 500 nm (A_{500nm}) normalized by cell density (OD_{600nm}) is plotted for *E. coli* with and without induction of protein expression (with 100 μM IPTG) and with and without NO exposure (~60 nM). Data for A_{500nm}/OD_{600nm} from *E. coli* transformed with a vector coding for both *Sw*H-NOX and *Sw*DGC, a vector coding for only *Sw*H-NOX, or a vector coding for only *Sw*DGC, relative to the A_{500nm}/OD_{600nm} for the empty vector under the same conditions are presented. Each data set was independently obtained a minimum of three times. The mean ± 1 standard deviation is reported.

Upon exposure to NO, wild-type *S. woodyi* experiences a decrease in c-di-GMP concentration and a decrease in biofilm thickness (Fig. 3-3). A decrease in EPS production from *E. coli* cells expressing *Sw*DGC/*Sw*H-NOX recombinantly was observed when NO was added to culture (Fig. 3-9), which is also indicative of a down-regulation in biofilm formation upon exposure to NO. These results are consistent with both an increase in phosphodiesterase activity and/or a decrease in di-guanylate cyclase activity, which is what is observed in steady-state kinetics assays of *Sw*DGC activity when *Sw*H-NOX and NO are present (Table 3-5 and Fig. 3-7).

In our model (Fig. 3-8), NO contributes to the regulation of biofilm formation in *S. woodyi* by simultaneously down-regulating the cyclase activity and up-regulating the phosphodiesterase activity of *Sw*DGC. Thus, we predict that NO could induce a rapid transition between biofilm and motility. In future experiments we plan to test this prediction using confocal microscopy of biofilms under flow conditions. Furthermore, this model suggests that molecules that act on the NO/H-NOX pathway have the potential to be potent anti-biofilm agents, a possibility that will be explored in future studies.

The mechanisms regulating biofilm dispersal are not well understood, but it is notable that NO has been shown to cause biofilm dispersal in several species [105]. Indeed, NO regulation of c-di-GMP levels has been implicated in the rapid dispersal of biofilms in *Pseudomonas aeruginosa* [105] as well as other *Shewanella* species under anaerobic conditions [184].

3.4.2 Biological function of H-NOX domains

Although there is relatively little information on the biological function of bacterial H-NOX domains to date, interestingly, it has consistently been demonstrated that NO-bound H-NOX inhibits the activity of an associated enzyme [114, 115]. This is in contrast to the well-understood role of NO/H-NOX in up-regulating the activity of mammalian sGCs [185]. Here, we demonstrate in a single H-NOX/enzyme system, that NO/H-NOX has both functions, that of inhibition and that of enhancement of enzymatic activity. NO-bound *Sw*H-NOX stimulates phosphodiesterase activity and inhibits di-guanylate cyclase activity, in comparison to ferrous unligated *Sw*H-NOX.

This is the first time that H-NOX activation of a bacterial enzyme has been reported. It is also the first time that H-NOX regulation of more than one enzymatic activity in the same protein has

been reported. In future studies we plan to elucidate a molecular-level understanding of how *Sw*H-NOX achieves variable regulation of multiple active sites (*S. woodyi* only codes for one H-NOX). In doing so, we should be able to gain insight into how H-NOX regulates enzymatic function in general, which would enhance understanding of both the bacterial and eukaryotic NO/H-NOX signal transduction pathways.

In order to understand the biological function of NO/H-NOX we are also planning to investigate how the *hnox* gene is regulated. It is possible that H-NOX is constitutively expressed, in order to quickly respond to changing NO concentrations. On the other hand, its expression may be regulated directly by NO or some other environmental signal (related to biofilm formation or anaerobic respiration, perhaps) or by growth phase or cell density.

3.4.3 C-di-GMP signaling in *Shewanella*

Although this study was primarily carried out as a model system to investigate the biological role of NO/H-NOX signaling in bacteria, there are several important implications for Shewanella biology suggested by our data.

Shewanella are ubiquitous in marine environments and are thought to play a role in regulating global carbon and nitrogen cycles as well as the biodegradation of marine pollutants [186]. *Shewanella* genomes generally have a very high number of GGDEF- and EAL-containing proteins; *S. oneidensis* is predicted to express 51 proteins with GGDEF domains, 27 proteins with EAL domains, and 20 proteins containing both GGDEF and EAL domains. *S. woodyi* carries genes for 45 GGDEF-containing proteins, 19 EAL-containing proteins, and 22 hybrid proteins. The high abundance of c-di-GMP synthesis and degradation proteins indicates a special

role for c-di-GMP signaling in *Shewanella*, possibly due to the importance of biofilm growth for these bacteria.

Although none of the other predicted GGDEF and EAL proteins in *S. woodyi* have been characterized, our data clearly indicate that *Swoo_2751* is not the only active di-guanylate cyclase in *S. woodyi* under our experimental conditions. In particular, Fig. 3 indicates that c-di-GMP levels do not drop to baseline either in the presence of NO, or absence of *Sw*H-NOX, both of which are conditions that down-regulate di-guanylate cyclase activity and up-regulate phosphodiesterase activity in the *Sw*H-NOX/*Sw*DGC system reported here. It is possible that each GGDEF/EAL protein may monitor a different environmental or cellular condition, and in response to that individual stimulus (oxygen levels, carbon levels, etc.), modulate the total c-di-GMP concentration in the cell. In this model, c-di-GMP-mediated cell adhesion is an individual cell's response to the synthesis of complex information. This is consistent with other models for c-di-GMP signaling in bacteria [31, 183, 187-189]. It is also supportive of the "local ecological adaptation of individuals" model of biofilm formation recently suggested [155, 190-192].

Nonetheless, in this study, evidence that *Sw*DGC has a relatively large effect on overall c-di-GMP concentrations and biofilm formation (Figs. 3-2 and 3-3) is presented. This large effect is underscored by the fact that *Sw*DGC is but 1 of 45 c-di-GMP metabolizing enzymes predicted in the genome of *S. woodyi*. This may be because of the importance of NO as an environmental cue for *Shewanella*.

Shewanella are able to use a wide variety of molecules as alternate electron acceptors to molecular oxygen in respiration under low oxygen tension [193]. Notably, NO is an endogenous product of anaerobic respiration on nitrite and nitrate [194, 195]. Thus, *S. woodyi* likely

encounter NO in their environment upon reduction of nitrite when nitrate or nitrite is being used as an alternative electron acceptor. Interestingly, the interior of biofilms are thought to be anaerobic [196], thus, generation of NO could occur in the interior of thick *S. woodyi* biofilms as a feedback signal, causing biofilm dispersal and thus preventing the biofilm community from getting too large.

In addition to respiration on nitrate or nitrite, we have also considered other sources of NO that *S. woodyi* may encounter, including NO generated by nitric oxide synthase enzymes due to gram-positive bacteria [197] that may be occupying the same niche as *S. woodyi*, or pathogenic or symbiotic association with eukaryotes (*S. woodyi* does not have a readily identifiable nitric oxide synthase gene in its genome). In support of a possible eukaryotic symbiotic role, *S. woodyi* is one of only a few members of the *Shewanellaceae* family that is bioluminescent, a trait that is sometimes associated with symbiosis [198]. Furthermore, *S. woodyi* was first discovered in association with squid ink [199].

At the present, the natural source of NO that causes biofilm dispersal (or reduced biofilm formation) in *S. woodyi* is not known, so it is difficult for us to further speculate on the role of NO/H-NOX in the biology of *S. woodyi*. We note, however, that if the source of NO is anaerobic respiration on nitrate/nitrite, one might expect other *Shewanella* species to have similar NO/biofilm responses. Interestingly, while other *Shewanella* have H-NOXs, they are not always predicted to be in the same operon as a DGC. For example, in *S. oneidensis*, *So*H-NOX is thought to regulate phosphorylation of a histidine kinase [114]. The downstream result of this phosphorylation is not known, however, so it is possible that NO/H-NOX in *S. oneidensis* still feeds into c-di-GMP signaling pathways.

Regardless, we do not suppose that the NO/*Sw*H-NOX/*Sw*DGC system reported here is the only mechanism for controlling biofilm growth in *S. woodyi.* Rather, we hypothesize that NO is one of perhaps many endogenous and exogenous signals that *S. woodyi* monitors in order to regulate planktonic v. sessile growth.

Chapter 4 Discover and characterize a *Sw*H-NOX regulated two-component signaling pathway in *Shewanella woodyi*

Key to the Chapter

This chapter reveals NO regulation of *S. woodyi* through a potential H-NOX/HK pathway, indicating a multi-effector H-NOX signaling network.

Abstract

In *Shewanella woodyi*, nitric oxide (NO) binds to NO sensor *Sw*H-NOX and mediates *Sw*HaCE diguanylate cyclase and phosphodiesterase activity, resulting in a decreased secondary messenger cyclic di-GMP level. The degradation of intracellular c-di-GMP leads to less biofilm formation. In this study, biofilm analysis of Δ*hace* mutant display a weaker response to NO comparing to wildtype, suggesting a potential second effector of H-NOX. SMART (Simple Module Architecture Research Tool) analysis suggests a swoo_2833 gene that is annotated as a histidine kinase (*Sw*HK) to be a target of *Sw*H-NOX. This protein is a homologue of *V. harveyi* HqsK, a protein that has been shown to interact with *Vh*H-NOX and participates in quorum sensing in response to NO. Biofilm formations of wildtype, Δ*hk*, Δ*hnox*/Δ*hk*, and Δ*hace*/Δ*hk* strains of *S. woodyi* are examined in the presence and absence of NO. Results indicate that *Sw*HK activity is affected by *Sw*H-NOX. Disrupting *hk* gene decreased biofilm formation as well as the response to NO. Further disruption of *hnox* in the Δ*hk* mutant abolishes NO regulation.

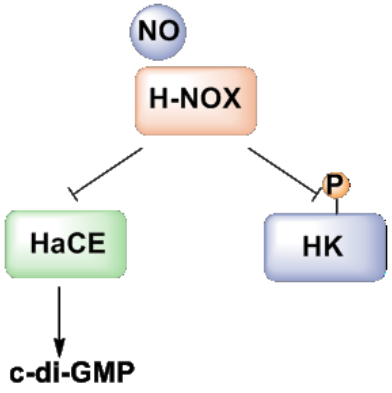

4.1 Introduction

NO regulation of biofilm formation and/or dispersal has been established in many bacterial species. Previous studies of several organisms have indicated that NO mediates bacterial biofilm level by acting on H-NOX proteins [88, 89, 111, 212], a homologue of the N-terminus sensory domain of sGC [112]. Thus far, H-NOXs regulation is limited to proteins encoded by adjacent genes of *hnox*. For example, in *S. woodyi* and *Legionella pneumophila*, H-NOX directly interacts with a DGC-PDE enzyme (*Sw*HaCE and *lpg*1057) [93, 115]. In *S. oneidensis*, *V. harveyi* and *Pseudoalteromonas atlantica,* NO-bound H-NOX inhibits autophosphorylation of the associated HK (*So*HnoK, *Vh*HqsK and *Pa*HahK) [97, 114, 200]. However, it is unclear whether an H-NOX only has a single effector. Given that H-NOX is the only NO sensor identified in these organisms, and NO can regulate various bacterial behaviors such as biofilm formation and bioluminescent production [93, 94, 97, 115, 116], it is probable that an H-NOX can have multiple targets.

In this study, a homologue of *Vh*HqsK is identified in *S. woodyi* (*Swoo*_2833, *Sw*HK). The purified *Sw*HK can interact with *Sw*H-NOX. Phenotypic analysis of gene disrupted mutants indicates that *Sw*HaCE and *Sw*HK are both regulated by *Sw*H-NOX. The two effectors respond to H-NOX synergistically, leading to a biofilm repressed phenotype upon NO exposure.

4.2 Materials and Methods

Bacterial strains and growth conditions. Strains used in this study are listed in Table 4-1. *E. coli* strains DH5α and BL21(DE3)pLysS were used throughout this study for plasmid amplification and protein purification. These strains were grown in Luria Broth (LB; 20 g/L; EMD chemicals) at 37 °C with agitation at 250 rpm. *E. coli* WM3064 was used as a donor for conjugation and was grown in LB complemented with 2,3-Diaminopropionic acid (DAP; 0.36

mM; Sigma Aldrich). *S. woodyi* strains were grown in Marine Media Broth (MM; 28 g/L; BD Difco) at 25 °C with agitation at 250 rpm. *Sw* transconjugants were grown on LB (10 g/L) / MM (14 g/L) / Bacto Agar (BA; 10 g/L; BD Difco) plates at 25 °C.

Table 4-1. Bacterial strains and PCR primers used in this chapter.

Strains and plasmids	Relevant characteristics	Ref.
Bacterial strains		
S. woodyi		
*Sw*MS32 (WT)	*Shewanella woodyi* MS32, ATCC 51908	[193]
Δ*hace*	*Sw*MS32 Δ*Swoo_2750*	This work
Δ*hnox*/Δ*hace*	*Sw*MS32 Δ*Swoo_2750*/Δ*Swoo_2751*	This work
Δ*hk*	*Sw*MS32 Δ*Swoo_2833*	This work
Δ*hnox*/Δ*hk*	*Sw*MS32 Δ*Swoo_2751*/*ΔSwoo_2833*	This work
Δ*hace*/Δ*hk*	*Sw*MS32 Δ*Swoo_2750*/*ΔSwoo_2833*	This work
E. coli		
WM3064	Mating strain	[201]
BL21(DE3) pLysS	Expression strain	
Plasmids		
pSMV3	Deletion vector, Km^r, *sacB*	[169]
pBBR1MCS-2	Broad range cloning vector, Km^r	[170]
pΔ*hk*	pSMV3 with 1kbp upstream and downstream of *hk*	This work
pΔ*hace*	pSMV3 with 1kbp upstream and downstream of *hace*	This work
pΔ*hnox/Δhace*	pSMV3 with 1kbp upstream and downstream of *hnox-hace*	This work
Primers		
Gene deletion primers		
hace-up-fw	*NNNGGATTC CACATAGTTTGGACACCTAAG	
hace-up-rv	*NNNGAATTC AACATTAGCCCCTGTTTTAA	
hace-down-fw	*NNNGAATTC TTATGAGTGCACTTGAGGACA	
hace-down-rv	*NNNNNNNNNGCGGCCGC CACAATAGAGAACTCATCTC	
hnox-up-fw	*NNNGGATCCCACATAGTTTGGACACCTAAG	
hnox-up-rev	*NNNGAATTCAACATTAGCCCCTGTTTTAA	
HK-up rv	AAAGAATTCAAACCAACAGCTTTCC	
HK-dw fw	AAAGAATTCTCAACTCGCCAGTTT	
HK-dw rv	AAACCACAACGCGGCCGCATTGCACGTGTCTATGC	
Confirmation primers		
PCRHK-KIFW	CATCTTATTGGAAAAAATTGC	
PCRHK-KIRV	GAGAGTGACCTTGATGGCTATCGACACC	
Complementation primers		

HK-KIFW	AAATTGAATTCTACAAGATAAAATTAGCAAGATAGGAAAGC
HK-KIRV	AAATTACTAGTTTAATTCAATGGATTCCATTTCATTAATATCG
Cloning primers	
GST-HK FW	AAGGAATTCCCATGAGTGATAAAGAGG
GST-HK RV	AAAGCGGCCGCTTAATTCAATGGATTCCATTTC

Construction of in-frame gene disruption mutant strains. The gene-deleted vectors were constructed as previously described [93]. PCR was used to amplify regions of gDNA flanking the target genes (*hnox/hace*, *hace, hk*) from *Shewanella woodyi* strain MS32 genomic DNA (ATCC strain 51908) using Phusion® polymerase (New England Biolabs). The 1kb upstream gDNA was amplified containing BamHI and EcoRI restriction sites, respectively. The downstream gDNA was amplified containing EcoRI and NotI restriction sites. The up- and downstream fragments were fused by ligation at the common EcoRI restriction site. This fused product was cloned into pSMV3 [202] using the NotI and BamHI restriction sites and sequenced (Stony Brook DNA sequencing facility). The following conjugation protocol is as previously reported [93]. In brief, the vectors were transformed into the plasmid donor strain *E. coli* WM3064 and mated with *Sw*MS32. The resulting *S. woodyi* transconjugants containing the deletion vector were then plated on LB/MM/BA plates containing 5% sucrose at 25 °C to select for double recombination events. Kanamycin sensitive colonies were screened by colony PCR to confirm gene deletion using primers hnox-up-fw, and hnox-down-rev (Table 4-1).

Biofilm imaging by confocal microscopy. CLSM images were taken as previously described [93] with some modifications. Overnight inoculum of *S. woodyi* wildtype and mutant strains were diluted (1:100) and grew in MM in 4-well glass microscope chamber slides at 25 °C for 24 hours. The slides were rinsed with distilled water and stained with the LIVE/DEAD BacLight^{TM}

kit (Invitrogen^{TM}). The biofilm formed at the air-liquid interface was then imaged and analyzed. Confocal images for each of three independently grown biofilms of each strain (wild-type, Δ*hk*, Δ*hnox*/Δ*hk* and Δ*hace*/Δ*hk* mutant *S. woodyi*) were separately obtained and analyzed.

Crystal violet (CV) staining for biofilm quantification. Steady-state biofilm was quantified in 96-well polyvinyl chloride (PVC) plates as has been previously described [93]. An overnight starting culture was diluted (1:100) into 100 µL subculture and incubated at 25 °C for 24 hours. After removing growth media and washing plates with water, remaining biofilm cells were stained with CV. Excess CV was then removed by washing and DMSO was added to solubilize the CV adsorbed by the biofilm cells. The absorbance of CV/DMSO solution that indicates biofilm mass was measured by a Perkin Elmer Victor^{TM} X5 multiplate reader at 570nm. For biofilms grown in the presence of NO, a final concentration of 200 µM diethylenetriamine NONOate (DETA/NO; Cayman Chemicals) was added as an NO donor (60-80nM NO).

Pull-down assay. Swoo_2833 gene (*Sw*HK) is cloned into a pGEX4T-2 (GE Life Science) vector using Pfu Turbo polymerase to incorporate a Glutathione S-transferase (GST) tag. Forward and reverse primers contained EcoRI and NotI restriction sites, respectively. GST constructs were purified from Bl21 cells (induced with 200 µM IPTG for 8 hrs at 16 ºC). The pull-down assay was done as previously described with a few modifications. Pellets were lysed by sonication and resulting supernatant was incubated with Glutathione sepharose beads for 30 min followed by washing (50 mM Tris, 500 mM KCl, 1 mM PMSF, 2 mM BME). The beads were incubated with 10 µM His_6 tagged *Sw*H-NOX in the same buffer for overnight at 4 ºC with gentle rocking. Beads were then washed three times to remove excess unbound protein and analyzed by SDS-PAGE followed by Western Blot analysis. Polyclonal anti-His antibody (Abcam) was used in 5% milk to detect the presence of His_6 tagged *Sw*H-NOX.

4.3 Results

4.3.1 NO regulates *S. woodyi* biofilm level by acting on *Sw*H-NOX to mediate *Sw*HaCE

Previously, we have shown that purified *Sw*H-NOX directly interacts with *Sw*HaCE *in vitro* and promotes PDE over DGC activity upon NO exposure [93]. To confirm the regulation of NO-bound H-NOX *in vivo*, gene disrupted Δ*hace* and Δ*hnox*/Δ*hace* mutant strains of *S. woodyi* were constructed and biofilm level was examined as a phenotype of NO regulation. The condition of biofilm formation was same as mentioned in Chapter 2 [93]. A DETA NONOate [173] was added as an NO donor to provide constant NO (60-80 nM) throughout biofilm formation process. Relative biofilm level with the absence and presence of NO was shown as Figure 4-1. The deletion of *hace* caused a modest decrease of biofilm comparing to wildtype. This was expected as *Sw*HaCE acts as a DGC in the presence of *Sw*H-NOX. Therefore, a disruption of *Sw*HaCE results in less accumulation of intracellular c-di-GMP [93]. The repression was not significant, since *S. woodyi* has a complex c-di-GMP metabolism network and the bacteria genome carries 45 GGDEF proteins, 19 EAL proteins, and 22 hybrid proteins [168]. Further disruption of *hnox* gene abolished NO regulation effect, suggesting that *Sw*HaCE was mediated by *Sw*H-NOX. Additionally, exposure to NO led to a repression of biofilm formation of Δ*hace*, indicating a potential *Sw*H-NOX effector other than *Sw*HaCE.

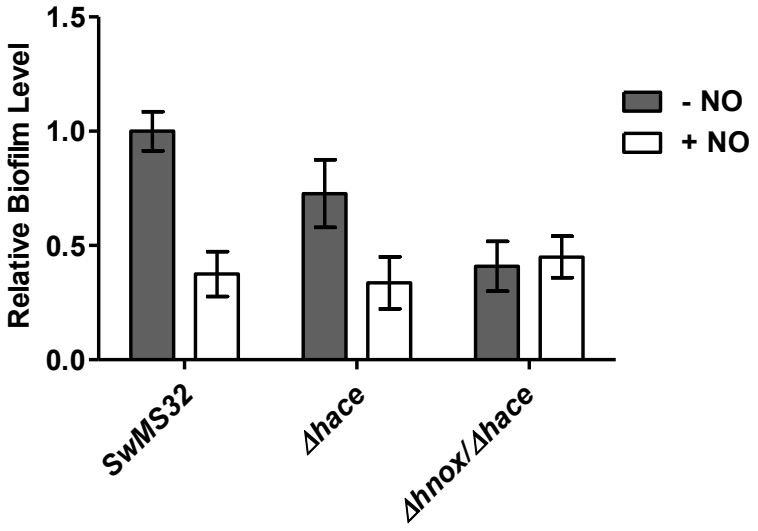

Figure 4-1. Biofilm CV quantification of wildtype, Δ*hace* and Δ*hnox*/Δ*hace* strains of *S. woodyi*.

4.3.2 *Sw*HK is a *Sw*H-NOX effector

To validate our theory, a SMART (Simple Module Architecture Research Tool) analysis was done to explore candidates of *Sw*H-NOX target based on neighborhood, gene fusion, occurrence and coexpression information in bacteria species that encodes for *hnox* genes [203, 204]. Among the three predicted functional partners (Swoo_2833, Swoo_4063, and Swoo_4721), the Swoo_2833 protein was the most probable one, due to its homology to *Vh*HqSK, a verified H-NOX effector in *V. harveyi* that participates in quorum sensing behavior [116]. Same as *Vh*HqSK, Swoo_2833 (*Sw*HK) is a LuxQ type two component histidine kinase that has both a kinase domain and a receiver domain. A CLUSTAL sequence alignment of *Sw*HK with several H-NOX related HKs from different organisms implied that it is a homologue (Figure 4-2), and therefore likely to be a *Sw*H-NOX effector.

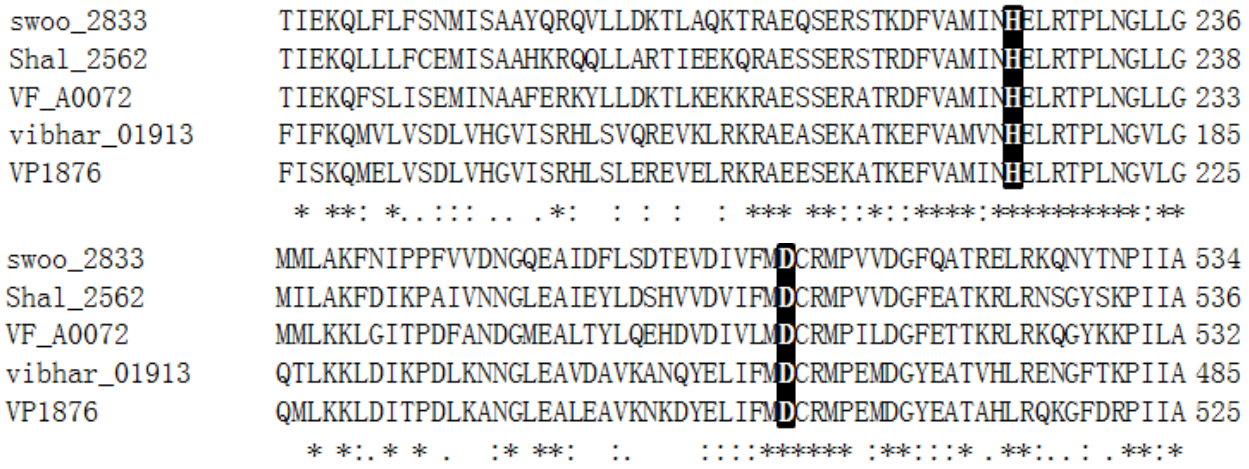

Figure 4-2. Partial BLAST alignment of *Sw*HK with LuxQ type H-NOX-adjacent HKs (Organisms from top to bottom: *S. woodyi*, *Shewanella halifaxensis*, *V. fischeri*, *V. harveyi* and *Vibrio parahaemolyticus*). Conserved autophosphorylation site (His) and phosphate acceptor (Asp) are labeled. A full length alignment is attached as Appendix 3.

To verify the hypothesis, a co-immunoprecipitation assay was performed with GST-tagged *Sw*HK and GST as bait to pull-down His_6-tagged *Sw*H-NOX from *E.coli* cell lysates. A small amount of *Sw*H-NOX is detected by anti-His antibody in the presence of *Sw*HK, indicating SwHK being a binding partner of *Sw*H-NOX *in vivo* (Figure 4-3).

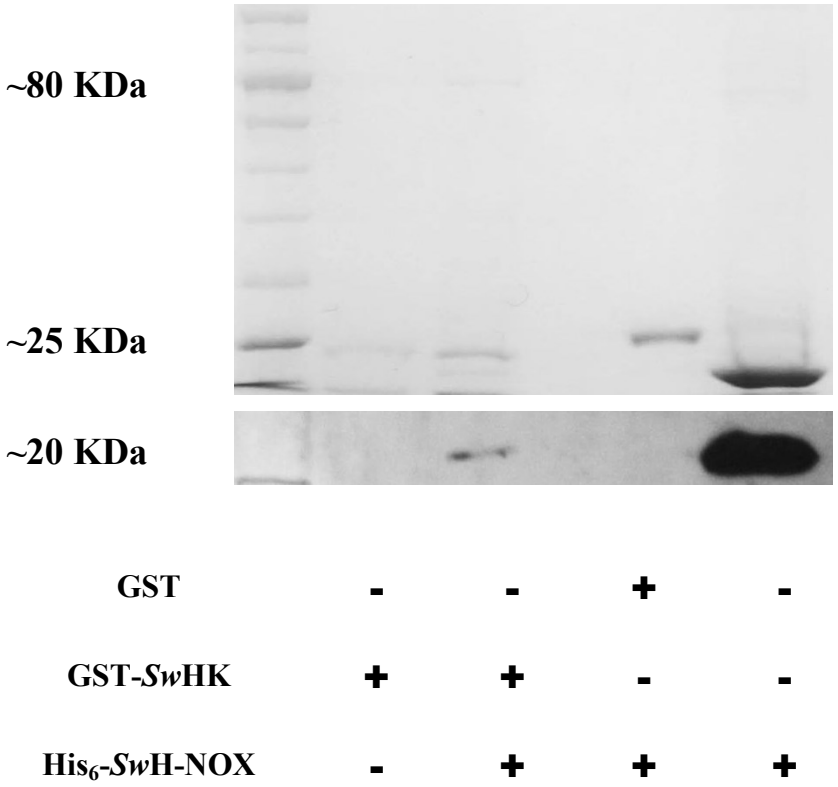

Figure 4-3. *Sw*HK can bind *Sw*H-NOX. Top: The far left lane is a molecular weight marker; the next lane to the right is GST-*Sw*HK alone (~92 KDa); the subsequent two lanes are GST-*Sw*HK or GST only (~ 27KDa) incubated with His_6-*Sw*H-NOX (~22 KDa), respectively. The far right lane is a positive control of His_6-*Sw*H-NOX. Bottom: Detection of *Sw*H-NOX pulled-down by *Sw*HK via Anti-His Western blot.

4.3.3 *Sw*HaCE and *Sw*HK act synergistically in response to NO-bound *Sw*H-NOX

Once the *Sw*H-NOX target was validated, we set out to explore detailed regulation mechanism. Gene disrupted mutants Δ*hk*, Δ*hnox*/Δ*hk* and Δ*hace*/Δ*hk* were made as previously described[93]. Quantitative crystal violet (CV) assay (Figure 4-3A) and qualitative confocal laser microscopic imagining (CLSM) (Figure 4-3B) were done to assess biofilm formation in *Sw*HK disrupted mutants.

A.

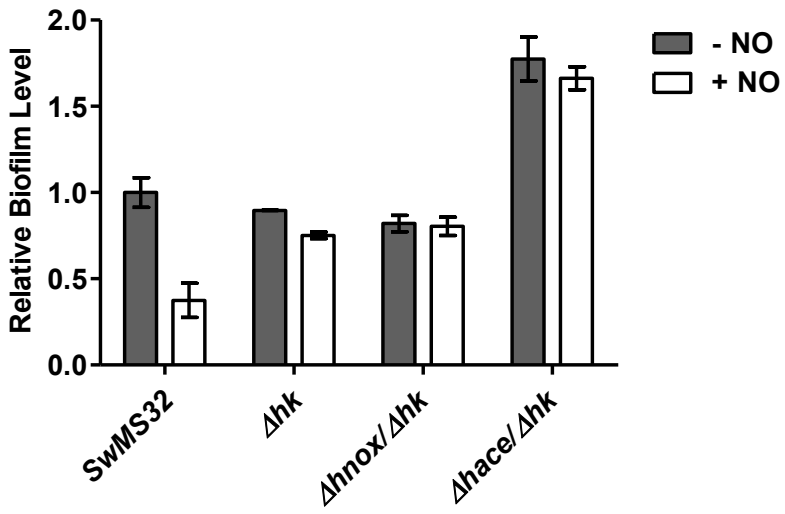

B.

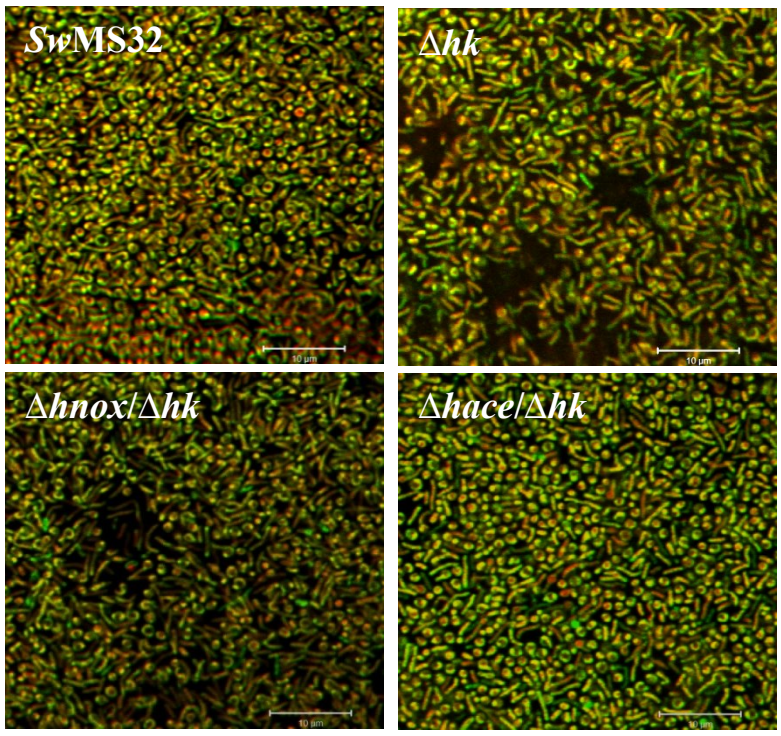

Figure 4-4. Biofilm formation of wild-type, Δ*hk*, Δ*hnox* and Δ*hace*/Δ*hk* mutant strains of *S.woodyi* analyzed by A) CV assay and B) CLSM; cells were stained with SYTO®9 (green; stains live cells) and propidium iodide (red; stains dead cells only). Bar = 10 μM.

The deletion of *hnox* gene in all of the wildtype or mutant strains abrogated the NO effect on biofilm level (Figure 4-1 and Figure 4-4A), suggesting that this phenotype is related to *Sw*H-NOX. As shown in Figure 3A, Δ*hk* biofilm was repressed by NO. This result consolidated our previous hypothesis that when exposed to NO, *Sw*H-NOX can enhance the PDE activity of *Sw*DGC, leading to a decrease in biofilm level. The great increase of biofilm when both *Sw*HaCE and *Sw*HK were disrupted showed a synergistic effect of biofilm enhancement when both enzymes are deactivated. The detailed mechanism was yet unclear. To corroborate with the CV quantification, confocal images of *S. woodyi* biofilms were taken for analysis. The disruption of *Sw*H-NOX and *Sw*HK resulted in a decrease of cell density due to an active *Sw*HaCE as a phosphodiesterase (Figure 4-4B). The Δ*hace*/Δ*hk* mutant formed a much denser biofilm.

4.4 Discussion

To date, very little is known about the molecular mechanism of NO regulation of bacterial biofilm at a low non-lethal level. So far the only known bacterial NO sensor is H-NOX. Previous studies have shown that H-NOXs are involved in signaling networks to mediate intracellular c-di-GMP level [93, 94]. However, all reports only identified a single effector encoded by the adjacent gene of *hnox* [93, 94, 97, 115, 200]. In this study, we extend H-NOX regulation to multiple effectors that can act synergistically *in vivo*. Results indicate that both *Sw*HaCE and *Sw*HK are under the regulation of H-NOX and lead to a repressed biofilm phenotype upon exposure to NO.

A possible explanation for the synergistic effect of *Sw*HaCE and *Sw*HK is that *Sw*HK is regulating multiple response regulators, in turn fine-tuning the intracellular c-di-GMP pool. The cross-talk between two RRs is typical in connecting distinct pathways [205]. One such example is the *Shewanella oneidensis* multi-component signaling network. The H-NOX related *So*HNOK

phosphorylates three receiver domains, and the HD-GYP domain containing RR HnoD inhibits PDE activity of HnoB, forming a feed-forward loop that provides extra tuning of c-di-GMP level [94]. In *S. woodyi*, among the predicted RRs of *Sw*HK by SMART, Swoo_1514 (RR) is in the same operon with a GGEEF containing RR (Swoo_1513, PleD) that is a homologue of *Caulobacter crescentus* PleD and a sensory hybrid histidine kinase (Swoo_1514, HHK) (Figure 4-5). As a cyclase, PleD synthesizes c-di-GMP and also receives a feed-back inhibition when c-di-GMP binds to allosteric sites [206]. Both *Sw*PleD and *Sw*RR receive phosphate groups from *Sw*HK and *Sw*HHK, and phosphorylated *Sw*RR inhibits the cyclase activity of *Sw*PleD, allowing a dual control of c-di-GMP production (Figure 4-6). To validate the hypothesis, *in vitro* phosphotransfer assay and confirmation of PleD cyclase activity is needed.

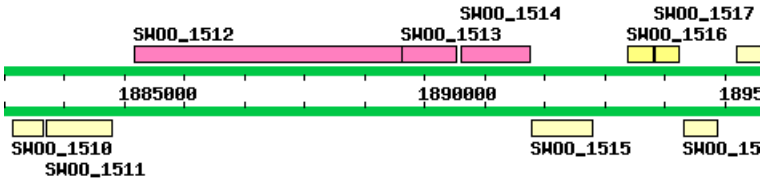

Figure 4-5. Organization of the *hhk*, *pled*, and *rr* genes.

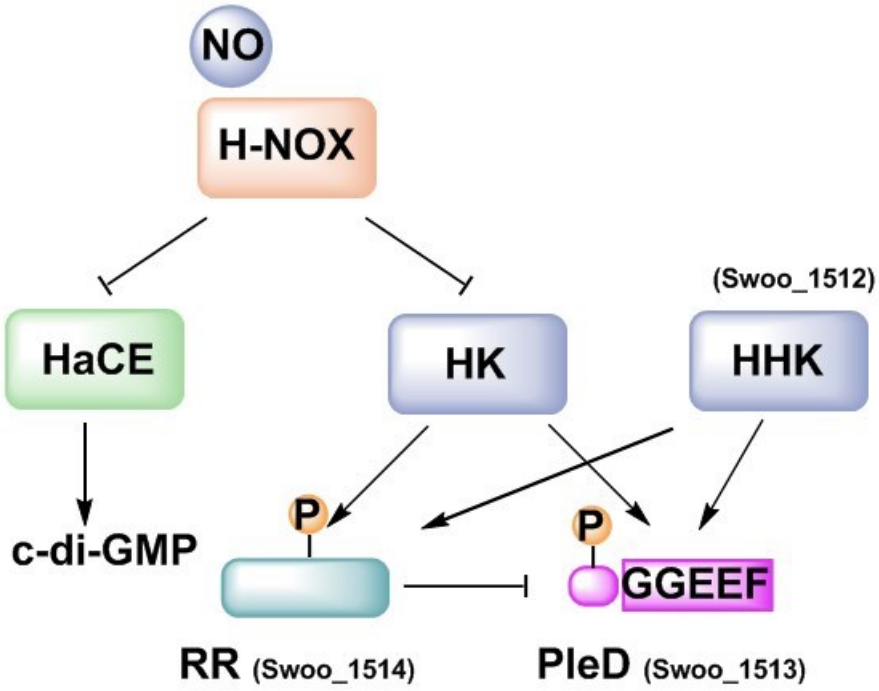

Figure 4-6. Model of H-NOX signaling network.

Chapter 5 Summary and Future Directions

In this dissertation, we have dedicated our effort towards exploring the mechanism of NO regulation of bacterial biofilms at a non-lethal level. Firstly, we validated our hypothesis that the H-NOX acts as a dedicated NO sensor in some bacteria species, and thereby mediates neighboring effector proteins upon NO exposure. Depends on the function of the downstream effector, the signaling pathway may vary. For H-NOX/HaCE systems, intracellular c-di-GMP synthesis and degradation is modified [93]. For H-NOX/HqSK systems, NO participates in a quorum sensing pathway, regulating bacterial behavior on a transcription level [116].

Secondly, we correlated biofilm phenotypes with NO regulation *in vivo* and proposed a mechanism. Based on the proteomics analysis of *V. harveyi*, it is probable that NO brings about a change of global protein expression, leading to a decrease in cell motility and facilitates initial attachment.

Lastly, we have extended the scope of H-NOX initiated signaling network and shown that it is not an isolated pathway, and the search for H-NOX effector may not be limited to adjacent proteins. Since NO is a broad-spectrum signaling molecule that mediates various bacterial behaviors, it is likely that H-NOX as the sensor can interact with multiple proteins and participates in different pathways. The cross-regulation between response regulators enables c-di-GMP to control cellular process at a wide range, owing to different affinities of c-di-GMP receptors [207].

Even as a small molecule, NO can target multiple physiological pathways at a high level with minimal drug resistance [98], at a low concentration level, the signaling effect is not unanimous. Bacteria species respond to NO at different concentration and displays diverse phenotypes.

Therefore, to harness the power of this behavioral modifier, more work needs to be done to identify dedicated NO sensors or proteins respond to NO as well as their effectors within organisms that do not encode for *hnox* genes. From there, we can develop NO substitutes for specific purposes and regulate bacterial behavior in a non-lethal way.

Reference

1. Henrici, A. T. (1933) Studies of Freshwater Bacteria: I. A Direct Microscopic Technique, *Journal of Bacteriology.* **25**, 277-287.
2. Geesey, G. G., R. Mutch, and Costerton, J. W. (1978) Sessile bacteria: An important component of the microbial population in small mountain streams, *the American Society of Limnology and Oceanography.* **23**, 1214-1223.
3. O'Toole, G., Kaplan, H. B. & Kolter, R. (2000) Biofilm Formation as Microbial Development, *Annual Review of Microbiology.* **54**, 49-79.
4. Costerton, J. W., Lewandowski, Z., Caldwell, D. E., Korber, D. R. & Lappin-Scott, H. M. (1995) Microbial Biofilms, *Annual Review of Microbiology.* **49**, 711-745.
5. Bryant, M. P., Wolin, E. A., Wolin, M. J. & Wolfe, R. S. (1967) *Methanobacillus omelianskii*, a symbiotic association of two species of bacteria, *Archiv Mikrobiol.* **59**, 20-31.
6. Davey, M. E. & O'toole, G. A. (2000) Microbial Biofilms: from Ecology to Molecular Genetics, *Microbiol Mol Biol Rev.* **64**, 847-867.
7. Flemming, H.-C. (1993) Biofilms and Environmental Protection, *Water Science & Technology.* **27**.
8. Davies, D. (2003) Understanding Biofilm Resistance to Antibacterial Agents, *Nat Rev Drug Discov.* **2**, 114-122.
9. McLeod, B. R., Fortun, S., Costerton, J. W. & Stewart, P. S. (1999) Enhanced bacterial biofilm control using electromagnetic fields in combination with antibiotics in *Methods in Enzymology* (Ron, J. D., ed) pp. 656-670, Academic Press.
10. Yu, F. P. & McFeters, G. A. (1994) Rapid in situ assessmetn of physiological activities in bacterial biofilms using fluorescent probes, *Journal of Microbiological Methods.* **20**, 1-10.
11. Ross, P., Weinhouse, H., Aloni, Y., Michaeli, D., Weinberger-Ohana, P., Mayer, R., Braun, S., de Vroom, E., van der Marel, G. A., van Boom, J. H. & Benziman, M. (1987) Regulation of cellulose synthesis in *Acetobacter xylinum* by cyclic diguanylic acid, *Nature.* **325**, 279-281.
12. Römling, U., Galperin, M. Y. & Gomelsky, M. (2013) Cyclic di-GMP: the First 25 Years of a Universal Bacterial Second Messenger, *Microbiology and Molecular Biology Reviews.* **77**, 1-52.
13. Paul, R., Weiser, S., Amiot, N. C., Chan, C., Schirmer, T., Giese, B. & Jenal, U. (2004) Cell cycle-dependent dynamic localization of a bacterial response regulator with a novel di-guanylate cyclase output domain, *Genes & Development.* **18**, 715-727.
14. Ryjenkov, D. A., Tarutina, M., Moskvin, O. V. & Gomelsky, M. (2005) Cyclic Diguanylate Is a Ubiquitous Signaling Molecule in Bacteria: Insights into Biochemistry of the GGDEF Protein Domain, *Journal of Bacteriology.* **187**, 1792-1798.
15. Aldridge, P. & Jenal, U. (1999) Cell cycle-dependent degradation of a flagellar motor component requires a novel-type response regulator, *Molecular Microbiology.* **32**, 379-391.
16. Aldridge, P., Paul, R., Goymer, P., Rainey, P. & Jenal, U. (2003) Role of the GGDEF regulator PleD in polar development of Caulobacter crescentus, *Molecular Microbiology.* **47**, 1695-1708.
17. Hecht, G. B. & Newton, A. (1995) Identification of a novel response regulator required for the swarmer-to-stalked-cell transition in *Caulobacter crescentus*, *Journal of Bacteriology.* **177**, 6223-9.

18. Schmidt, A. J., Ryjenkov, D. A. & Gomelsky, M. (2005) The Ubiquitous Protein Domain EAL Is a Cyclic Diguanylate-Specific Phosphodiesterase: Enzymatically Active and Inactive EAL Domains, *Journal of Bacteriology.* **187**, 4774-4781.
19. Ryan, R. P., Fouhy, Y., Lucey, J. F., Crossman, L. C., Spiro, S., He, Y.-W., Zhang, L.-H., Heeb, S., Cámara, M., Williams, P. & Dow, J. M. (2006) Cell–cell signaling in *Xanthomonas campestris* involves an HD-GYP domain protein that functions in cyclic di-GMP turnover, *Proceedings of the National Academy of Sciences.* **103**, 6712-6717.
20. Christen, M., Christen, B., Folcher, M., Schauerte, A. & Jenal, U. (2005) Identification and Characterization of a Cyclic di-GMP-specific Phosphodiesterase and Its Allosteric Control by GTP, *Journal of Biological Chemistry.* **280**, 30829-30837.
21. Mills, E., Pultz, I. S., Kulasekara, H. D. & Miller, S. I. (2011) The bacterial second messenger c-di-GMP: mechanisms of signalling, *Cellular Microbiology.* **13**, 1122-1129.
22. Chang, A. L., Tuckerman, J. R., Gonzalez, G., Mayer, R., Weinhouse, H., Volman, G., Amikam, D., Benziman, M. & Gilles-Gonzalez, M.-A. (2001) Phosphodiesterase A1, a Regulator of Cellulose Synthesis in *Acetobacter xylinum*, Is a Heme-Based Sensor†, *Biochemistry.* **40**, 3420-3426.
23. Tuckerman, J. R., Gonzalez, G., Sousa, E. H. S., Wan, X., Saito, J. A., Alam, M. & Gilles-Gonzalez, M.-A. (2009) An Oxygen-Sensing Diguanylate Cyclase and Phosphodiesterase Couple for c-di-GMP Control, *Biochemistry.* **48**, 9764-9774.
24. Spiers, A. J., Bohannon, J., Gehrig, S. M. & Rainey, P. B. (2003) Biofilm formation at the air–liquid interface by the *Pseudomonas fluorescens* SBW25 wrinkly spreader requires an acetylated form of cellulose, *Molecular Microbiology.* **50**, 15-27.
25. Drenkard, E. & Ausubel, F. M. (2002) *Pseudomonas* biofilm formation and antibiotic resistance are linked to phenotypic variation, *Nature.* **416**, 740-743.
26. Ueda, A. & Wood, T. K. (2009) Connecting Quorum Sensing, c-di-GMP, Pel Polysaccharide, and Biofilm Formation in *Pseudomonas aeruginosa* through Tyrosine Phosphatase TpbA (PA3885), *PLoS Pathog.* **5**, e1000483.
27. Ryan, R. P., McCarthy, Y., Andrade, M., Farah, C. S., Armitage, J. P. & Dow, J. M. (2010) Cell–cell signal-dependent dynamic interactions between HD-GYP and GGDEF domain proteins mediate virulence in *Xanthomonas campestris*, *Proceedings of the National Academy of Sciences.* **107**, 5989-5994.
28. Malone, J. G., Jaeger, T., Manfredi, P., Dötsch, A., Blanka, A., Bos, R., Cornelis, G. R., Häussler, S. & Jenal, U. (2012) The YfiBNR Signal Transduction Mechanism Reveals Novel Targets for the Evolution of Persistent *Pseudomonas aeruginosa* in Cystic Fibrosis Airways, *PLoS Pathog.* **8**, e1002760.
29. Andrade, M. O., Alegria, M. C., Guzzo, C. R., Docena, C., Pareda Rosa, M. C., Ramos, C. H. I. & Farah, C. S. (2006) The HD-GYP domain of RpfG mediates a direct linkage between the Rpf quorum-sensing pathway and a subset of diguanylate cyclase proteins in the phytopathogen *Xanthomonas axonopodis* pv citri, *Molecular Microbiology.* **62**, 537-551.
30. Kulesekara, H., Lee, V., Brencic, A., Liberati, N., Urbach, J., Miyata, S., Lee, D. G., Neely, A. N., Hyodo, M., Hayakawa, Y., Ausubel, F. M. & Lory, S. (2006) Analysis of *Pseudomonas aeruginosa* diguanylate cyclases and phosphodiesterases reveals a role for bis-(3′-5′)-cyclic-GMP in virulence, *Proceedings of the National Academy of Sciences of the United States of America.* **103**, 2839-2844.

31. Lim, B., Beyhan, S., Meir, J. & Yildiz, F. H. (2006) Cyclic-diGMP signal transduction systems in *Vibrio cholerae*: modulation of rugosity and biofilm formation, *Molecular Microbiology.* **60**, 331-348.
32. Lee, V. T., Matewish, J. M., Kessler, J. L., Hyodo, M., Hayakawa, Y. & Lory, S. (2007) A cyclic-di-GMP receptor required for bacterial exopolysaccharide production, *Molecular Microbiology.* **65**, 1474-1484.
33. Chin, K.-H., Lee, Y.-C., Tu, Z.-L., Chen, C.-H., Tseng, Y.-H., Yang, J.-M., Ryan, R. P., McCarthy, Y., Dow, J. M., Wang, A. H. J. & Chou, S.-H. (2010) The cAMP Receptor-Like Protein CLP Is a Novel c-di-GMP Receptor Linking Cell–Cell Signaling to Virulence Gene Expression in *Xanthomonas campestris*, *Journal of Molecular Biology.* **396**, 646-662.
34. Tischler, A. D. & Camilli, A. (2005) Cyclic Diguanylate Regulates *Vibrio cholerae* Virulence Gene Expression, *Infection and Immunity.* **73**, 5873-5882.
35. Simm, R., Morr, M., Kader, A., Nimtz, M. & Römling, U. (2004) GGDEF and EAL domains inversely regulate cyclic di-GMP levels and transition from sessility to motility, *Molecular Microbiology.* **53**, 1123-1134.
36. Sultan, S. Z., Pitzer, J. E., Boquoi, T., Hobbs, G., Miller, M. R. & Motaleb, M. A. (2011) Analysis of the HD-GYP Domain Cyclic Dimeric GMP Phosphodiesterase Reveals a Role in Motility and the Enzootic Life Cycle of *Borrelia burgdorferi*, *Infection and Immunity.* **79**, 3273-3283.
37. Purcell, E. B., McKee, R. W., McBride, S. M., Waters, C. M. & Tamayo, R. (2012) Cyclic Diguanylate Inversely Regulates Motility and Aggregation in *Clostridium difficile*, *Journal of Bacteriology.* **194**, 3307-3316.
38. Savakis, P., De Causmaecker, S., Angerer, V., Ruppert, U., Anders, K., Essen, L.-O. & Wilde, A. (2012) Light-induced alteration of c-di-GMP level controls motility of *Synechocystis* sp. PCC 6803, *Molecular Microbiology.* **85**, 239-251.
39. Paul, K., Nieto, V., Carlquist, W. C., Blair, D. F. & Harshey, R. M. The c-di-GMP Binding Protein YcgR Controls Flagellar Motor Direction and Speed to Affect Chemotaxis by a "Backstop Brake" Mechanism, *Molecular Cell.* **38**, 128-139.
40. Fang, X. & Gomelsky, M. (2010) A post-translational, c-di-GMP-dependent mechanism regulating flagellar motility, *Molecular Microbiology.* **76**, 1295-1305.
41. Girgis, H. S., Liu, Y., Ryu, W. S. & Tavazoie, S. (2007) A Comprehensive Genetic Characterization of Bacterial Motility, *PLoS Genet.* **3**, e154.
42. Boyd, C. D. & O'Toole, G. A. (2012) Second Messenger Regulation of Biofilm Formation: Breakthroughs in Understanding c-di-GMP Effector Systems, *Annual Review of Cell and Developmental Biology.* **28**, 439-462.
43. Jenal, U. & Malone, J. (2006) Mechanisms of Cyclic-di-GMP Signaling in Bacteria, *Annual Review of Genetics.* **40**, 385-407.
44. Merritt, J. H., Brothers, K. M., Kuchma, S. L. & O'Toole, G. A. (2007) SadC Reciprocally Influences Biofilm Formation and Swarming Motility via Modulation of Exopolysaccharide Production and Flagellar Function, *Journal of Bacteriology.* **189**, 8154-8164.
45. Weber, H., Pesavento, C., Possling, A., Tischendorf, G. & Hengge, R. (2006) Cyclic-di-GMP-mediated signalling within the σS network of *Escherichia coli*, *Molecular Microbiology.* **62**, 1014-1034.
46. Sudarsan, N., Lee, E. R., Weinberg, Z., Moy, R. H., Kim, J. N., Link, K. H. & Breaker, R. R. (2008) Riboswitches in Eubacteria Sense the Second Messenger Cyclic Di-GMP, *Science.* **321**, 411-413.

47. Lee, E. R., Baker, J. L., Weinberg, Z., Sudarsan, N. & Breaker, R. R. (2010) An Allosteric Self-Splicing Ribozyme Triggered by a Bacterial Second Messenger, *Science.* **329**, 845-848.
48. Miller, M. B., Skorupski, K., Lenz, D. H., Taylor, R. K. & Bassler, B. L. (2002) Parallel Quorum Sensing Systems Converge to Regulate Virulence in *Vibrio cholerae*, *Cell.* **110**, 303-314.
49. Waters, C. M. & Bassler, B. L. (2005) QUORUM SENSING: Cell-to-Cell Communication in Bacteria, *Annual Review of Cell and Developmental Biology.* **21**, 319-346.
50. Miller, M. B. & Bassler, B. L. (2001) QUORUM SENSING IN BACTERIA, *Annual Review of Microbiology.* **55**, 165-199.
51. Nealson, K. H. & Hastings, J. W. (1979) Bacterial bioluminescence: its control and ecological significance, *Microbiological Reviews.* **43**, 496-518.
52. Henke, J. M. & Bassler, B. L. (2004) Quorum Sensing Regulates Type III Secretion in *Vibrio harveyi* and *Vibrio parahaemolyticus*, *Journal of Bacteriology.* **186**, 3794-3805.
53. Bassler, B. L., Wright, M., Showalter, R. E. & Silverman, M. R. (1993) Intercellular signalling in *Vibrio harveyi*: sequence and function of genes regulating expression of luminescence, *Molecular Microbiology.* **9**, 773-786.
54. Tortosa, P., Logsdon, L., Kraigher, B., Itoh, Y., Mandic-Mulec, I. & Dubnau, D. (2001) Specificity and Genetic Polymorphism of the *Bacillus* Competence Quorum-Sensing System, *Journal of Bacteriology.* **183**, 451-460.
55. Waters, C. M., Antiporta, M. H., Murray, B. E. & Dunny, G. M. (2003) Role of the *Enterococcus faecalis* GelE Protease in Determination of Cellular Chain Length, Supernatant Pheromone Levels, and Degradation of Fibrin and Misfolded Surface Proteins, *Journal of Bacteriology.* **185**, 3613-3623.
56. Eijsink, V. G., Brurberg, M. B., Middelhoven, P. H. & Nes, I. F. (1996) Induction of bacteriocin production in *Lactobacillus sake* by a secreted peptide, *Journal of Bacteriology.* **178**, 2232-7.
57. Ng, W.-L. & Bassler, B. L. (2009) Bacterial Quorum-Sensing Network Architectures, *Annual Review of Genetics.* **43**, 197-222.
58. Visick, K. L. & McFall-Ngai, M. J. (2000) An Exclusive Contract: Specificity in the *Vibrio fischeri-Euprymna scolopes* Partnership, *Journal of Bacteriology.* **182**, 1779-1787.
59. Seed, P. C., Passador, L. & Iglewski, B. H. (1995) Activation of the *Pseudomonas aeruginosa* lasI gene by LasR and the Pseudomonas autoinducer PAI: an autoinduction regulatory hierarchy, *Journal of Bacteriology.* **177**, 654-9.
60. Ji, G., Beavis, R. C. & Novick, R. P. (1995) Cell density control of staphylococcal virulence mediated by an octapeptide pheromone, *Proceedings of the National Academy of Sciences.* **92**, 12055-12059.
61. Ng, W.-L., Perez, L. J., Wei, Y., Kraml, C., Semmelhack, M. F. & Bassler, B. L. (2011) Signal production and detection specificity in *Vibrio* CqsA/CqsS quorum-sensing systems, *Molecular Microbiology.* **79**, 1407-1417.
62. Wei, Y., Perez, L. J., Ng, W.-L., Semmelhack, M. F. & Bassler, B. L. (2011) Mechanism of *Vibrio cholerae* Autoinducer-1 Biosynthesis, *ACS Chemical Biology.* **6**, 356-365.
63. Schauder, S. & Bassler, B. L. (2001) The languages of bacteria, *Genes & Development.* **15**, 1468-1480.
64. Henke, J. M. & Bassler, B. L. (2004) Three Parallel Quorum-Sensing Systems Regulate Gene Expression in *Vibrio harveyi*, *Journal of Bacteriology.* **186**, 6902-6914.

65. Cao, J. G. & Meighen, E. A. (1989) Purification and structural identification of an autoinducer for the luminescence system of *Vibrio harveyi*, *Journal of Biological Chemistry.* **264**, 21670-21676.
66. Surette, M. G., Miller, M. B. & Bassler, B. L. (1999) Quorum sensing in *Escherichia coli, Salmonella typhimurium,* and *Vibrio harveyi:* A new family of genes responsible for autoinducer production, *Proceedings of the National Academy of Sciences.* **96**, 1639-1644.
67. Miller, S. T., Xavier, K. B., Campagna, S. R., Taga, M. E., Semmelhack, M. F., Bassler, B. L. & Hughson, F. M. *Salmonella typhimurium* Recognizes a Chemically Distinct Form of the Bacterial Quorum-Sensing Signal AI-2, *Molecular Cell.* **15**, 677-687.
68. Xavier, K. B. & Bassler, B. L. (2003) LuxS quorum sensing: more than just a numbers game, *Current Opinion in Microbiology.* **6**, 191-197.
69. Neiditch, M. B., Federle, M. J., Pompeani, A. J., Kelly, R. C., Swem, D. L., Jeffrey, P. D., Bassler, B. L. & Hughson, F. M. Ligand-Induced Asymmetry in Histidine Sensor Kinase Complex Regulates Quorum Sensing, *Cell.* **126**, 1095-1108.
70. Bassler, B. L., Wright, M. & Silverman, M. R. (1994) Multiple signalling systems controlling expression of luminescence in *Vibrio harveyi*: sequence and function of genes encoding a second sensory pathway, *Molecular Microbiology.* **13**, 273-286.
71. Federle, M. J. & Bassler, B. L. (2003) Interspecies communication in bacteria, *The Journal of Clinical Investigation.* **112**, 1291-1299.
72. Miller, M. B., Skorupski, K., Lenz, D. H., Taylor, R. K. & Bassler, B. L. Parallel Quorum Sensing Systems Converge to Regulate Virulence in *Vibrio cholerae*, *Cell.* **110**, 303-314.
73. Higgins, D. A., Pomianek, M. E., Kraml, C. M., Taylor, R. K., Semmelhack, M. F. & Bassler, B. L. (2007) The major *Vibrio cholerae* autoinducer and its role in virulence factor production, *Nature.* **450**, 883-886.
74. Freeman, J. A. & Bassler, B. L. (1999) Sequence and Function of LuxU: a Two-Component Phosphorelay Protein That Regulates Quorum Sensing in *Vibrio harveyi*, *Journal of Bacteriology.* **181**, 899-906.
75. Freeman, J. A., Lilley, B. N. & Bassler, B. L. (2000) A genetic analysis of the functions of LuxN: a two-component hybrid sensor kinase that regulates quorum sensing in *Vibrio harveyi*, *Molecular Microbiology.* **35**, 139-149.
76. Freeman, J. A. & Bassler, B. L. (1999) A genetic analysis of the function of LuxO, a two-component response regulator involved in quorum sensing in *Vibrio harveyi*, *Molecular Microbiology.* **31**, 665-677.
77. Lilley, B. N. & Bassler, B. L. (2000) Regulation of quorum sensing in *Vibrio harveyi* by LuxO and Sigma-54, *Molecular Microbiology.* **36**, 940-954.
78. Lenz, D. H., Mok, K. C., Lilley, B. N., Kulkarni, R. V., Wingreen, N. S. & Bassler, B. L. (2004) The Small RNA Chaperone Hfq and Multiple Small RNAs Control Quorum Sensing in *Vibrio harveyi* and *Vibrio cholerae*, *Cell.* **118**, 69-82.
79. Swartzman, E., Silverman, M. & Meighen, E. A. (1992) The luxR gene product of *Vibrio harveyi* is a transcriptional activator of the lux promoter, *Journal of Bacteriology.* **174**, 7490-7493.
80. Ignarro, L. J., Byrns, R. E., Buga, G. M. & Wood, K. S. (1987) Endothelium-derived relaxing factor from pulmonary artery and vein possesses pharmacologic and chemical properties identical to those of nitric oxide radical, *Circulation Research.* **61**, 866-79.
81. Culotta, E. & Koshland, D. (1992) NO news is good news, *Science.* **258**, 1862-1865.

82. Arnold, W. P., Mittal, C. K., Katsuki, S. & Murad, F. (1977) Nitric Oxide Activates Guanylate Cyclase and Increases Guanosine 3'-5' cyclic Monophosphate Levels in Various Tissue Preparations, *Proceedings of the National Academy of Sciences of the United States of America.* **74**, 3203-3207.
83. Jain, R. & Chan, M. (2003) Mechanisms of ligand discrimination by heme proteins, *J Biol Inorg Chem.* **8**, 1-11.
84. Ohlstein, E. H., Wood, K. S. & Ignarro, L. J. (1982) Purification and properties of heme-deficient hepatic soluble guanylate cyclase: Effects of heme and other factors on enzyme activation by NO, NO-heme, and protoporphyrin IX, *Archives of Biochemistry and Biophysics.* **218**, 187-198.
85. Denninger, J. W. & Marletta, M. A. (1999) Guanylate cyclase and the ·NO/cGMP signaling pathway, *Biochimica et Biophysica Acta (BBA) - Bioenergetics.* **1411**, 334-350.
86. Hofmann, F., Bernhard, D., Lukowski, R. & Weinmeister, P. (2009) cGMP Regulated Protein Kinases (cGK) in *cGMP: Generators, Effectors and Therapeutic Implications* (Schmidt, H. H. W., Hofmann, F. & Stasch, J.-P., eds) pp. 137-162, Springer Berlin Heidelberg.
87. Moncada, S., Palmer, R. M. & Higgs, E. A. (1991) Nitric oxide: physiology, pathophysiology, and pharmacology, *Pharmacological Reviews.* **43**, 109-142.
88. Pacher, P., Beckman, J. S. & Liaudet, L. (2007) Nitric Oxide and Peroxynitrite in Health and Disease, *Physiol Rev.* **87**, 315-424.
89. Nathan, C. (1992) Nitric oxide as a secretory product of mammalian cells, *The FASEB Journal.* **6**, 3051-64.
90. Prast, H. & Philippu, A. (2001) Nitric oxide as modulator of neuronal function, *Progress in Neurobiology.* **64**, 51-68.
91. Bogdan, C. (2001) Nitric oxide and the immune response, *Nat Immunol.* **2**, 907-916.
92. Lowenstein, C. J., Dinerman, J. L. & Snyder, S. H. (1994) Nitric Oxide: A Physiologic Messenger, *Annals of Internal Medicine.* **120**, 227-237.
93. Liu, N., Xu, Y., Hossain, S., Huang, N., Coursolle, D., Gralnick, J. A. & Boon, E. M. (2012) Nitric Oxide Regulation of Cyclic di-GMP Synthesis and Hydrolysis in *Shewanella woodyi*, *Biochemistry.* **51**, 2087-2099.
94. Plate, L. & Marletta, M. A. (2012) Nitric oxide modulates bacterial biofilm formation through a multicomponent cyclic-di-GMP signaling network, *Mol Cell.* **46**, 449-460.
95. McDougald, D., Rice, S. A., Barraud, N., Steinberg, P. D. & Kjelleberg, S. (2012) Should we stay or should we go: mechanisms and ecological consequences for biofilm dispersal, *Nat Rev Micro.* **10**, 39-50.
96. Davidson, S. K., Koropatnick, T. A., Kossmehl, R., Sycuro, L. & McFall-Ngai, M. J. (2004) NO means 'yes' in the squid-vibrio symbiosis: nitric oxide (NO) during the initial stages of a beneficial association, *Cellular Microbiology.* **6**, 1139-1151.
97. Henares, B. M., Higgins, K. E. & Boon, E. M. (2012) Discovery of a Nitric Oxide Responsive Quorum Sensing Circuit in *Vibrio harveyi*, *ACS Chemical Biology.* **7**, 1331-1336.
98. Privett, B. J., Broadnax, A. D., Bauman, S. J., Riccio, D. A. & Schoenfisch, M. H. (2012) Examination of bacterial resistance to exogenous nitric oxide, *Nitric Oxide.* **26**, 169-173.
99. Carpenter, A. W. & Schoenfisch, M. H. (2012) Nitric oxide release: Part II. Therapeutic applications, *Chemical Society Reviews.* **41**, 3742-3752.
100. Kers, J. A., Wach, M. J., Krasnoff, S. B., Widom, J., Cameron, K. D., Bukhalid, R. A., Gibson, D. M., Crane, B. R. & Loria, R. (2004) Nitration of a peptide phytotoxin by bacterial nitric oxide synthase, *Nature.* **429**, 79-82.

101. Wasser, I. M., de Vries, S., Moënne-Loccoz, P., Schröder, I. & Karlin, K. D. (2002) Nitric Oxide in Biological Denitrification: Fe/Cu Metalloenzyme and Metal Complex NOx Redox Chemistry, *Chemical Reviews.* **102**, 1201-1234.
102. Schmidt, I., Steenbakkers, P. J. M., op, d. C. H. J. M., Schmidt, K. & Jetten, M. S. M. (2004) Physiologic and proteomic evidence for a role of nitric oxide in biofilm formation by *Nitrosomonas europaea* and other ammonia oxidizers, *J Bacteriol.* **186**, 2781-2788.
103. Barraud, N., Hassett, D. J., Hwang, S.-H., Rice, S. A., Kjelleberg, S. & Webb, J. S. (2006) Involvement of nitric oxide in biofilm dispersal of *Pseudomonas aeruginosa*, *J Bacteriol.* **188**, 7344-7353.
104. Barraud, N., Storey, M. V., Moore, Z. P., Webb, J. S., Rice, S. A. & Kjelleberg, S. (2009) Nitric oxide-mediated dispersal in single- and multi-species biofilms of clinically and industrially relevant microorganisms, *Microb Biotechnol.* **2**, 370-378.
105. Barraud, N., Schleheck, D., Klebensberger, J., Webb, J. S., Hassett, D. J., Rice, S. A. & Kjelleberg, S. (2009) Nitric oxide signaling in *Pseudomonas aeruginosa* biofilms mediates phosphodiesterase activity, decreased cyclic Di-GMP levels, and enhanced dispersal, *J Bacteriol.* **191**, 7333-7342.
106. Li, Y., Heine, S., Entian, M., Sauer, K. & Frankenberg-Dinkel, N. (2013) NO-induced biofilm dispersion in *Pseudomonas aeruginosa* is mediated by an MHYT domain-coupled phosphodiesterase, *J Bacteriol.* **195**, 3531-3542.
107. Galperin, M. Y., Gaidenko, T. A., Mulkidjanian, A. Y., Nakano, M. & Price, C. W. (2001) MHYT, a new integral membrane sensor domain, *FEMS Microbiology Letters.* **205**, 17-23.
108. Morgan, R., Kohn, S., Hwang, S.-H., Hassett, D. J. & Sauer, K. (2006) BdlA, a Chemotaxis Regulator Essential for Biofilm Dispersion in *Pseudomonas aeruginosa*, *Journal of Bacteriology.* **188**, 7335-7343.
109. Weinert, E. E., Phillips-Piro, C. M., Tran, R., Mathies, R. A. & Marletta, M. A. (2011) Controlling Conformational Flexibility of an O2-Binding H-NOX Domain, *Biochemistry.* **50**, 6832-6840.
110. Karow, D. S., Pan, D., Tran, R., Pellicena, P., Presley, A., Mathies, R. A. & Marletta, M. A. (2004) Spectroscopic Characterization of the Soluble Guanylate Cyclase-like Heme Domains from *Vibrio cholerae* and *Thermoanaerobacter tengcongensis*†, *Biochemistry.* **43**, 10203-10211.
111. Boon, E. M., Davis, J. H., Tran, R., Karow, D. S., Huang, S. H., Pan, D., Miazgowicz, M. M., Mathies, R. A. & Marletta, M. A. (2006) Nitric Oxide Binding to Prokaryotic Homologs of the Soluble Guanylate Cyclase β1 H-NOX Domain, *Journal of Biological Chemistry.* **281**, 21892-21902.
112. Iyer, L., Anantharaman, V. & Aravind, L. (2003) Ancient conserved domains shared by animal soluble guanylyl cyclases and bacterial signaling proteins, *BMC Genomics.* **4**, 5.
113. Boon, E. M. & Marletta, M. A. (2005) Ligand specificity of H-NOX domains: from sGC to bacterial NO sensors, *Journal of Inorganic Biochemistry.* **99**, 892-902.
114. Price, M. S., Chao, L. Y. & Marletta, M. A. (2007) *Shewanella oneidensis* MR-1 H-NOX Regulation of a Histidine Kinase by Nitric Oxide†, *Biochemistry.* **46**, 13677-13683.
115. Carlson, H. K., Vance, R. E. & Marletta, M. A. (2010) H-NOX regulation of c-di-GMP metabolism and biofilm formation in *Legionella pneumophila*, *Molecular Microbiology.* **77**, 930-942.
116. Henares, B., Xu, Y. & Boon, E. (2013) A Nitric Oxide-Responsive Quorum Sensing Circuit in *Vibrio harveyi* Regulates Flagella Production and Biofilm Formation, *International Journal of Molecular Sciences.* **14**, 16473-16484.

117. Costerton, J. W., Stewart, P. S. & Greenberg, E. P. (1999) Bacterial Biofilms: A Common Cause of Persistent Infections, *Science.* **284**, 1318-1322.
118. Hall-Stoodley, L., Costerton, J. W. & Stoodley, P. (2004) Bacterial biofilms: from the Natural environment to infectious diseases, *Nat Rev Micro.* **2**, 95-108.
119. Donlan, R. M. & Costerton, J. W. (2002) Biofilms: Survival Mechanisms of Clinically Relevant Microorganisms, *Clinical Microbiology Reviews.* **15**, 167-193.
120. Stewart, P. S. & William Costerton, J. (2001) Antibiotic resistance of bacteria in biofilms, *The Lancet.* **358**, 135-138.
121. Daniels, R., Vanderleyden, J. & Michiels, J. (2004) Quorum sensing and swarming migration in bacteria, *FEMS Microbiology Reviews.* **28**, 261-289.
122. Bjarnsholt, T., Jensen, P. Ø., Jakobsen, T. H., Phipps, R., Nielsen, A. K., Rybtke, M. T., Tolker-Nielsen, T., Givskov, M., Høiby, N., Ciofu, O. & the Scandinavian Cystic Fibrosis Study, C. (2010) Quorum Sensing and Virulence of *Pseudomonas aeruginosa* during Lung Infection of Cystic Fibrosis Patients, *PLoS ONE.* **5**, e10115.
123. Nealson, K. H. & Hastings, J. W. (1979) Bacterial bioluminescence: its control and ecological significance, *Microbiol Rev.* **43**, 496-518.
124. McCarter, L. L. (1998) OpaR, a Homolog of *Vibrio harveyi* LuxR, Controls Opacity of *Vibrio parahaemolyticus*, *Journal of Bacteriology.* **180**, 3166-3173.
125. Enos-Berlage, J. L. & McCarter, L. L. (2000) Relation of Capsular Polysaccharide Production and Colonial Cell Organization to Colony Morphology in *Vibrio parahaemolyticus*, *Journal of Bacteriology.* **182**, 5513-5520.
126. Fidopiastis, P. M., Miyamoto, C. M., Jobling, M. G., Meighen, E. A. & Ruby, E. G. (2002) LitR, a new transcriptional activator in *Vibrio fischeri*, regulates luminescence and symbiotic light organ colonization, *Molecular Microbiology.* **45**, 131-143.
127. Yildiz, F. H., Liu, X. S., Heydorn, A. & Schoolnik, G. K. (2004) Molecular analysis of rugosity in a *Vibrio cholerae* O1 El Tor phase variant, *Molecular Microbiology.* **53**, 497-515.
128. Zhu, J. & Mekalanos, J. J. (2003) Quorum Sensing-Dependent Biofilms Enhance Colonization in *Vibrio cholerae*, *Developmental Cell.* **5**, 647-656.
129. Waters, C. M., Lu, W., Rabinowitz, J. D. & Bassler, B. L. (2008) Quorum Sensing Controls Biofilm Formation in Vibrio cholerae through Modulation of Cyclic Di-GMP Levels and Repression of vpsT, *Journal of Bacteriology.* **190**, 2527-2536.
130. Waters, C. M. & Bassler, B. L. (2006) The *Vibrio harveyi* quorum-sensing system uses shared regulatory components to discriminate between multiple autoinducers, *Genes & Development.* **20**, 2754-2767.
131. Yildiz, F. H. & Visick, K. L. (2009) *Vibrio* biofilms: so much the same yet so different, *Trends in microbiology.* **17**, 109-118.
132. Liu, N., Xu, Y., Hossain, S., Huang, N., Coursolle, D., Gralnick, J. A. & Boon, E. M. (2012) Nitric Oxide Regulation of Cyclic di-GMP Synthesis and Hydrolysis in Shewanella woodyi, *Biochemistry.* **51**, 2087-2099.
133. Plate, L. & Marletta, Michael A. (2012) Nitric Oxide Modulates Bacterial Biofilm Formation through a Multicomponent Cyclic-di-GMP Signaling Network, *Molecular cell.* **46**, 449-460.
134. Römling, U. & Amikam, D. (2006) Cyclic di-GMP as a second messenger, *Current Opinion in Microbiology.* **9**, 218-228.

135. Jenal, U. (2004) Cyclic di-guanosine-monophosphate comes of age: a novel secondary messenger involved in modulating cell surface structures in bacteria?, *Current Opinion in Microbiology.* **7**, 185-191.
136. Bassler, B. L., Wright, M. & Silverman, M. R. (1994) Sequence and function of LuxO, a negative regulator of luminescence in Vibrio harveyi, *Molecular Microbiology.* **12**, 403-412.
137. Miller, S. T., Xavier, K. B., Campagna, S. R., Taga, M. E., Semmelhack, M. F., Bassler, B. L. & Hughson, F. M. (2004) Salmonella typhimurium Recognizes a Chemically Distinct Form of the Bacterial Quorum-Sensing Signal AI-2, *Molecular cell.* **15**, 677-687.
138. Schmidt, I., Steenbakkers, P. J. M., op den Camp, H. J. M., Schmidt, K. & Jetten, M. S. M. (2004) Physiologic and Proteomic Evidence for a Role of Nitric Oxide in Biofilm Formation by Nitrosomonas europaea and Other Ammonia Oxidizers, *Journal of Bacteriology.* **186**, 2781-2788.
139. O'Toole, G. A. & Kolter, R. (1998) Flagellar and twitching motility are necessary for *Pseudomonas aeruginosa* biofilm development, *Molecular Microbiology.* **30**, 295-304.
140. Pratt, L. A. & Kolter, R. (1998) Genetic analysis of *Escherichia coli* biofilm formation: roles of flagella, motility, chemotaxis and type I pili, *Molecular Microbiology.* **30**, 285-293.
141. Watnick, P. I. & Kolter, R. (1999) Steps in the development of a *Vibrio cholerae* El Tor biofilm, *Molecular Microbiology.* **34**, 586-595.
142. Barak, R. & Eisenbach, M. (1992) Correlation between phosphorylation of the chemotaxis protein CheY and its activity at the flagellar motor, *Biochemistry.* **31**, 1821-1826.
143. Clegg, D. O. & Koshland, D. E. (1984) The role of a signaling protein in bacterial sensing: behavioral effects of increased gene expression, *Proceedings of the National Academy of Sciences.* **81**, 5056-5060.
144. Ravid, S., Matsumura, P. & Eisenbach, M. (1986) Restoration of flagellar clockwise rotation in bacterial envelopes by insertion of the chemotaxis protein CheY, *Proceedings of the National Academy of Sciences.* **83**, 7157-7161.
145. Wolfe, A. J., Conley, M. P., Kramer, T. J. & Berg, H. C. (1987) Reconstitution of signaling in bacterial chemotaxis, *Journal of Bacteriology.* **169**, 1878-1885.
146. Lupp, C. & Ruby, E. G. (2005) *Vibrio fischeri* Uses Two Quorum-Sensing Systems for the Regulation of Early and Late Colonization Factors, *Journal of Bacteriology.* **187**, 3620-3629.
147. Nadell, C. D., Xavier, J. B., Levin, S. A. & Foster, K. R. (2008) The Evolution of Quorum Sensing in Bacterial Biofilms, *PLoS Biol.* **6**, e14.
148. Parsek, M. R. & Greenberg, E. P. (2005) Sociomicrobiology: the connections between quorum sensing and biofilms, *Trends in Microbiology.* **13**, 27-33.
149. Coggan, K. A. a. W., Matthew C. (2012) Global Regulatory Pathways and Cross-talk Control *Pseudomonas aeruginosa* Environmental Lifestyle and Virulence Phenotype, *Curr Issues Mol Biol.* **14**, 47-70.
150. Williams, P. & Cámara, M. (2009) Quorum sensing and environmental adaptation in *Pseudomonas aeruginosa*: a tale of regulatory networks and multifunctional signal molecules, *Current Opinion in Microbiology.* **12**, 182-191.
151. Davey, M. E. & O'Toole G, A. (2000) Microbial biofilms: from ecology to molecular genetics, *Microbiology and Molecular Biology Reviews.* **64**, 847-67.
152. Nablo, B. J., Chen, T. Y. & Schoenfisch, M. H. (2001) Sol-gel derived nitric-oxide releasing materials that reduce bacterial adhesion, *J Am Chem Soc.* **123**, 9712-3.
153. Hetrick, E. M., Shin, J. H., Paul, H. S. & Schoenfisch, M. H. (2009) Anti-biofilm efficacy of nitric oxide-releasing silica nanoparticles, *Biomaterials.* **30**, 2782-9.

154. Privett, B. J., Nutz, S. T. & Schoenfisch, M. H. (2010) Efficacy of surface-generated nitric oxide against Candida albicans adhesion and biofilm formation, *Biofouling.* **26**, 973-983.
155. Monds, R. D. & O'Toole, G. A. (2009) The developmental model of microbial biofilms: ten years of a paradigm up for review, *Trends in Microbiology.* **17**, 73-87.
156. Romling, U. (2011) Cyclic di-GMP, an established secondary messenger still speeding up, *Environ Microbiol*.
157. D'Argenio, D. A. & Miller, S. I. (2004) Cyclic di-GMP as a bacterial second messenger, *Microbiology.* **150**, 2497-502.
158. Tischler, A. D. & Camilli, A. (2004) Cyclic diguanylate (c-di-GMP) regulates *Vibrio cholerae* biofilm formation, *Molecular Microbiology.* **53**, 857-869.
159. Ausmees, N., Mayer, R., Weinhouse, H., Volman, G., Amikam, D., Benziman, M. & Lindberg, M. (2001) Genetic data indicate that proteins containing the GGDEF domain possess diguanylate cyclase activity, *FEMS Microbiol Lett.* **204**, 163-7.
160. Simm, R., Morr, M., Kader, A., Nimtz, M. & Romling, U. (2004) GGDEF and EAL domains inversely regulate cyclic di-GMP levels and transition from sessility to motility, *Mol Microbiol.* **53**, 1123-34.
161. Galperin, M. Y., Nikolskaya, A. N. & Koonin, E. V. (2001) Novel domains of the prokaryotic two-component signal transduction systems, *FEMS Microbiol Lett.* **203**, 11-21.
162. Rajagopal, S., Key, J. M., Purcell, E. B., Boerema, D. J. & Moffat, K. (2004) Purification and initial characterization of a putative blue light-regulated phosphodiesterase from Escherichia coli, *Photochemistry and photobiology.* **80**, 542-7.
163. Karatan, E., Duncan, T. R. & Watnick, P. I. (2005) NspS, a predicted polyamine sensor, mediates activation of Vibrio cholerae biofilm formation by norspermidine, *Journal of bacteriology.* **187**, 7434-43.
164. Boon, E. M. & Marletta, M. A. (2005) Ligand discrimination in soluble guanylate cyclase and the H-NOX family of heme sensor proteins, *Curr Opin Chem Biol.* **9**, 441-6.
165. Boon, E. M., Huang, S. H. & Marletta, M. A. (2005) A molecular basis for NO selectivity in soluble guanylate cyclase, *Nat Chem Biol.* **1**, 53-59.
166. Boon, E. M. & Marletta, M. A. (2006) Sensitive and selective detection of nitric oxide using an H-NOX domain, *J Am Chem Soc.* **128**, 10022-3.
167. Wang, Y., Dufour, Y. S., Carlson, H. K., Donohue, T. J., Marletta, M. A. & Ruby, E. G. (2010) H-NOX-mediated nitric oxide sensing modulates symbiotic colonization by Vibrio fischeri, *Proc Natl Acad Sci U S A.* **107**, 8375-80.
168. Liu, N., Pak, T. & Boon, E. M. (2010) Characterization of a diguanylate cyclase from Shewanella woodyi with cyclase and phosphodiesterase activities, *Mol Biosyst.* **6**, 1561-4.
169. Saltikov, C. W. & Newman, D. K. (2003) Genetic identification of a respiratory arsenate reductase, *Proceedings of the National Academy of Sciences.* **100**, 10983-10988.
170. Kovach, M. E., Elzer, P. H., Steven Hill, D., Robertson, G. T., Farris, M. A., Roop Ii, R. M. & Peterson, K. M. (1995) Four new derivatives of the broad-host-range cloning vector pBBR1MCS, carrying different antibiotic-resistance cassettes, *Gene.* **166**, 175-176.
171. Waters, C. M., Lu, W., Rabinowitz, J. D. & Bassler, B. L. (2008) Quorum sensing controls biofilm formation in Vibrio cholerae through modulation of cyclic di-GMP levels and repression of vpsT, *J Bacteriol.* **190**, 2527-36.
172. Lawrence, J. R., Korber, D. R., Hoyle, B. D., Costerton, J. W. & Caldwell, D. E. (1991) Optical sectioning of microbial biofilms, *Journal of bacteriology.* **173**, 6558-67.

173. Maragos, C. M., Wang, J. M., Hrabie, J. A., Oppenheim, J. J. & Keefer, L. K. (1993) Nitric Oxide/Nucleophile Complexes Inhibit the *in Vitro* Proliferation of A375 Melanoma Cells via Nitric Oxide Release, *Cancer Research.* **53**, 564-568.
174. Keefer, L. K., Nims, R. W., Davies, K. M. & Wink, D. A. (1996) "NONOates" (1-substituted diazen-1-ium-1,2-diolates) as nitric oxide donors: convenient nitric oxide dosage forms, *Methods Enzymol.* **268**, 281-93.
175. Pasto, M., Serrano, E., Urocoste, E., Barbacanne, M. A., Guissani, A., Didier, A., Delisle, M. B., Rami, J. & Arnal, J. F. (2001) Nasal polyp-derived superoxide anion: dose-dependent inhibition by nitric oxide and pathophysiological implications, *American journal of respiratory and critical care medicine.* **163**, 145-51.
176. Pervin, S., Singh, R. & Chaudhuri, G. (2001) Nitric oxide-induced cytostasis and cell cycle arrest of a human breast cancer cell line (MDA-MB-231): potential role of cyclin D1, *Proc Natl Acad Sci U S A.* **98**, 3583-8.
177. Warwood, T. L., Ohls, R. K., Lambert, D. K., Leve, E. A., Veng-Pedersen, P. & Christensen, R. D. (2006) Urinary excretion of darbepoetin after intravenous vs subcutaneous administration to preterm neonates, *J Perinatol.* **26**, 636-9.
178. De, N., Navarro, M. V. A. S., Raghavan, R. V. & Sondermann, H. (2009) Determinants for the Activation and Autoinhibition of the Diguanylate Cyclase Response Regulator WspR, *Journal of Molecular Biology.* **393**, 619-633.
179. Costerton, J. W., Cheng, K. J., Geesey, G. G., Ladd, T. I., Nickel, J. C., Dasgupta, M. & Marrie, T. J. (1987) Bacterial biofilms in nature and disease, *Annual review of microbiology.* **41**, 435-64.
180. Palmer, R. J., Jr. & Stoodley, P. (2007) Biofilms 2007: broadened horizons and new emphases, *J Bacteriol.* **189**, 7948-60.
181. Stone, J. R. & Marletta, M. A. (1996) Spectral and kinetic studies on the activation of soluble guanylate cyclase by nitric oxide, *Biochemistry.* **35**, 1093-9.
182. Boon, E. M., Huang, S. H. & Marletta, M. A. (2005) A molecular basis for NO selectivity in soluble guanylate cyclase, *Nat Chem Biol.* **1**, 53-9.
183. Garcia, B., Latasa, C., Solano, C., Garcia-del Portillo, F., Gamazo, C. & Lasa, I. (2004) Role of the GGDEF protein family in Salmonella cellulose biosynthesis and biofilm formation, *Mol Microbiol.* **54**, 264-77.
184. Thormann, K. M., Duttler, S., Saville, R. M., Hyodo, M., Shukla, S., Hayakawa, Y. & Spormann, A. M. (2006) Control of formation and cellular detachment from Shewanella oneidensis MR-1 biofilms by cyclic di-GMP, *J Bacteriol.* **188**, 2681-91.
185. Denninger, J. W. & Marletta, M. A. (1999) Guanylate cyclase and the NO/cGMP signaling pathway, *Biochimica et Biophysica Acta.* **1411**, 334-350.
186. Fredrickson, J. K., Romine, M. F., Beliaev, A. S., Auchtung, J. M., Driscoll, M. E., Gardner, T. S., Nealson, K. H., Osterman, A. L., Pinchuk, G., Reed, J. L., Rodionov, D. A., Rodrigues, J. L. M., Saffarini, D. A., Serres, M. H., Spormann, A. M., Zhulin, I. B. & Tiedje, J. M. (2008) Towards environmental systems biology of *Shewanella*, *Nature Reviews Microbiology.* **6**, 592-603.
187. Kulasakara, H., Lee, V., Brencic, A., Liberati, N., Urbach, J., Miyata, S., Lee, D. G., Neely, A. N., Hyodo, M., Hayakawa, Y., Ausubel, F. M. & Lory, S. (2006) Analysis of Pseudomonas aeruginosa diguanylate cyclases and phosphodiesterases reveals a role for bis-(3'-5')-cyclic-GMP in virulence, *Proc Natl Acad Sci U S A.* **103**, 2839-44.

188. Simm, R., Lusch, A., Kader, A., Andersson, M. & Romling, U. (2007) Role of EAL-containing proteins in multicellular behavior of Salmonella enterica serovar Typhimurium, *J Bacteriol.* **189**, 3613-23.
189. Sommerfeldt, N., Possling, A., Becker, G., Pesavento, C., Tschowri, N. & Hengge, R. (2009) Gene expression patterns and differential input into curli fimbriae regulation of all GGDEF/EAL domain proteins in Escherichia coli, *Microbiology.* **155**, 1318-31.
190. Klausen, M., Heydorn, A., Ragas, P., Lambertsen, L., Aaes-Jorgensen, A., Molin, S. & Tolker-Nielsen, T. (2003) Biofilm formation by Pseudomonas aeruginosa wild type, flagella and type IV pili mutants, *Molecular Microbiology.* **48**, 1511-24.
191. Klausen, M., Gjermansen, M., Kreft, J. U. & Tolker-Nielsen, T. (2006) Dynamics of development and dispersal in sessile microbial communities: examples from Pseudomonas aeruginosa and Pseudomonas putida model biofilms, *FEMS microbiology letters.* **261**, 1-11.
192. Ghigo, J. M. (2003) Are there biofilm-specific physiological pathways beyond a reasonable doubt?, *Research in microbiology.* **154**, 1-8.
193. Makemson, J. C., Fulayfil, N. R., Landry, W., Van Ert, L. M., Wimpee, C. F., Widder, E. A. & Case, J. F. (1997) *Shewanella woodyi* sp. nov., an Exclusively Respiratory Luminous Bacterium Isolated from the Alboran Sea, *Int J Syst Bacteriol.* **47**, 1034-1039.
194. Zumft, W. G. (2002) Nitric oxide signaling and NO dependent transcriptional control in bacterial denitrification by members of the FNR-CRP regulator family, *J Mol Microbiol Biotechnol.* **4**, 277-86.
195. Ji, X. B. & Hollocher, T. C. (1988) Reduction of nitrite to nitric oxide by enteric bacteria, *Biochem Biophys Res Commun.* **157**, 106-8.
196. Stewart, P. S. & Franklin, M. J. (2008) Physiological heterogeneity in biofilms, *Nat Rev Microbiol.* **6**, 199-210.
197. Schreiber, F., Beutler, M., Enning, D., Lamprecht-Grandio, M., Zafra, O., Gonzalez-Pastor, J. & de Beer, D. (2011) The role of nitric-oxide-synthase-derived nitric oxide in multicellular traits of *Bacillus subtilis* 3610: biofilm formation, swarming, and dispersal, *BMC Microbiology.* **11**, 111.
198. Widder, E. A. (2010) Bioluminescence in the Ocean: Origins of Biological, Chemical, and Ecological Diversity, *Science.* **328**, 704-708.
199. Makemson, J. C., Fulayfil, N. R., Landry, W., Van Ert, L. M., Wimpee, C. F., Widder, E. A. & Case, J. F. (1997) Shewanella woodyi sp. nov., an exclusively respiratory luminous bacterium isolated from the Alboran Sea, *Int J Syst Bacteriol.* **47**, 1034-9.
200. Arora, D. P. & Boon, E. M. (2012) Nitric oxide regulated two-component signaling in *Pseudoalteromonas atlantica*, *Biochemical and Biophysical Research Communications.* **421**, 521-526.
201. Dehio, C. & Meyer, M. (1997) Maintenance of broad-host-range incompatibility group P and group Q plasmids and transposition of Tn5 in *Bartonella henselae* following conjugal plasmid transfer from *Escherichia coli*, *Journal of Bacteriology.* **179**, 538-40.
202. Saltikov, C. W. & Newman, D. K. (2003) Genetic identification of a respiratory arsenate reductase, *Proceedings of the National Academy of Sciences of the United States of America.* **100**, 10983-8.
203. Schultz, J., Milpetz, F., Bork, P. & Ponting, C. P. (1998) SMART, a simple modular architecture research tool: Identification of signaling domains, *Proceedings of the National Academy of Sciences.* **95**, 5857-5864.

204. Letunic, I., Doerks, T. & Bork, P. (2012) SMART 7: recent updates to the protein domain annotation resource, *Nucleic Acids Research.* **40**, D302-D305.
205. Mitrophanov, A. Y. & Groisman, E. A. (2008) Signal integration in bacterial two-component regulatory systems, *Genes & Development.* **22**, 2601-2611.
206. Wassmann, P., Chan, C., Paul, R., Beck, A., Heerklotz, H., Jenal, U. & Schirmer, T. (2007) Structure of BeF3--Modified Response Regulator PleD: Implications for Diguanylate Cyclase Activation, Catalysis, and Feedback Inhibition, *Structure.* **15**, 915-927.
207. Hengge, R. (2009) Principles of c-di-GMP signalling in bacteria, *Nat Rev Micro.* **7**, 263-273.

Appendix 1 Vector map of Δ*hnox*, Δ*hace*, Δ*hnox*/Δ*hace* and Δ*hk* in pSMV3

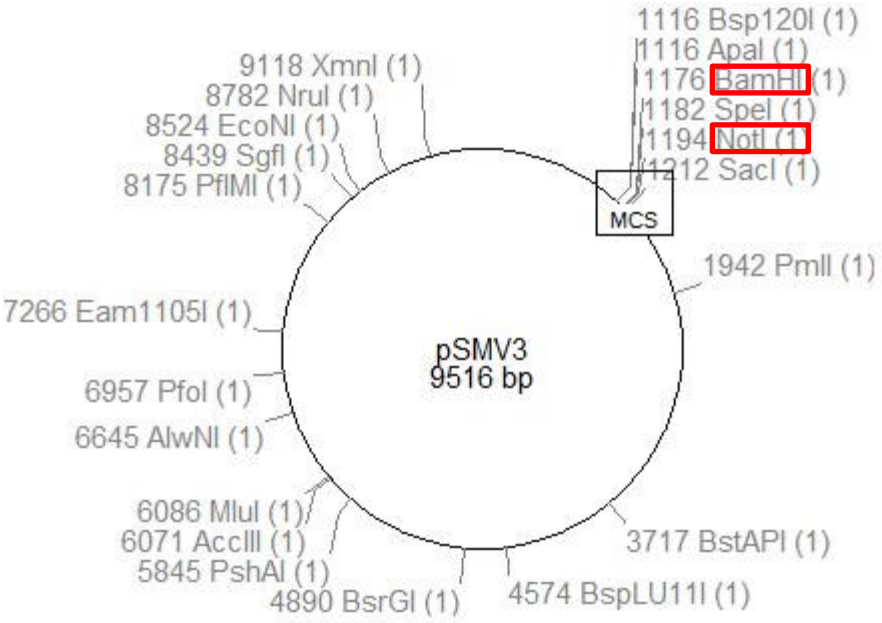

Appendix 2 List of protein expression changes in *V. harveyi* as a function of NO.

Peptides obtained after growth in the presence of 0, 50, 100, or 200 nM nitric oxide are represented by isobaric tags that produce signature ions at m/z 114, 115, 116 and 117 respectively. Standard deviations (S.D.) were obtained from readings of different significant fragmented peptides concentrations of the same protein. Downregulated values are shown in red and upregulated values are shown in green.

	Peptide abundance at (50/0) nM NO		Peptide abundance at (100/0) nM NO		Peptide abundance at (200/0) nM NO	
Protein Name	115/114	115/114 S.D.	116/114	116/114 S.D.	117/114	117/114 S.D.
adaA; methylphosphotriester-DNA alkyltransferase	0.197	0.040	0.142	0.031	0.327	0.014
uncharacterized protein	0.214	0.031	0.114	0.022	0.054	0.031
pyruvate dehydrogenase E1 component, alpha subunit	0.214	0.065	0.141	0.090	0.128	0.098
4-hydroxyphenylpyruvate dioxygenase	0.268	0.058	0.127	0.095	0.092	0.077
flagellin	0.365	0.091	0.625	0.201	0.813	0.228
flagellin	0.421	0.035	0.637	0.063	1.013	0.105
flagellin	0.425	0.102	0.705	0.104	1.000	0.065
flagellin	0.443	0.231	0.673	0.168	0.955	0.165
pknB; probable serine/threonine-protein kinase;	0.490	0.029	0.338	0.030	0.191	0.030
grxA; glutaredoxin 1	0.494	0.349	1.995	1.043	0.371	0.020
Type II secretory pathway, pseudopilin	0.535	0.189	0.450	0.186	0.393	0.382
Transcription antitermination protein nusG	0.580	0.038	0.527	0.020	0.402	0.064
OstA; OstA-like protein	0.589	0.129	0.927	0.110	0.464	0.112
Formimidoylglutamase	0.592	0.058	0.630	0.101	0.866	0.075
Enolase2	0.602	0.087	0.215	0.025	0.165	0.033
putative thioredoxin-like protein	0.606	0.101	0.955	0.056	0.308	0.262
gram_neg_porins	0.607	0.226	0.892	0.157	1.867	0.295
trpB; Tryptophan synthase beta chain	0.615	0.369	0.464	0.321	0.188	0.140
ATP-dependent zinc metalloprotease FtsH	0.629	0.307	0.619	0.299	0.859	0.341
L-allo-threonine aldolase	0.636	0.177	0.686	0.147	0.420	0.115
AcrR; Transcriptional regulator [Transcription]	0.637	0.091	1.472	0.138	3.794	1.061
Imidazolonepropionase	0.638	0.071	0.577	0.055	0.855	0.155
Amidinotransf; Amidinotransferase	0.660	0.126	0.681	0.165	0.367	0.079
Trypsin-like serine proteases, typically periplasmic, contain C-terminal PDZ domain	0.664	0.155	0.558	0.121	0.302	0.051
gamma-glutamyltransferase	0.665	0.135	0.842	0.104	0.599	0.096
Peptidase B	0.666	0.060	0.534	0.106	0.777	0.096
Urocanate hydratase	0.669	0.173	0.844	0.146	0.879	0.171

Integration host factor subunit alpha	0.672	0.125	0.933	0.119	2.036	0.417
Domain of unknown function	0.673	0.016	0.493	0.024	0.238	0.055
aroK; Shikimate kinase	0.674	0.247	0.624	0.375	0.352	0.290
ABC-type dipeptide transport system, periplasmic component	0.675	0.409	0.573	0.441	0.505	0.454
IgA1 protease	0.676	0.118	0.519	0.008	0.815	0.030
Salmonella repeat of unknown function (DUF823)	0.678	0.184	0.599	0.083	0.483	0.069
arginine N-succinyltransferase	0.687	0.094	0.653	0.085	0.805	0.087
fliY	0.688	0.488	0.467	0.271	0.374	0.404
nucleoid DNA-binding protein	0.707	0.252	1.125	0.344	2.666	1.107
inorganic pyrophosphatase	0.707	0.107	0.729	0.101	0.556	0.065
antioxidant, AhpC/TSA family protein	0.717	0.072	0.613	0.054	0.385	0.116
DNA-directed RNA polymerase sigma subunit	0.725	0.179	0.430	0.133	0.472	0.172
Single-stranded DNA-binding protein	0.727	0.122	1.215	0.130	1.361	0.132
entS; EntS/YbdA MFS transporter	0.732	0.038	0.579	0.107	0.496	0.061
OmpH; Outer membrane protein (OmpH-like)	0.733	0.035	0.775	0.168	0.662	0.331
50S ribosomal protein L3	0.736	0.121	0.976	0.201	1.343	0.273
leucine transcriptional activator	0.736	0.147	1.260	0.824	5.737	5.229
D-lactate dehydrogenase	0.742	0.105	0.803	0.112	0.786	0.166
Acyl-[acyl-carrier-protein]--UDP-N-acetylglucosamine O-acyl	0.743	0.041	0.758	0.035	0.666	0.253
Aspartate-semialdehyde dehydrogenase	0.744	0.111	0.614	0.066	0.608	0.115
coxB; cytochrome c oxidase	0.745	0.091	0.633	0.147	0.652	0.360
anti-RNA polymerase sigma 70 factor	0.747	0.054	0.608	0.117	0.347	0.082
FMN_red; NADPH-dependent FMN reductase	0.747	0.078	0.800	0.077	0.359	0.069
non supervised orthologous group	0.750	0.353	0.594	0.144	0.383	0.190
ATP-dependent Clp protease proteolytic subunit	0.752	0.153	0.678	0.122	0.707	0.134
Protein of unknown function (DUF2750)	0.755	0.287	0.873	0.335	0.747	0.076
Adenosine deaminase 1	0.761	0.034	0.945	0.038	0.764	0.055
UPF0312 protein; YceI; YceI-like domain	0.762	0.188	0.772	0.235	0.507	0.179
D-3-phosphoglycerate dehydrogenase	0.762	0.157	0.670	0.179	2.698	0.752
Protein of unknown function (DUF1451)	0.766	0.169	0.716	0.181	0.288	0.093
ABC-type oligopeptide transport system, periplasmic component	0.767	0.178	0.577	0.180	0.592	0.152
aminopeptidase N	0.776	0.188	0.614	0.138	1.090	0.342
Peptide chain release factor 3	0.784	0.018	0.648	0.044	0.903	0.248
Protein of unknown function	0.784	0.152	0.763	0.227	0.340	0.084
DNA-binding transcriptional regulator Crl	0.786	0.177	0.656	0.143	0.381	0.103
3,4-dihydroxy-2-butanone 4-phosphate synthase	0.792	0.186	0.856	0.110	0.964	0.172
Chaperone protein hscA homolog	0.795	0.158	0.970	0.172	0.981	0.177
ABC amino acid transporter periplasmic ligand binding protein	0.795	0.175	0.660	0.007	0.614	0.046
chemotaxis protein CheX	0.797	0.132	0.991	0.058	0.596	0.094
Putative translation initiation inhibitor, yjgF family	0.804	0.159	0.929	0.194	0.573	0.150
30S ribosomal protein S11	0.809	0.448	0.798	0.507	1.481	1.002
ribosome-associated protein Y	0.810	0.173	1.166	0.451	1.515	0.987
3-isopropylmalate dehydrogenase	0.810	0.045	0.728	0.078	0.456	0.079

OmpR; osmolarity response regulator	0.811	0.320	0.740	0.316	0.518	0.226
aroC; Chorismate synthase	0.813	0.056	0.744	0.041	0.464	0.042
greA2; Transcription elongation factor	0.814	0.132	1.041	0.270	0.595	0.252
glycerol-3-phosphate dehydrogenase	0.819	0.027	0.594	0.044	1.403	0.071
Fe-S_biosyn; Iron-sulphur cluster biosynthesis	0.824	0.086	0.971	0.081	0.557	0.095
Arginine deiminase	0.824	0.081	0.929	0.214	1.109	0.375
GAF domain-containing protein	0.824	0.094	0.777	0.134	0.558	0.146
Asparaginyl-tRNA synthetase	0.827	0.139	0.562	0.133	0.849	0.202
UPF0502 protein	0.827	0.177	1.455	0.353	2.150	0.559
Phosphate-starvation-inducible E	0.828	0.167	0.937	0.090	0.722	0.061
sthA; Soluble pyridine nucleotide transhydrogenase	0.828	0.139	0.581	0.092	0.493	0.107
ferric uptake regulator	0.829	0.114	1.066	0.085	0.764	0.092
Probable cytosol aminopeptidase	0.830	0.149	1.441	0.250	4.428	1.101
Protein of unknown function (DUF1499)	0.834	0.062	0.911	0.071	0.468	0.055
50S ribosomal protein	0.836	0.304	0.772	0.359	1.408	0.762
Glutaminyl-tRNA synthetase	0.839	0.245	0.930	0.277	0.911	0.248
trimethylamine-N-oxide reductase	0.841	0.054	1.081	0.155	0.519	0.097
50S ribosomal protein L6	0.846	0.131	1.037	0.228	1.195	0.197
DNA-binding transcriptional regulator TorR	0.851	0.129	1.842	0.302	6.595	1.184
deoC; Deoxyribose-phosphate aldolase	0.858	0.076	0.667	0.117	0.551	0.167
Dihydrodipicolinate reductase	0.860	0.109	0.805	0.103	0.623	0.110
bifunctional phosphoribosylaminoimidazolecarboxamide formyltransferase/IMP cyclohydrolase, Bifunctional purine biosynthesis protein purH	0.860	0.097	0.669	0.113	0.263	0.034
ATP synthase epsilon chain 1	0.862	0.153	0.567	0.251	0.624	0.585
Protein-disulfide isomerase	0.863	0.097	1.086	0.173	1.001	0.166
Nitrogen regulatory protein PII	0.864	0.033	1.026	0.087	0.717	0.016
LUXS S-ribosylhomocysteine lyase	0.866	0.137	1.091	0.221	0.652	0.101
4,5-dioxygenase	0.868	0.091	0.733	0.211	0.422	0.028
fatty acid reductase	0.876	0.299	0.892	0.335	1.279	0.322
	0.881	0.099	1.449	0.093	0.813	0.428
	0.881	0.071	0.990	0.105	1.358	0.140
oxidoreductase	0.883	0.120	0.892	0.017	0.851	0.079
N-succinylglutamate 5-semialdehyde dehydrogenase	0.883	0.103	0.426	0.068	0.286	0.076
Protein of unknown function (DUF339)	0.884	0.115	0.969	0.091	0.557	0.074
bifunctional 2',3'-cyclic nucleotide 2'-phosphodiesterase/3'-nucleotidase periplasmic precursor protein	0.885	0.156	0.962	0.111	0.892	0.206
argD; bifunctional N-succinyldiaminopimelate-aminotransferase/acetylornithine transaminase protein	0.885	0.106	0.519	0.137	0.471	0.137
Acetyl-coenzyme A synthetase 2	0.886	0.047	0.477	0.063	0.574	0.032
phosphoheptose isomerase	0.887	0.165	0.999	0.158	0.680	0.161
Gamma-glutamyl phosphate reductase	0.888	0.128	0.763	0.092	1.165	0.126
phosphomannomutase	0.889	0.048	0.394	0.027	0.238	0.027
carboxy-terminal protease	0.892	0.166	0.772	0.204	0.928	0.292
ribonuclease E	0.895	0.170	1.008	0.123	1.578	0.722

ATP-dependent Clp protease ATP-binding subunit	0.896	0.094	0.644	0.050	0.304	0.100
Dihydroorotase	0.897	0.183	1.360	0.349	0.856	0.177
Serine proteases of the peptidase family S9A	0.910	0.127	1.026	0.168	0.913	0.188
ABC-type Zn2+ transport system, periplasmic component/surface adhesin	0.914	0.372	0.895	0.395	0.600	0.086
Cell division protein zapB	0.915	0.140	1.093	0.143	0.567	0.091
Peptide deformylase OS	0.916	0.104	0.984	0.070	0.762	0.124
Serine hydroxymethyltransferase	0.917	0.134	1.007	0.180	0.493	0.095
50S ribosomal protein L18	0.919	0.196	0.972	0.340	1.299	0.489
Cysteine desulfurase	0.922	0.231	0.835	0.372	1.203	0.583
choloylglycine hydrolase	0.924	0.086	1.284	0.098	1.066	0.104
Spermidine/putrescine-binding periplasmic protein	0.924	0.079	1.070	0.060	0.716	0.002
Uracil phosphoribosyltransferase	0.925	0.150	1.108	0.275	0.530	0.086
Purine nucleoside phosphorylase deoD-type 2	0.926	0.223	0.794	0.146	0.744	0.147
UPF0319 protein	0.926	0.175	1.113	0.208	0.666	0.178
50S ribosomal protein L13	0.928	0.204	1.001	0.182	1.577	0.254
DNA-binding protein H-NS	0.929	0.706	1.558	1.742	2.513	3.902
30S ribosomal protein S6	0.929	0.161	1.134	0.164	1.307	0.215
Sporulation control protein	0.930	0.154	0.789	0.032	1.100	0.092
fdx; ferredoxin, 2Fe-2S	0.930	0.187	1.133	0.362	0.641	0.228
antioxidant, AhpC/Tsa family	0.934	0.398	1.032	0.249	0.852	0.306
phosphoglucomutase	0.937	0.198	0.922	0.129	0.292	0.083
Fatty acid metabolism regulator protein	0.937	0.105	1.133	0.177	0.623	0.083
Elongation factor Tu	0.937	0.499	0.907	0.307	0.507	0.211
uncharacterized protein	0.938	0.116	0.921	0.120	0.884	0.139
50S ribosomal protein L7/L12	0.940	0.413	1.388	0.710	0.900	0.501
50S ribosomal protein L24	0.940	0.355	1.220	0.110	1.239	0.357
Protein of unknown function (DUF541)	0.941	0.045	0.896	0.123	1.171	0.082
30S ribosomal protein S14	0.942	0.337	0.787	0.272	1.335	0.720
uncharacterized protein	0.944	0.078	1.151	0.138	0.624	0.063
glyceraldehyde 3-phosphate dehydrogenase	0.944	0.823	0.679	0.161	0.887	0.318
DNA-directed RNA polymerase subunit beta	0.944	0.178	0.992	0.178	3.305	0.701
ATP synthase subunit delta 1	0.944	0.150	1.008	0.303	0.678	0.137
HlyU; Transcriptional activator HlyU	0.946	0.148	0.925	0.102	0.500	0.067
Porphobilinogen deaminase	0.946	0.093	0.977	0.248	0.604	0.138
trans-2-enoyl-CoA reductase	0.947	0.122	0.821	0.079	0.606	0.153
ABC-type Fe3+ transport system, periplasmic component	0.947	0.451	0.767	0.124	0.852	0.135
ATP-dependent protease	0.949	0.163	0.967	0.271	3.234	1.233
acetyl-CoA synthetase	0.949	0.126	0.507	0.101	0.600	0.097
Phosphoglucosamine mutase	0.950	0.459	0.848	0.524	1.217	1.147
phosphoribosylformylglycinamidine synthase	0.952	0.116	0.874	0.179	1.389	0.419
acetyl-CoA carboxylase biotin carboxylase subunit	0.954	0.225	0.761	0.166	0.699	0.153
Putative heme iron utilization protein	0.955	0.285	0.836	0.261	0.449	0.198
Amidophosphoribosyltransferase	0.956	0.131	1.049	0.133	2.584	0.361
50S ribosomal protein L19	0.958	0.055	0.900	0.077	1.333	0.146
Manganese superoxide dismutase	0.962	0.043	0.249	0.045	0.104	0.043

30S ribosomal protein S16	0.963	0.149	1.135	0.246	1.126	0.179
glycerophosphodiester phosphodiesterase	0.963	0.430	1.016	0.457	0.905	0.356
Probable Fe(2+)-trafficking protein	0.964	0.457	0.927	0.099	0.504	0.147
Pyridoxine 5'-phosphate synthase	0.966	0.125	1.000	0.121	0.958	0.136
Peptidyl-prolyl cis-trans isomerase	0.970	0.085	1.107	0.086	0.822	0.168
Peptidyl-prolyl cis-trans isomerase	0.971	0.207	1.133	0.332	0.497	0.142
phosphoribosylamine--glycine ligase	0.972	0.111	0.975	0.107	0.367	0.090
maltose ABC transporter periplasmic protein	0.973	0.248	1.002	0.229	0.821	0.179
peptidase	0.973	0.087	0.913	0.118	1.325	0.315
Iron-sulfur cluster insertion protein erpA	0.977	0.097	1.218	0.223	0.880	0.041
30S ribosomal protein S3	0.979	0.091	0.833	0.111	2.479	0.153
Peptide chain release factor 1	0.979	0.312	1.010	0.142	0.734	0.111
pknB; probable serine/threonine-protein kinase	0.979	0.730	0.885	0.079	0.538	0.117
30S ribosomal protein S4	0.982	0.172	1.095	0.141	1.882	0.393
Uroporphyrinogen decarboxylase	0.982	0.210	1.170	0.118	1.482	0.280
nitroreductase A	0.982	0.059	0.870	0.342	0.614	0.029
Nitroreductase	0.984	0.107	1.283	0.096	1.017	0.151
50S ribosomal protein L4	0.985	0.355	1.082	0.520	1.752	0.818
fumC; fumarate hydratase	0.985	0.094	0.348	0.045	0.127	0.039
putative manganese-dependent inorganic pyrophosphatase	0.985	0.220	1.155	0.186	0.878	0.157
DNA-directed RNA polymerase subunit beta	0.986	0.202	0.970	0.199	3.089	0.840
putative type I restriction-modification system, methyltransferase subunit	0.987	0.078	1.096	0.125	0.913	0.097
50S ribosomal protein L5	0.987	0.087	1.023	0.090	2.237	0.357
Glycine dehydrogenase [decarboxylating]	0.989	0.198	1.260	0.261	3.787	1.124
oxygen-independent coproporphyrinogen III oxidase	0.990	0.100	0.819	0.085	0.527	0.068
adenylate cyclase	0.991	0.159	0.736	0.102	0.430	0.030
Acyl carrier protein	0.992	0.202	1.247	0.287	0.602	0.269
Peptidyl-prolyl cis-trans isomerase	0.994	0.117	0.979	0.163	0.534	0.167
PKCI_related; Protein Kinase C Interacting protein related (PKCI): PKCI and related proteins belong to the ubiquitous HIT family of hydrolases that act on alpha-phosphates of ribonucleotides	0.995	0.116	0.984	0.137	0.401	0.063
3-hydroxydecanoyl-[acyl-carrier-protein] dehydratase	0.995	0.187	1.313	0.233	2.303	0.648
50S ribosomal protein L16	0.995	0.088	1.102	0.108	2.233	0.260
3'(2'),5'-bisphosphate nucleotidase	0.995	0.153	0.776	0.024	0.737	0.021
30S ribosomal protein	1.000	0.310	1.078	0.194	1.424	0.251
2-dehydro-3-deoxyphosphooctonate aldolase	1.000	0.114	1.174	0.105	1.017	0.124
isoprenoid biosynthesis protein with amidotransferase-like domain	1.001	0.256	0.906	0.137	0.601	0.545
Glycine cleavage system H protein	1.001	0.129	1.628	0.307	0.850	0.122
Bifunctional protein folD	1.003	0.110	1.342	0.198	0.885	0.104
Phosphoglycerate kinase	1.003	0.430	0.934	0.499	0.411	0.340
50S ribosomal protein L21	1.004	0.418	1.076	0.196	1.341	0.358
peptidase	1.006	0.396	0.712	0.111	0.855	0.130
Phosphate transport regulator (distant homolog of PhoU)~	1.008	0.110	0.823	0.085	0.401	0.066

30S ribosomal protein S9	1.013	0.160	1.059	0.178	2.393	0.458
aromatic amino acid aminotransferase	1.014	0.067	0.641	0.273	0.886	0.139
alkanal monooxygenase alpha chain	1.014	0.312	0.923	0.253	1.063	0.301
Aspartyl-tRNA synthetase	1.014	0.137	0.809	0.129	0.978	0.161
Isoleucyl-tRNA synthetase	1.014	0.215	1.059	0.249	1.592	0.357
nucleotide sugar dehydrogenase	1.017	0.223	0.597	0.034	0.266	0.026
50S ribosomal protein L14	1.017	0.287	1.387	0.478	2.282	0.986
scaffold protein	1.021	0.351	1.396	0.572	0.940	0.377
HTH-type transcriptional repressor purR	1.021	0.339	0.949	0.350	1.452	0.843
Adenylate kinase	1.021	0.163	1.166	0.228	0.733	0.171
3-methyl-2-oxobutanoate hydroxymethyltransferase	1.021	0.324	1.177	0.241	1.422	0.312
Triosephosphate isomerase	1.023	0.813	1.038	0.210	0.726	0.169
DNA polymerase I	1.023	0.041	0.811	0.048	2.026	0.618
50S ribosomal protein	1.024	0.139	1.161	0.126	1.394	0.129
Protein of unknown function (DUF1244)	1.024	0.102	1.280	0.075	0.824	0.105
30S ribosomal protein S21	1.025	0.085	1.067	0.078	1.348	0.161
Ribonucleoside-diphosphate reductase	1.028	0.010	0.775	0.053	1.167	0.053
coxB; cytochrome c oxidase, subunit II	1.028	0.537	1.575	0.524	1.430	1.005
Ribulose-phosphate 3-epimerase	1.029	0.163	1.184	0.235	1.012	0.184
adenylosuccinate synthetase	1.029	0.462	0.567	0.248	0.264	0.116
Thiol:disulfide interchange protein DsbA	1.032	0.115	1.076	0.127	0.640	0.179
Fe/S biogenesis protein nfuA	1.032	0.063	1.799	0.171	0.645	0.059
6,7-dimethyl-8-ribityllumazine synthase	1.034	0.126	1.058	0.111	1.185	0.126
thiamine transporter substrate binding subunit	1.035	0.341	0.783	0.086	0.920	0.182
plasmid pVIBHAR	1.036	0.247	0.944	0.314	0.248	0.076
signal recognition particle GTPase	1.037	0.169	1.168	0.226	0.955	0.282
Erythronate-4-phosphate dehydrogenase	1.040	0.105	0.901	0.055	1.373	0.042
carboxypeptidase	1.040	0.166	0.729	0.111	0.972	0.233
surA; survival protein SurA	1.041	0.134	1.187	0.193	0.897	0.152
Arginyl-tRNA synthetase	1.041	0.139	0.966	0.133	1.510	0.208
50S ribosomal protein L9	1.042	0.300	1.131	0.175	1.465	0.284
uncharacterized protein	1.042	0.006	1.199	0.072	0.761	0.267
aromatic amino acid aminotransferase	1.043	0.175	0.968	0.115	1.683	0.317
GTP cyclohydrolase 1	1.043	0.060	1.207	0.154	0.981	0.103
Succinylglutamate desuccinylase	1.047	0.127	0.830	0.125	1.520	0.359
UPF0265 protein	1.047	0.111	1.057	0.112	0.511	0.064
AcrR; Transcriptional regulator [Transcription]	1.050	0.516	1.278	0.361	3.873	1.628
prolyl oligopeptidase	1.051	0.185	1.052	0.181	0.937	0.153
cheY; chemotaxis protein CheY	1.052	0.074	0.953	0.052	0.455	0.030
Oligoribonuclease	1.053	0.049	0.995	0.092	0.600	0.091
Phosphoribosylglycinamide formyltransferase 2	1.055	0.246	0.953	0.207	0.953	0.177
pyruvate-formate lyase	1.055	0.220	1.175	0.208	2.547	0.760
ATP-dependent protease La	1.057	0.257	0.861	0.177	0.897	0.304
3,4-dihydroxy-2-butanone 4-phosphate synthase	1.057	0.291	1.021	0.392	0.614	0.187
2-oxoglutarate dehydrogenase E1 component	1.059	0.167	0.930	0.156	2.711	0.558
50S ribosomal protein L17	1.061	0.192	1.222	0.254	1.228	0.201

hypothetical protein	1.062	0.080	1.026	0.249	2.944	0.549
GMP synthase [glutamine-hydrolyzing]	1.064	0.046	1.225	0.102	3.042	0.406
tryptophanyl-tRNA synthetase	1.066	0.046	1.081	0.198	1.157	0.376
predicted iron-dependent peroxidase	1.068	0.240	1.176	0.140	1.323	0.858
50S ribosomal protein L11	1.068	0.574	1.090	0.188	1.310	0.479
cytochrome b562	1.069	0.047	1.294	0.174	0.854	0.128
30S ribosomal protein S18	1.072	0.491	0.941	0.196	1.863	0.620
Tryptophan synthase alpha chain	1.074	0.075	1.067	0.201	0.787	0.206
Glutamate-1-semialdehyde 2,1-aminomutase	1.075	0.363	0.855	0.313	0.338	0.122
glutamate dehydrogenase	1.076	0.371	0.676	0.129	1.041	0.322
Carbamoyl-phosphate synthase large chain	1.078	0.133	1.101	0.134	1.371	0.195
33 kDa chaperonin	1.079	0.210	1.353	0.206	1.149	0.243
30S ribosomal protein S19	1.079	0.179	1.361	0.248	1.338	0.048
ADP-ribose diphosphatase NudE	1.079	0.177	0.898	0.124	0.884	0.141
Peptidase_M14-like_4; A functionally uncharacterized subgroup of the M14 family of metallocarboxypeptidases (MCPs).	1.080	0.295	1.212	0.451	0.840	0.224
thioredoxin	1.081	0.143	1.195	0.108	0.769	0.096
Pyruvate dehydrogenase E1 component	1.082	0.220	1.055	0.191	3.234	0.918
Pyruvate kinase	1.083	0.177	0.951	0.151	1.645	0.273
pyrazinamidase/nicotinamidase	1.086	0.337	1.198	0.350	0.889	0.100
iron-containing alcohol dehydrogenase	1.086	0.292	1.485	0.164	0.492	0.137
Phosphopantetheine attachment site	1.087	0.243	1.024	0.163	0.548	0.134
Peptidyl-prolyl cis-trans isomerase	1.087	0.298	1.215	0.345	0.766	0.287
cb-type cytochrome oxidase subunit III	1.088	0.098	1.693	0.379	0.677	0.091
30S ribosomal protein S8	1.090	0.098	1.047	0.093	2.114	0.216
Elongation factor P	1.090	0.216	1.179	0.329	1.108	0.301
Polyribonucleotide nucleotidyltransferase	1.090	0.591	1.084	0.702	1.998	1.740
heat shock protein	1.092	0.156	1.540	0.293	3.063	0.741
Ribosome-recycling factor	1.092	0.207	1.200	0.271	0.789	0.269
UPF0149 protein	1.093	0.121	1.067	0.101	0.582	0.118
Zn-dependent oligopeptidase	1.093	0.198	0.885	0.111	1.691	0.374
Seryl-tRNA synthetase	1.093	0.168	1.250	0.254	1.049	0.192
50S ribosomal protein L2	1.094	0.159	1.160	0.104	2.053	0.456
succinate dehydrogenase iron-sulfur subunit	1.095	0.222	1.245	0.164	3.122	0.453
DNA gyrase subunit B	1.096	0.121	0.806	0.049	1.117	0.247
Threonyl-tRNA synthetase	1.097	0.127	0.889	0.092	1.209	0.151
50S ribosomal protein L28	1.099	0.082	1.110	0.124	1.739	0.219
phosphoenolpyruvate-protein phosphotransferase	1.099	0.128	1.110	0.222	1.235	0.306
phosphoribosylaminoimidazole carboxylase ATPase subunit	1.102	0.097	1.152	0.147	1.231	0.155
UPF0133 protein	1.103	0.271	1.253	0.358	0.929	0.338
Fructose-1,6-bisphosphatase class 1	1.105	0.190	1.118	0.213	1.340	0.291
Chaperone protein dnaJ	1.106	0.067	0.896	0.013	0.834	0.036
Translation initiation factor IF-2	1.107	0.356	0.857	0.256	1.236	0.502
50S ribosomal protein L32	1.108	0.405	1.529	0.670	1.540	0.642
Phosphoserine aminotransferase	1.108	0.037	0.911	0.142	0.751	0.141
NAD-dependent malic enzyme	1.110	0.184	1.012	0.166	3.261	0.773

50S ribosomal protein L22	1.110	0.702	0.993	0.404	1.432	0.680
50S ribosomal protein L10	1.110	0.178	1.206	0.257	1.625	0.418
Aspartate carbamoyltransferase regulatory chain	1.110	0.030	1.105	0.009	1.554	0.106
carbonic anhydrase	1.115	0.207	1.210	0.205	0.845	0.193
UDP-N-acetylglucosamine 2-epimerase	1.116	0.190	1.075	0.194	0.284	0.076
Protein-export protein secB	1.117	0.166	1.171	0.151	0.909	0.340
Chaperone protein dnaK	1.118	0.647	1.289	0.501	0.898	0.358
peroxiredoxin	1.118	0.102	0.981	0.083	0.514	0.175
RNA polymerase sigma factor	1.119	0.205	0.981	0.127	2.440	0.687
Peptidase_M75; Imelysin	1.120	0.164	1.148	0.233	0.858	0.263
Trigger factor	1.120	0.725	1.674	1.350	1.988	1.876
zinc-carboxypeptidase	1.120	0.082	1.059	0.078	1.198	0.097
asparagine synthetase B	1.121	0.254	0.690	0.083	0.367	0.119
archaeal Glu-tRNA(Gln) amidotransferase, subunit E containing GAD domain	1.122	0.136	1.374	0.224	0.786	0.161
Leucyl-tRNA synthetase	1.122	0.223	1.203	0.202	1.791	0.311
ADP-L-glycero-D-manno-heptose-6-epimerase	1.122	0.097	0.865	0.129	1.016	0.172
phenylalanyl-tRNA synthetase subunit beta	1.122	0.156	1.062	0.121	1.973	0.275
Catalase	1.123	0.145	1.547	0.269	1.478	0.272
DNA-directed RNA polymerase subunit alpha	1.124	0.224	1.207	0.251	2.076	0.422
Transcriptional regulators of sugar metabolism	1.128	0.023	0.859	0.133	1.054	0.023
putative alcohol dehydrogenase	1.130	0.110	0.739	0.112	0.662	0.062
50S ribosomal protein L1	1.130	0.286	1.248	0.288	1.344	0.276
glutathione synthetase	1.132	0.228	1.133	0.287	1.166	0.426
Histidyl-tRNA synthetase	1.134	0.270	1.086	0.253	1.925	1.040
Xaa-Pro aminopeptidase	1.135	0.176	0.900	0.099	1.739	0.261
Elongation factor G 2	1.135	0.310	0.998	0.187	1.467	0.319
malate oxidoreductase	1.137	0.155	1.211	0.139	1.293	0.199
FMN reductase	1.137	0.140	1.002	0.131	0.820	0.108
6-phosphofructokinase	1.141	0.161	0.961	0.083	1.223	0.013
Transaldolase	1.142	0.261	1.034	0.254	0.986	0.348
Delta-aminolevulinic acid dehydratase	1.145	0.178	1.092	0.232	0.993	0.271
putative nucleotide-binding protein	1.146	0.376	1.422	0.427	1.178	0.232
dihydrodipicolinate synthase	1.147	0.129	1.190	0.127	0.289	0.051
UPF0176 protein	1.149	0.203	1.312	0.300	0.662	0.095
Diaminopimelate decarboxylase	1.150	0.139	1.001	0.107	1.232	0.143
beta-hexosaminidase	1.151	0.077	0.961	0.084	1.484	0.302
Lysyl-tRNA synthetase	1.151	0.133	0.982	0.196	0.633	0.110
30S ribosomal protein S5	1.152	0.234	1.233	0.300	2.146	0.461
UDP-N-acetylglucosamine 1-carboxyvinyltransferase	1.157	0.519	0.908	0.507	1.534	0.732
positive response regulator for pho regulon	1.157	0.069	1.053	0.077	0.942	0.096
Sulfite reductase [NADPH] hemoprotein beta-component	1.160	0.257	1.772	0.501	1.603	0.430
phosphoenolpyruvate synthase	1.161	0.212	1.186	0.220	2.395	0.592
3-oxoacyl-[acyl-carrier-protein] synthase 2	1.163	0.074	1.013	0.113	0.683	0.122
alkanal monooxygenase beta chain	1.164	0.292	0.930	0.177	1.475	0.348
TelA; Toxic anion resistance protein (TelA)	1.165	0.250	1.368	0.266	1.103	0.334
ATP-dependent protease	1.168	0.190	1.101	0.179	1.418	0.217

60 kDa chaperonin	1.169	0.269	1.030	0.219	1.319	0.303
Enolase 1	1.173	0.358	1.238	0.292	0.665	0.241
phosphoribosylaminoimidazole carboxylase catalytic subunit	1.173	0.209	1.252	0.296	1.597	0.205
general secretory pathway protein E	1.175	0.103	1.145	0.130	1.494	0.133
Phosphoenolpyruvate carboxykinase [ATP]	1.176	0.448	0.946	0.271	1.453	0.402
30S ribosomal protein S7	1.178	0.276	1.111	0.181	1.971	0.439
Transcription termination factor Rho	1.185	0.429	0.903	0.283	0.857	0.499
Aspartate carbamoyltransferase	1.187	0.235	0.977	0.210	2.000	0.673
stringent starvation protein A	1.187	0.109	0.931	0.071	1.909	0.214
Alanyl-tRNA synthetase	1.193	0.325	1.321	0.529	1.528	0.481
Succinyl-CoA ligase [ADP-forming] subunit beta	1.193	0.451	1.336	0.295	0.997	0.260
Glycerol kinase	1.195	0.121	0.952	0.140	2.899	0.373
DNA polymerase III subunit beta	1.198	0.206	1.450	0.211	1.762	0.175
ribosome-associated protein Y	1.198	0.112	1.176	0.067	1.465	0.095
putative ABC transporter ATP-binding protein	1.200	0.257	1.084	0.146	0.498	0.204
Alanine dehydrogenase	1.203	0.221	0.848	0.138	1.754	0.310
Glutamyl-tRNA synthetase	1.205	0.112	0.981	0.078	0.713	0.138
2,3-bisphosphoglycerate-independent phosphoglycerate mutase	1.206	0.586	0.969	0.311	0.705	0.190
phosphocarrier protein PtsH	1.208	0.139	1.399	0.025	0.678	0.019
Inosine-5'-monophosphate dehydrogenase	1.208	0.503	0.986	0.526	0.449	0.171
30S ribosomal protein S2	1.210	0.350	1.105	0.365	1.668	0.839
transcription elongation factor NusA	1.211	0.281	1.106	0.290	1.205	0.342
Elongation factor G 1	1.211	0.094	1.121	0.163	1.152	0.161
Valyl-tRNA synthetase	1.215	0.182	1.321	0.206	1.258	0.189
EntF; Non-ribosomal peptide synthetase modules and related proteins	1.216	0.111	0.582	0.081	0.184	0.035
ribonucleotide-diphosphate reductase subunit beta	1.216	0.171	1.340	0.159	1.929	0.979
Glucose-6-phosphate 1-dehydrogenase	1.217	0.217	1.071	0.200	2.274	0.639
transketolase	1.218	0.285	1.067	0.262	1.611	0.397
ketol-acid reductoisomerase	1.218	0.354	0.980	0.198	1.115	0.251
Glutamine synthetase	1.222	0.444	1.014	0.218	1.508	0.246
GTP-binding protein engA	1.224	0.376	0.828	0.309	0.854	0.328
Thioredoxin reductase	1.225	0.668	1.041	0.079	0.951	0.130
Glutamate--cysteine ligase	1.225	0.196	1.135	0.195	1.124	0.293
Glucose-6-phosphate isomerase	1.226	0.198	1.147	0.214	1.508	0.467
bifunctional proline dehydrogenase/pyrroline-5-carboxylate dehydrogenase	1.226	0.252	1.060	0.143	1.696	0.380
succinate dehydrogenase flavoprotein subunit	1.229	0.230	1.185	0.208	1.861	0.577
Dihydrolipoyl dehydrogenase	1.229	0.246	1.468	0.337	2.191	0.647
Isocitrate dehydrogenase [NADP]	1.229	0.510	0.932	0.270	0.562	0.179
glyS; Glycyl-tRNA synthetase beta subunit	1.232	0.272	1.061	0.265	0.557	0.115
ATP synthase gamma chain	1.232	0.365	1.039	0.233	1.721	0.708
Cytidylate kinase	1.236	0.284	1.439	0.154	0.874	0.145
Carbon storage regulator homolog	1.236	0.144	1.189	0.461	0.990	0.032
Putative Mg2+ and Co2+ transporter	1.238	0.271	1.435	0.317	1.247	0.351
ABC amino acid transporter periplasmic	1.238	0.225	1.750	0.392	1.557	0.336

component						
DUF1887; Protein of unknown function,	1.239	0.147	1.194	0.209	2.318	0.370
Serine hydroxymethyltransferase	1.241	0.231	0.869	0.166	0.348	0.205
PTS system glucose-specific transporter subunit	1.248	0.963	1.100	0.581	0.609	0.240
4-hydroxy-3-methylbut-2-en-1-yl diphosphate synthase	1.250	0.045	1.193	0.068	1.108	0.086
Spermidine/putrescine-binding periplasmic protein	1.254	0.849	0.803	0.268	0.579	0.349
50S ribosomal protein L23	1.255	0.400	1.334	0.462	1.671	0.556
glucosamine--fructose-6-phosphate aminotransferase	1.257	0.173	1.217	0.179	1.414	0.214
uncharacterized protein	1.258	0.291	1.748	0.314	0.893	0.218
Aminomethyltransferase	1.259	0.423	1.402	0.473	1.493	0.536
uncharacterized protein	1.264	0.142	1.626	0.193	0.648	0.146
malonyl CoA-acyl carrier protein transacylase	1.266	0.005	1.202	0.015	0.590	0.004
Phosphoribosylaminoimidazole-succinocarboxamide synthase	1.269	0.234	0.881	0.143	0.326	0.112
Protein translocase subunit secA	1.269	0.358	0.791	0.157	1.004	0.236
YceI; YceI-like domain	1.270	0.477	1.323	0.117	0.955	0.212
prfB; protein chain release factor B	1.271	0.262	1.212	0.224	0.504	0.126
transketolase	1.272	0.184	1.043	0.172	1.621	0.279
ATP synthase subunit alpha 1	1.272	0.377	0.956	0.205	1.944	0.568
6-phosphogluconate dehydrogenase, decarboxylating	1.272	0.286	1.268	0.389	1.685	0.431
Prolyl-tRNA synthetase	1.273	0.425	1.090	0.340	1.554	0.544
dihydrolipoamide acetyltransferase	1.277	0.275	1.301	0.306	1.920	0.489
glutamate decarboxylase	1.277	0.241	1.225	0.218	1.254	0.340
hypoxanTHIne ribosyl transferase	1.278	0.092	1.195	0.098	1.080	0.099
Ubiquinol-cytochrome c reductase iron-sulfur subunit	1.285	0.255	2.094	0.141	1.566	0.354
typA, bipA, yihK, yjhK; putative GTP-binding factor	1.285	0.636	1.755	0.933	4.672	2.848
ferredoxin/oxidoreductase	1.286	0.280	0.903	0.134	0.949	0.052
carbamoyl phosphate synthase small subunit	1.290	0.296	1.387	0.368	0.924	0.248
ATP-dependent hsl protease ATP-binding subunit	1.291	0.422	0.923	0.223	0.837	0.237
Methionyl-tRNA synthetase	1.291	0.415	1.291	0.400	2.579	0.897
6-phosphogluconolactonase/Glucosamine-6-phosphate isomerase/deaminase	1.299	0.095	1.122	0.022	1.396	0.089
Aconitate hydratase 2	1.300	0.279	1.340	0.300	1.450	0.361
cheW; CheW positive regulator of CheA protein activity	1.300	0.135	1.251	0.151	1.158	0.139
ubiquinone/menaquinone biosynthesis methyltransferase	1.301	0.323	0.943	0.171	0.574	0.169
2,3,4,5-tetrahydropyridine-2-carboxylate N-succinyltransferase	1.305	0.197	0.825	0.067	0.820	0.180
cysteinyl-tRNA synthetase	1.308	0.175	1.193	0.121	1.946	0.319
pterin-4-alpha-carbinolamine dehydratase	1.309	0.180	1.693	0.362	1.422	0.180
Tyrosyl-tRNA synthetase	1.313	0.185	1.123	0.201	0.909	0.050
30S ribosomal protein S1	1.322	0.278	1.531	0.389	1.958	0.517
fructose-bisphosphate aldolase	1.323	0.850	0.931	0.344	1.204	0.579

UPF0082 protein	1.323	0.408	1.375	0.445	0.949	0.184
Phosphatidylserine/phosphatidylglycerophosphate/cardiolipin synthases and related enzymes [Lipid metabolism	1.325	0.116	1.250	0.030	3.161	0.291
ferritin	1.332	0.582	1.114	0.340	1.106	0.666
acetyl-CoA acetyltransferase	1.341	0.527	0.886	0.394	0.430	0.242
Phosphate acetyltransferase	1.343	0.249	0.888	0.235	0.718	0.196
adenylosuccinate lyase	1.343	0.259	1.185	0.278	2.926	0.893
metK; S-adenosylmethionine synthase	1.345	0.093	0.979	0.064	0.492	0.063
nitrate/sulfonate/bicarbonate transport systems, periplasmic components	1.345	0.205	1.525	0.321	1.371	0.286
Ribose-5-phosphate isomerase A	1.348	0.722	1.140	0.144	1.164	0.179
Pantothenate synthetase	1.380	0.166	1.161	0.157	1.606	0.310
AckA Acetate kinase	1.380	0.091	0.921	0.095	0.542	0.169
CTP synthase	1.383	0.380	1.142	0.367	0.631	0.289
Elongation factor Ts	1.387	0.755	1.467	0.439	1.430	0.500
Protein of unknown function (DUF3549)	1.392	0.198	1.072	0.041	0.440	0.008
Protein grpE	1.396	0.577	1.705	0.454	1.375	0.430
clpB; heat shock protein	1.399	0.542	1.093	0.669	0.613	0.352
DNA gyrase subunit A	1.403	0.490	1.255	0.602	3.725	1.903
Orotidine 5'-phosphate decarboxylase	1.411	0.162	1.215	0.095	1.190	0.068
inositol monophosphate family protein	1.412	0.563	1.986	1.243	2.292	1.229
Adenine phosphoribosyltransferase	1.426	0.121	1.238	0.202	0.343	0.079
ATP synthase subunit beta 1	1.429	0.406	1.060	0.238	2.193	0.499
Thiamine-phosphate pyrophosphorylase	1.438	0.144	1.053	0.121	1.131	0.190
Cysteine synthase	1.442	0.250	1.646	0.222	0.896	0.334
Nucleoside diphosphate kinase	1.454	0.125	1.312	0.150	0.506	0.070
Universal stress protein UspA and related nucleotide-binding proteins	1.455	0.099	0.822	0.056	0.573	0.064
Cold shock proteins	1.456	0.648	1.743	0.857	0.626	0.304
Succinyl-CoA ligase [ADP-forming] subunit alpha	1.460	0.602	1.465	0.578	1.121	0.466
Chaperone protein htpG	1.460	0.334	1.280	0.308	2.242	0.821
Dihydroorotate dehydrogenase	1.463	0.584	1.180	0.683	1.160	0.836
Malate dehydrogenase	1.464	0.797	1.204	0.320	0.875	0.282
ABC-type tungstate transport system, permease component	1.468	0.285	2.454	0.533	1.774	0.573
sulfite reductase (NADPH) flavoprotein subunit alpha	1.470	0.396	1.459	0.285	3.560	1.621
Citrate synthase	1.471	0.218	0.895	0.163	0.376	0.116
Phosphoadenosine phosphosulfate reductase	1.474	0.389	1.646	0.645	2.332	1.235
putative glutathione S-transferase YghU	1.476	0.397	1.523	0.256	0.973	0.194
long-chain-fatty-acid ligase	1.477	0.771	0.942	0.496	0.779	0.439
Lipoyl synthase	1.479	0.220	1.653	0.371	1.238	0.230
Orotate phosphoribosyltransferase	1.483	0.208	1.077	0.145	1.137	0.194
type II secretion pathway protein E	1.493	0.860	2.396	2.192	3.044	2.142
(Dimethylallyl)adenosine tRNA methylthiotransferase miaB	1.494	0.132	1.831	0.205	0.768	0.132
aspartate ammonia-lyase	1.504	0.335	1.213	0.191	2.521	0.605
2-amino-3-ketobutyrate coenzyme A ligase	1.510	0.329	1.578	0.316	3.336	0.926

LUXD Acyl transferase	1.527	0.528	1.231	0.370	1.379	0.440
hypothetical protein	1.534	0.190	1.539	0.216	2.010	0.283
Phosphoribosylformylglycinamidine cyclo-ligase	1.541	0.668	2.358	1.411	2.350	1.880
alkyl hydroperoxide reductase c22 protein	1.545	0.100	2.192	0.532	2.055	0.446
Thiazole synthase	1.552	0.158	1.592	0.207	2.085	0.337
anthranilate synthase component I	1.566	0.179	1.190	0.121	1.741	0.266
dihydrolipoamide succinyltransferase	1.568	0.380	1.295	0.395	3.315	1.249
Uridylate kinase	1.571	0.320	1.531	0.309	2.138	0.460
Phenylalanyl-tRNA synthetase alpha chain	1.572	0.369	1.377	0.321	1.856	0.410
thiamine biosynthesis protein ThiC	1.581	0.390	1.919	0.419	4.353	1.255
cAMP-regulatory protein	1.648	0.309	1.813	0.403	3.364	0.625
Transposase_31; Putative transposase, YhgA-like	1.658	0.335	1.532	0.799	0.765	0.150
3-ketoacyl-(acyl-carrier-protein) reductase	1.664	0.090	1.613	0.074	0.804	0.087
GTP-dependent nucleic acid-binding protein EngD	1.677	1.123	1.458	1.048	1.818	1.279
Elongation factor P-like protein	1.684	0.554	2.335	0.845	1.037	0.433
Glycyl-tRNA synthetase alpha subunit	1.718	0.168	1.131	0.118	1.588	0.253
Autonomous glycyl radical cofactor	1.724	0.463	1.975	0.519	1.279	0.385
10 kDa chaperonin	1.752	1.163	1.000	0.238	1.153	0.592
aminoacyl-histidine dipeptidase	1.760	0.986	1.130	0.104	1.897	0.476
Ribose-phosphate pyrophosphokinase	1.762	0.614	1.357	0.515	0.751	0.319
Sulfate adenylyltransferase subunit 2	1.777	0.150	1.378	0.152	1.544	0.333
50S ribosomal protein	1.802	0.722	0.821	0.279	2.013	0.747
fumarate hydratase, class I	1.846	0.292	2.391	0.664	2.126	0.492
L-threonine 3-dehydrogenase	1.874	0.446	1.807	0.445	2.623	0.701
Protein RecA	1.886	0.736	1.509	0.750	0.996	0.218
DNA-binding protein	2.031	1.452	1.256	0.222	4.703	2.486
ribosomal protein S20	2.082	2.074	2.522	2.509	1.498	1.363
Molybdenum cofactor biosynthesis protein	2.152	0.519	2.509	0.526	1.055	0.178
3-oxoacyl-[acyl-carrier-protein] synthase I	2.162	1.153	1.898	1.173	0.672	0.424
fructose 1,6-bisphosphatase II	2.537	3.077	4.349	6.085	6.988	10.905
azurin	2.796	2.386	0.865	0.285	0.625	0.075
heavy metal-(Cd/Co/Hg/Pb/Zn)-translocating P-type ATPase	2.949	0.143	0.889	0.012	0.997	0.094
regulatory ATPase RavA	4.023	2.230	1.229	0.452	0.897	0.230
Cell division protein ftsZ	4.288	4.935	5.264	6.442	5.162	7.002
Phasin_2; Phasin protein	4.990	3.994	4.017	3.935	2.167	1.604

Appendix 3 Sequence alignment of Swoo_2833 with LuxQ type H-NOX-adjacent HKs.

Organisms from top to bottom: *S. woodyi*, *Shewanella halifaxensis*, *V. fischeri*, *V. harveyi* and *Vibrio parahaemolyticus*.

```
swoo_2833          MSDKEAD-LIKTIAVLTRKAQRERSARLEAEKLLNQKSRELYFAKQEVEASLFSIQEKSD 59
Shal_2562          MPNDEFNSLTEKVNLLSRKIEREKAAKKAAEKLLEEKSRELYAAKQLVEDSLMNIKEKSE 60
VF_A0072           MD------VDKTIELLNRKIKREKAARKAAEGLLERKSHELYMAKQLVEDTLFTVQEKAE 54
vibhar_01913       ------------------------------------------------MALKKLEMKSQ 11
VP1876             ---------MTGNSSLERKLKREIASRKAAELLLEQKSYELYESTQKLSVALKKLELRSE 51
                                                                    :* .:: :::

swoo_2833          QDTALIGLKSNLESILLEFNQNFLQQPLSNDLLQSLMDTLAKLKHVESSQLVFKNEQKTS 119
Shal_2562          QDIALLHFKTYLESILLDFNQLFLQKPISDLLLQRLLDDLIGIDEVKACRIRFNALTSEK 120
VF_A0072           KDVVLLEFKSYLDSILLDYNQRLLKEQPTQMLLQSLINDLGCLNSIQSVCLSFSSNANET 114
vibhar_01913       KDLCKFEFEEQIDATLIKFGRTFLSSTFGESMITSFLEQLTLNSIVLGAYLYLVP-ENVS 70
VP1876             SDLRKFEFEEKIDATLIRFGRTFLSSTFDETMIASFLEQLTSNSVITASYLYLDP-VQLT 110
                   .*   : ::  ::: *: :.: :*..   : ::  ::: *   . : .  : :    . .

swoo_2833          HQANFSAG---TFTQWAPHNKGQTTDSEYPQRQLIVKIGENQHTLGSLYINLSVPNNWLS 176
Shal_2562          KAKTFYAGNKLLFQSELKANSALYWSEDYQQLNIIINAEAN--ILGGLTLVIDAPRTWQN 178
VF_A0072           -LTQLYAGKHQEFETLSQASYPVQWNESLTQITVFFELENIESGAIQLIFNTSPNTMWRD 173
vibhar_01913       PLRNHQFG-----YLQLANNRPIQSKPHWRKNCLHLPIIIGSTTFGELIFSLELDQVEQE 125
VP1876             SLRRHHFG-----HLDLKSDKPIARTPNWQNEALHLPIIIDERVVGELIFSVSLEQIEQA 165
                          *          .          :  : .          * .

                                                                  H box
swoo_2833          TIEKQLFLFSNMISAAYQRQVLLDKTLAQKTRAEQSERSTKDFVAMINHELRTPLNGLLG 236
Shal_2562          TIEKQLLLFCEMISAAHKRQQLLARTIEEKQRAESSERSTRDFVAMINHELRTPLNGLLG 238
VF_A0072           TIEKQFSLISEMINAAFERKYLLDKTLKEKKRAESSERATRDFVAMINHELRTPLNGLLG 233
vibhar_01913       FIFKQMVLVSDLVHGVISRHLSVQREVKLRKRAEASEKATKEFVAMVNHELRTPLNGVLG 185
VP1876             FISKQMELVSDLVHGVISRHLSLEREVELRKRAEESEKATKEFVAMINHELRTPLNGVLG 225
                    * **: *.:::: .. .*:  : : :  : *** **::*::****:**********:**

swoo_2833          NTELMIETRLSDYQEKLIKNMVQSGELLKVIINDLLDISKINAGMLELNEVAFSTLELTN 296
Shal_2562          SAELMSDTQLTPHQRQLLNTMHQSGELLRVIINDLLDLSKMSAGMLQIVEISFSPRQVCT 298
VF_A0072           SAELMEDTEITDYQKKLLETIHQSGQMLRIIINDLLDFSKMSAGMLELKMANFKPCILVK 293
vibhar_01913       SADLLDKTLLDDEQQQYLSNLIHSGDLLRVIINDLLDFSKMNAGMMEIIDKVFAWKDLEN 245
VP1876             SADLLSKTQLGEDQRQYLGNLIQSGDLLRVIINDLLDFSKMNAGMMEIIDKVFAWDDLEK 285
                   .::*: .* :   *.: : .: :**::*::*******:**:.***:::    *    :

                                                                  N box
swoo_2833          AIQNTFAPQAAEKGLAFDFEIDPKTPENLSGDPDRIKQIFVNLIGNAIKFTDKGKISIKI 356
Shal_2562          MIYDIFKQRTAEFGLSFAFNYHTEVPERLLGDPDRIKQLFVNLIGNSIKFTQSGQITVDI 358
VF_A0072           TIEQIFTPQMAEKCLRFDIHIADNLPQTLMGDIDRVQQILVNLIGNAFKFTKSGHISLKV 353
vibhar_01913       ALTGVFAAKAAEKRIHFSIDKKLGIPEFLIGDFERVTQILVNLIGNAIKFTNLGGVVLRV 305
VP1876             AITGVFAAKAAEKRIHFSIDKKLGIPEFLIGDLERITQILVNLIGNAIKFTHLGGVVLRV 345
                    :   *  : **  : * :.     *: * ** :*: *::******::***. * : : :
```


G1
F
swoo_2833 DWHESSFRFVISDTGCGIPKEHLANLFDPFTQVNNRSNRLYEGTGLGLTICKLLVNEMLG 416
Shal_2562 EWQDGQFCFSVTDTGCGIPADKVDTLFDPFTQVNNSSNRVYEGTGLGLAICKHLVDEMHG 418
VF_A0072 GWQKNALVLIVSDTGCGIPQDKQKLLFEPFTQVDNSSQRQFEGTGLGLSICKLLVDAMSG 413
vibhar_01913 EWQNGYANFEVEDTGIGIPLEAQKALFDPFVQADRSTKRSFEGSGLGLAICKNLVDLMGG 365
VP1876 EWVNGTAFFEVEDTGIGIPLAAQSSLFDPFVQVDRSAKRSFEGSGLGLAICKNLVDLMQG 405
QIALESQPDKGSSFTVTLPLAVTQAQ-QISQPAEF-NYTDFDSLTVLVVEDSHINQTLIK 474
DLTLTSELDKGTQFNIRLPLKLAPPS-QKPNHTHE-VDVAIDAMTVLVVEDSPVNQVLIE 476
ELSFKSELGEGSEFQVKLPLEVVCEQRTHSSEDNQ-LSFSIENLSILAVEDIKMNQVILN 472
DISFASVPRQGTMFKLKIPLKKGEAQGRGSGDVSDGKHIELAGRSVLVVDDIRMNQVIVT 425
EISFESEERKGTTFKVSIPLKEGQAQGAASGELAVVERSDLAGRSILVVDDIRMNQVIVT 465
MMLAKFNIPPFVVDNGQEAIDFLSDTEVDIVFMDCRMPVVDGFQATRELRKQNYTNPIIA 534
MILAKFDIKPAIVNNGLEAIEYLDSHVVDVIFMDCRMPVVDGFEATKRLRNSGYSKPIIA 536
MMLKKLGITPDFANDGMEALTYLQEHDVDIVLMDCRMPILDGFETTKRLRKQGYKKPILA 532
QTLKKLDIKPDLKNNGLEAVDAVKANQYELIFMDCRMPEMDGYEATVHLRENGFTKPIIA 485
QMLKKLDITPDLKANGLEALEAVKNKDYELIFMDCRMPEMDGYEATAHLRQKGFDRPIIA 525
LTAGTTSTEIEQCKQCGMDDIVCKPYKIADLKAILMKWNPLN- 576
LTASTTSTETEQCYLCGMNGIINKPYQKQEIRNVLTEWWAKIK 579
LTAGTTSMEVEACIEAGMDDTLSKPYKAIELEAMLKLWGSKYV 575
LTAGTTLEERQKCIESGMNDILTKPYTAADIEQIMCKWLGE-- 526
LTAGTTIEERQKCIDSGMDDILTKPYTATDIEQIMCKWLEQ-- 566

Appendix 4 Vector map for SwHK in pGEX4T-2

S. woodyi HK was cloned in to vector with restrictions sites at EcoRI and NotI to give an N-terminal GST-tagged HK.

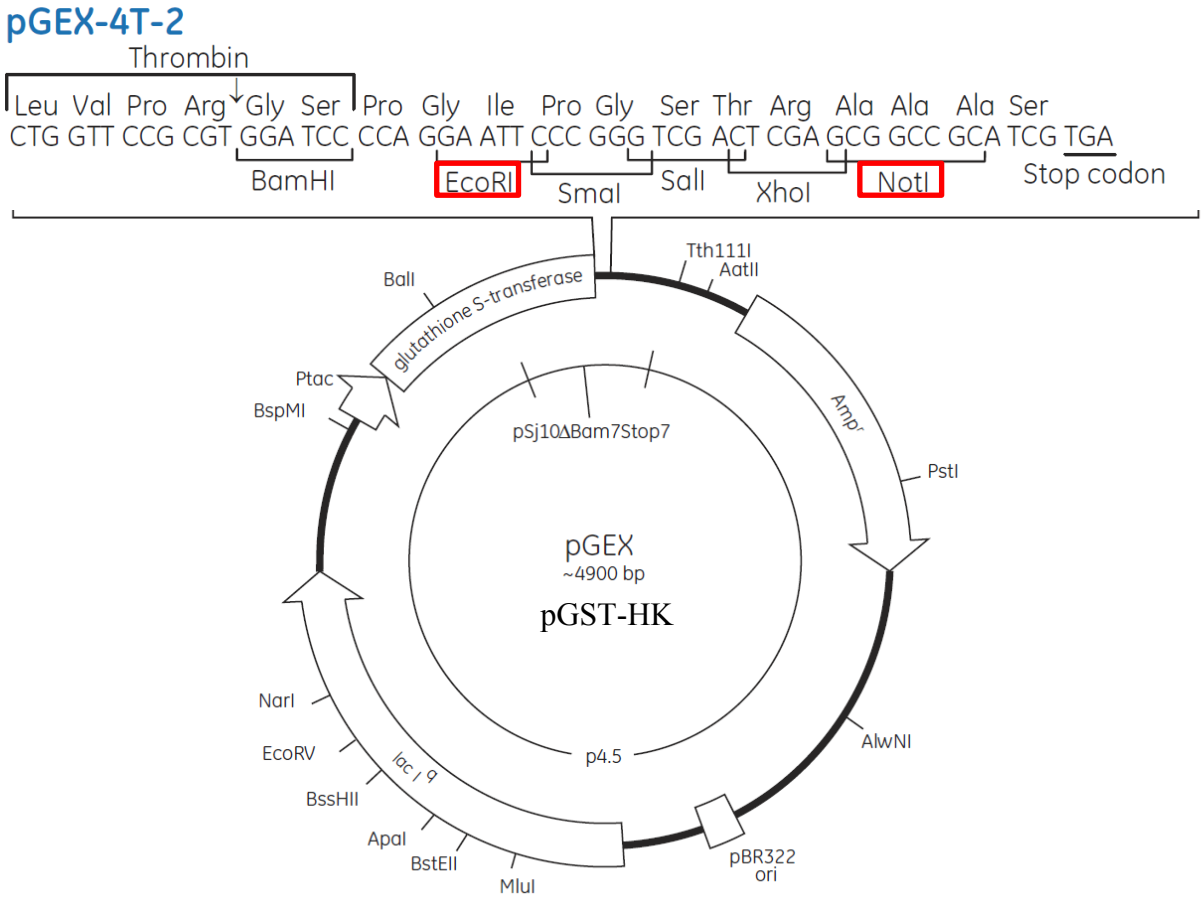

Appendix 5 Clustal equence alignment of Swoo_1513 and *Caulobacter crescentus* PleD.

```
PleD        MS--ARILVVDDIEANVRLLEAKLTAEYYEVSTAMDGPTALAMAAR-ICPTIILLDVMMP 57
Swoo_1513   MSDKATILLVDDTRTNIELLAGCLQKT-YNLKVAMNGKRCLELAESEPVPDLILLDVIMP 59
            **  * **:*** .:*:.** . *    *::..**:*  .* :*     * :*****:**

PleD        GMDGFTVCRKLKDDPTTRHIPVVLITALDGRGDRIQGLESGASDFLTKPIDDVMLFARVR 117
Swoo_1513   DMDGYDVCRQLKDNSSTKDIPIMFVTGKDSDEDEELGLQLGAVDYITKPIR--------- 110
            .***: ***:***:.:*:.**::::*. *.  *.  **: ** *::****

PleD        SLTRFKLVIDELRQREASGRRMGVIAGAAARLDGLGGRVLIVDDNERQAQRVAAELGVEH 177
Swoo_1513   ------------------------------------------------------------


PleD        RPVIESDPEKAKISAGGPVDLVIVNAAAKNFDGLRFTAALRSEERTRQLPVLAMVDPDDR 237
Swoo_1513   ------------------------------------------------------------


PleD        GRMVKALEIGVNDILSRPIDPQELSARVKTQIQRKRCTDYLRNNLDHSLELAVTDQLTGL 297
Swoo_1513   ----------------------PAIVTARVGTQVILKQQSDTLRS-------MALHDQLTSL 143
                                  *  ::*** **:  *: :* **.       :*: ****.*

PleD        HNRRYMTGQLDSLVKRATLGGDPVSALLIDIDFFKKINDTFGHDIGDEVLREFALRLASN 357
Swoo_1513   FNRHYLIEAANSKVARIKRHGGTLSLMMIDIDYFKLVNDKFGHQAGDTVLRAVASVLSSG 203
            .**:*:    :* * * .  *..:* ::****:** :**.***: ** *** .*  *:*.
```

c-di-GMP binding site

```
PleD        VRAIDLPCRYGGEEFVVIMPDTALADALRIAERIRMHVSGSPFTVAHGREMLNVTISIGV 417
Swoo_1513   SRKEDVVARFGGEEFVVLLDDCSILDADDKAEQLRSLIEQ---LIPEG---ISVTASFGI 257
            *  *: .*:*****:: * :: **   **::*  :.     :..*   :.** *:*:

PleD        SATAGEGDTPEALLKRADEGVYQAKASGRNAVVGKAA------- 454
Swoo_1513   AELDPDGETFEHLLARADQAVYLAKEQGRNCVVQAKSELDIKED 301
            :    :*:* * ** ***:.** ** .***.**   :
```